Surface Evolution of Mountains and Drainage Basins under Climatic and Tectonic Forcings

Yinbing Zhu

A thesis submitted in fulfilment of the requirements
for the degree of Doctor of Philosophy

School of Geosciences

Faculty of Science

University of Sydney

Australia

2026

Statement of Originality

I certify that the intellectual content of this thesis is the product of my own work and that all the assistance received in preparing this thesis and sources have been acknowledged. This thesis has not been submitted for any degree or other purposes.

Yinbing Zhu

Statement of Gen AI Attribution

During the preparation of the thesis, the author used ChatGPT for the purposes of optimizing the code used to analyze the output of numerical models. The author confirms that where text was modified by generative AI, the content was reviewed for possible errors, inaccuracies, and bias. The author takes full responsibility for the submitted thesis and ensures the work is their own and has used generative AI within the parameters of use (refer to the University of Sydney generative AI guide for researchers).

Yinbing Zhu

Supervisors

Prof. Patrice F. Rey

A/Prof. Tristan Salles

Acknowledgments

The advantage of numerical models is that parameters can be set. You can add any constraints you want to the model, and the model will run according to the set parameters. This is a controllable operation; everything seems predictable. However, life cannot be accurately parameterized. In the next second, the next day, the next month, the next year, anything can happen. Whether good or bad, you must learn to accept it. When I received the scholarship from the China Scholarship Council and the offer from the University of Sydney, life seemed perfect. Writing a few articles and getting a Ph.D. seemed easy. However, the complex model of life doesn't allow for smooth sailing. 2020 was the year I graduated with my master's degree, and also the year the model began to run strangely. Why did such results appear out of nowhere? I didn't understand, because the results touched upon areas unknown to me. Learning to adapt and accept is a good way to deal with the results. Also in that year, COVID-19 spread throughout the world. Australia's borders closed, and after a year of continuously applying for extensions, in 2021, I finally set foot on Australian soil for the first time. During my studies in Australia, there were both surprises and disappointments. Sometimes I had companions, and sometimes I walked alone.

My supervisor, Prof. Patrice Rey, is one of the few people who has information about my research and personal life. He gave me care and help that went beyond the duties of a supervisor. Although my progress was slow, I was always driven by the desire not to let him down. This thesis represents my humble effort to present a satisfactory conclusion to this journey. I also want to thank my other supervisor, A/Prof. Tristan Salles, who helped me become familiar with numerical models. Without his help, this thesis would have been even more challenging to complete. The people I met at the University of Sydney, such as Joe, Jono, Chris, Faranak, Puqing, Eric, Sinan, Utpal, and others, also brought me warmth with their friendliness. In addition, there is a friend at UNSW who helped me overcome many difficulties. I hope this friend will have fewer troubles and more happiness in the future.

The journey of studying abroad has been both a test and a reward.

Authorship Attribution Statement

Article 1: Zhu, Y., Rey, P., & Salles, T. (2025). Rainfall and tectonic forcing lead to contrasting headwater slope evolutions. ***Earth Surf. Dynam. (Accepted)***

Y.Z. designed and ran the simulations, analyzed the results, and wrote the manuscript. P.F.R. contributed to the result analysis and manuscript revision. T.S. developed the model code and contributed to the manuscript revision.

Article 2: Zhu, Y., Rey, P., & Salles, T. (2025). Diagnostic Signals of Rainfall and Tectonic Uplift: Insights from Divide Migration and Landscape Relaxation Times. ***(Submitted to Australian Journal of Earth Sciences)***

Y.Z. designed and ran the simulations, analyzed the results, and wrote the manuscript. P.F.R. contributed to the result analysis and manuscript revision. T.S. developed the model code and contributed to the manuscript revision.

Article 3: Zhu, Y., Rey, P., & Salles, T. (2025). Evaluating Central Andean Altiplano uplift histories with numerical model: a quantitative comparison of fold setups and uplift scenarios. (Prepared for submission to *Earth Surface Processes and Landforms*)

Y.Z. designed and ran the simulations, analyzed the results, and wrote the manuscript. P.F.R. contributed to the result analysis and manuscript revision. T.S. developed the model code and contributed to the manuscript revision.

In addition to the authorship attribution statements above, in cases where I am not the corresponding author of a published item, permission to include the published material has been granted by the corresponding author.

Yinbing Zhu, 30th December 2025

As supervisor for the candidature upon which this thesis is based, I can confirm that the authorship attribution statements above are correct.

Prof. Patrice F. Rey, 30th December 2025

ABSTRACT

The landscape on Earth's surface is a natural archive that records past climate change, tectonic events, and their interactions. The evolution of mountains and drainage basins reflects the complex coupling of surface processes at different spatial and temporal scales. Although previous researchers have attempted to interpret this archive through various means and successfully reconstructed the evolutionary history of some orogenic belts, in complex natural systems, the landscape signals generated by tectonic uplift and climate change (especially rainfall) often overlap, making it difficult to accurately separate and quantify the contribution of each forcing. Therefore, extracting diagnostic signals from landscape features and interpreting climatic and tectonic history remain major challenges for modern geomorphology. To address these challenges, this thesis uses landscape evolution modeling to investigate the transient and steady-state characteristics of landscapes under climatic and tectonic forcing, and to explore the uplift history of the Andean Plateau (Altiplano) by comparing modelled and natural landscapes.

The first part of the thesis develops a comparative theoretical framework using the landscape evolution model Badlands. Idealised experiments investigate the response of drainage basins to changes in rainfall rate and uplift rate under uniform and orographic rainfall conditions. The study combines quantitative metrics, including the channel steepness index (k_{sn}) and drainage-divide migration. The results show that transient changes in headwater channel slope provide an effective diagnostic signal for distinguishing climatic from tectonic forcing. Changes in rainfall rate can lead to a transient slope change reversal at the headwaters, caused by the time lag between hillslope diffusion and river incision response. In contrast, tectonic uplift causes the slope to remain unchanged before the arrival of the erosion wave. In addition, the study finds that landscape relaxation times are asymmetric under rainfall changes. Under orographic rainfall conditions, divide migration is highly sensitive to rainfall changes but relatively insensitive to tectonic uplift. These contrasting responses provide important indicators of the relative roles of climatic and tectonic forcing.

The second part of the thesis applies the theoretical framework to the Altiplano in the Central Andes to investigate the long-standing controversy over its uplift history. The study designs a combination experiment consisting of five uplift scenarios (earlier rapid, rapid, slow and steady, stepwise, and uniform and slow) and three fold setups (no folds, vertical folds, fold shortening). The similarity between modeling results and modern landscapes is quantitatively evaluated by using the Earth Mover's Distance (EMD) algorithm. The results indicate that fold shortening is a key factor in reproducing the N-S tributary pattern and knickpoint distribution on the eastern side of the Altiplano. Among all tested cases, the landscape generated by the stepwise uplift under horizontal fold shortening is most consistent with the modern landscape.

Overall, this thesis contributes to understanding the surface evolution of mountain ranges and drainage basins in two ways. First, through comparative numerical experiments, it establishes a theoretical framework for distinguishing climatic from tectonic forcing. Second, it shows how the framework can be applied to a natural orogenic system to constrain its uplift history. More broadly, the thesis demonstrates that by integrating analyses of channel profiles, divide migration, and large-scale drainage organisation, it is possible to link modern landscapes to the climatic and tectonic processes that shaped them. This contributes to a more quantitative and process-based interpretation of landscape evolution in tectonically active mountain ranges.

Contents

1 Introduction

The Earth's surface is uneven, featuring mountains, plains, hills, and basins, which are collectively known as landscapes. Modern landscapes result from the long-term combined action of internal forces (e.g., plate tectonics and mantle convection) and external forces (e.g., biological activity and river erosion). The characteristics of landscapes record the dynamic changes of the Earth throughout geological history and are therefore often used to study the processes that shaped landscape evolution. The landscapes of most interest in modern geomorphic research are mountains and drainage basins, which are common landscapes widely distributed on Earth. Mountains and drainage basins are usually coupled, with mountain uplift often accompanied by the development of adjacent drainage basins.

Tectonic activity and climate processes strongly influence the evolution of both. Under continuous and stable tectonic activity and climate, landscapes can reach a state of dynamic equilibrium over time, where the rate of material uplift equals the rate of erosion. However, this dynamic equilibrium is easily disrupted by tectonic uplift and climate change. After the perturbation, the landscape enters a transient adjustment state, which is a crucial period for studying the source of the perturbation. However, it is not easy to determine whether a landscape is in a transient state and to extract effective dynamic information from it, because the widely studied mountains and drainage basins may not be influenced solely by tectonics and climate. Their geomorphic characteristics are complex and diverse, and the characteristic signals usually contain signals influenced by other factors. Although there has been considerable research on mountains and drainage basins, our understanding of their dynamic processes and mechanisms of evolution remains incomplete.

In the following sections, I first introduce the climatic and tectonic control on the evolution of mountains and drainage basins. I then review various modeling ideas and landscape evolution models (LEMs) used in quantitative research on surface processes. The introduction chapter concludes with an overview of the research scope of this thesis.

1.1 Dynamics Factors of Surface Evolution

Tectonic activity and climatic processes are major controls on landscape evolution. Both shape the Earth's surface and interact with one another. Understanding landscape evolution, therefore, requires consideration of both factors. This section outlines crustal responses driven by tectonics and topographic erosion driven by climate.

1.1.1 Tectonic Drivers of Surface Uplift and Deformation

Tectonic activity occurs both at plate boundaries and within plates, shaping surface roughness and influencing the pace of landscape evolution. Its essential function is to change the pattern of uplift and subsidence, and the erosion base level, thereby providing initial potential energy and boundary conditions for external force erosion and deposition processes. Plate tectonics is one of the most important tectonic mechanisms that can establish significant topographic elevation differences at the regional scale (Figure 1.1).

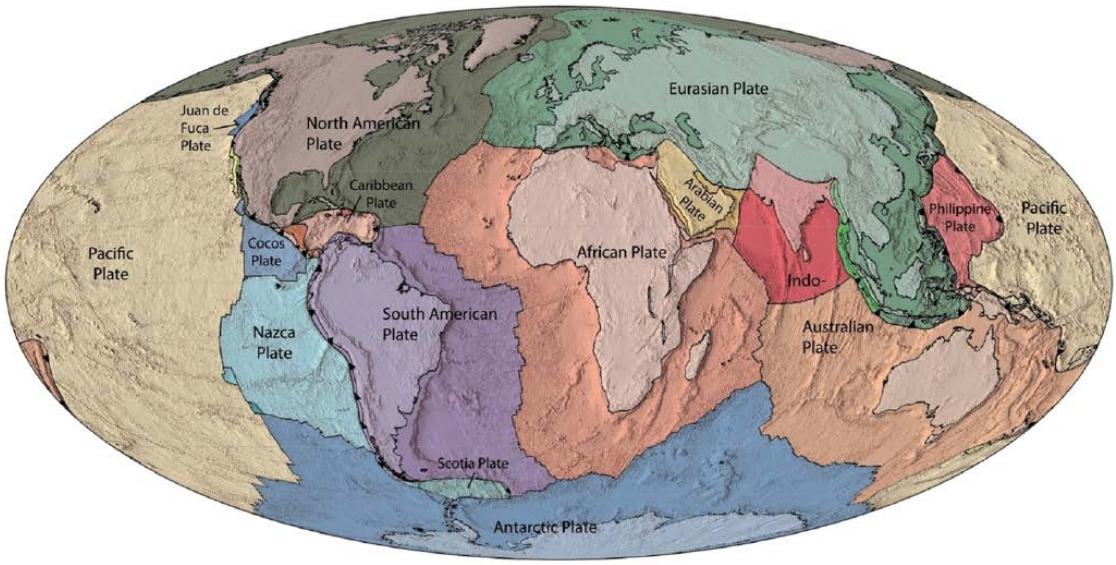

Figure 1.1. Present-day configuration of Earth's tectonic plates. The seven principal plates and multiple smaller plates are bounded by divergent margins (mid-ocean ridges), transform boundaries, and convergent margins (subduction zones). Adapted from Scotese and van der Pluijm (2020).

In the continental-continental collision zone, the crust is strongly compressed and shortened, accompanied by crustal thickening and rock uplift, forming high-altitude orogenic belts (Figure 1.2a). The Himalayan orogenic belt is a typical example, and its formation is closely related to the continuous convergence of the Indian Plate and the Eurasian Plate (Molnar & Tapponnier, 1975; Yin & Harrison, 2000). At the boundary of subducting plates, subducting plates trigger forearc to backarc tectonic deformation and volcanic activity (e.g., Heuret & Lallemand, 2005; Stern, 2002). The hanging plate thickens and uplifts as a whole under compression, thus developing long and continuous mountain ranges (Figure 1.2b) (Anderson et al., 2017; Garzione et al., 2017; Manea et al., 2017). The Andes Mountains in South America are a classic example of this mechanism.

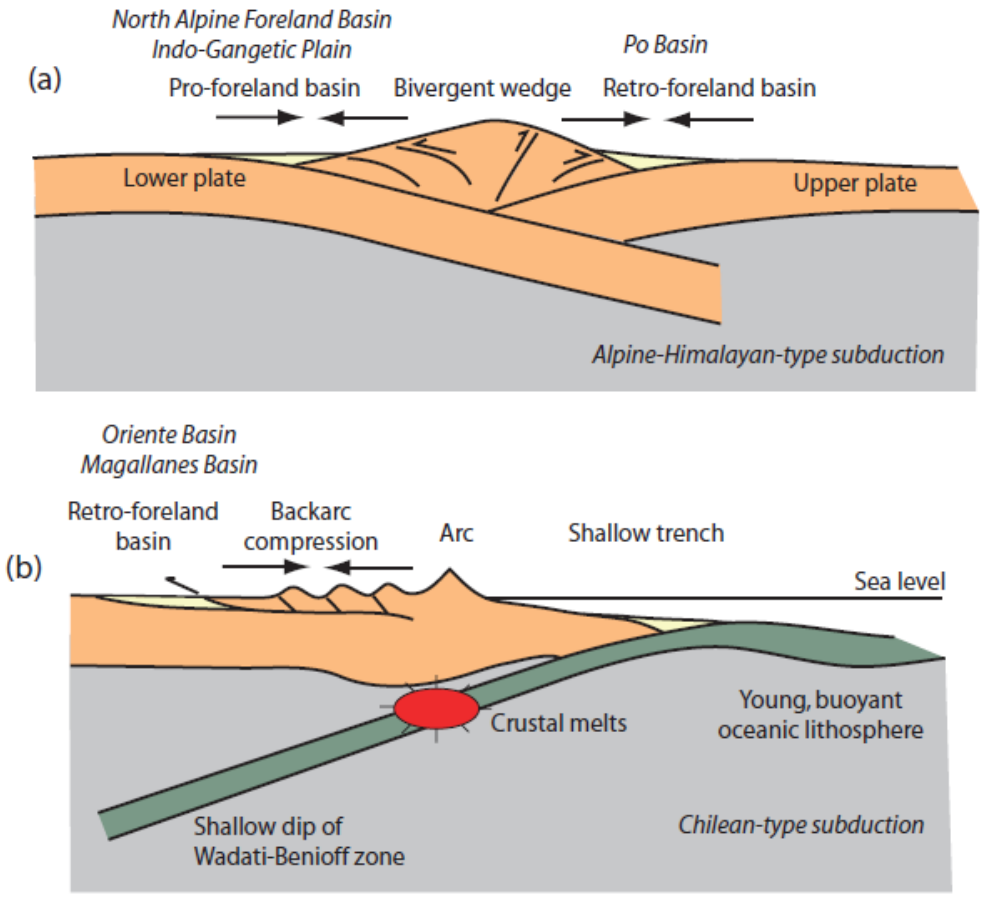

Figure 1.2. Cross-sectional diagram illustrating (a) continental collision (Himalayas) and (b) subduction zone dynamics (Andes). Adapted from Allen; and Allen (2013).

In addition to plate boundaries, intraplate processes are important drivers of large-scale vertical movements. Isostatic adjustment adjusts the height of the crust by changing the load (Figure 1.3a) (Tucker & Slingerland, 1994). A large amount of erosion or glacier melting can cause unloading, leading to crustal rebound and uplift. If a large amount of sediment accumulates and causes loading, it may induce crustal subsidence. The equilibrium rebound after the melting of glaciers in Southern Patagonia provides a clear example (Dietrich et al., 2010). Mantle convection can generate dynamic topography on a thousand-kilometer scale, causing slow and widespread uplift or subsidence of the Earth's surface (Figure 1.3b) (Flament et al., 2013).

All these horizontal shortening and crustal thickening due to collisions and subduction, and the isostatic response of the crust are constrained by the internal dynamics. Internal dynamics define the original state and the basic boundary conditions of the landscape (Upadhyay, 2025). Therefore, the intensity, location, and scale of the subsequent erosion, transport, and deposition are also greatly influenced by internal forces.

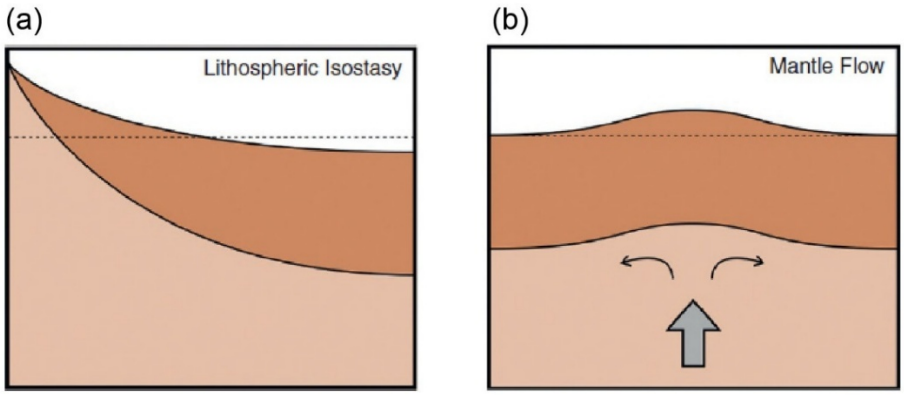

Figure 1.3. Surface movement caused by the isostasy and mantle flow. Modified from Hoggard et al. (2021).

1.1.2 Climatic Influences on Erosion and River Dynamics

After tectonic uplift and the establishment of initial topography, climate becomes one of the dominant factors controlling external processes. Climate directly controls erosion efficiency and material transport by regulating water volume, temperature, and freezing conditions (e.g., Li et al., 2021; Zhang et al., 2021). Therefore, it can transform and reorganize the rough landscape formed by tectonics. Among various external forces, river erosion driven by rainfall runoff is usually the most important factor. The incision strength of rivers is jointly controlled by flow rate, flow velocity, and sediment concentration, and affects the response of the river slope to tectonic uplift and rainfall changes (K. X. Whipple et al., 2013). The channel steepness index (k_s) is often used as a quantitative indicator of the longitudinal profile response of a river channel (Smith et al., 2022). High values usually indicate higher uplift rates or stronger erosion rates (Kirby & Whipple, 2012). However, its explanation is also constrained by factors such as rock erodibility, sediment supply, and channel shape adjustment (Kirby & Whipple, 2012).

In cold or high-altitude areas, glacier erosion can dominate for a longer period of time. Glaciers can quickly shape steep and typical landscape units such as U-shaped valleys, cirques, and horns through abrasion, plucking, and transport, and significantly alter the elevation distribution and slope structure within the drainage area (Figure 1.4) (Fraedrich, 2023). At the same time, the weathering process provides materials for erosion. Physical weathering and chemical weathering control the thickness, particle size composition, and supply of movable substances in the weathering crust. Its rate and dominant type are strongly influenced by temperature, rainfall, and vegetation cover, with vegetation being an important "mediator variable" connecting climate and erosion (H. R. G. K. Hack, 2020; Murphy et al., 2016; Xie et al., 2022). Therefore, climate not only affects erosion rates but also changes the landscape style.

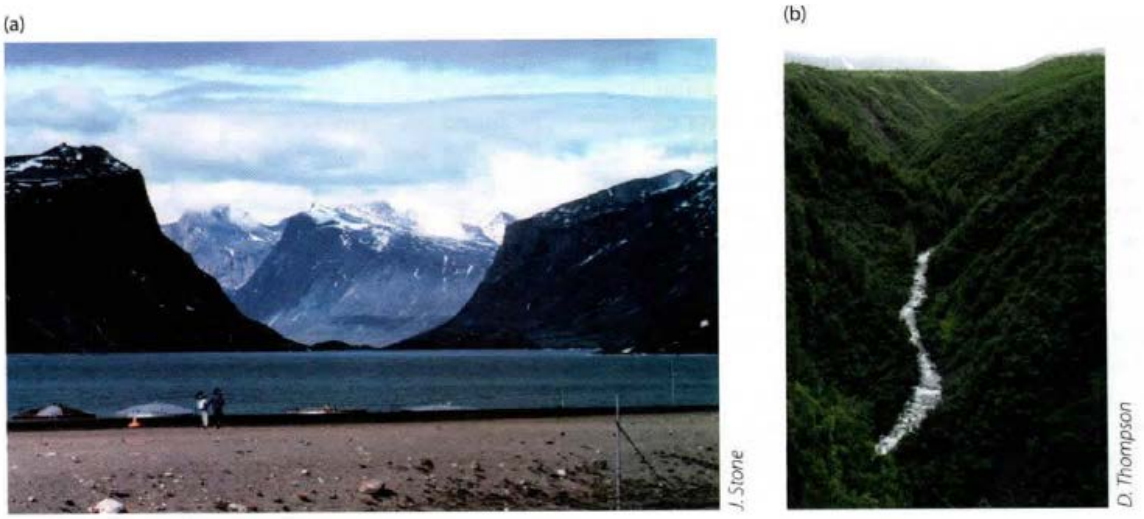

Figure 1.4. (a) A U-shaped valley formed by glacier erosion and (b) a V-shaped valley formed by river erosion. Adapted from P.R. Bierman and D.R. Montgomery (2019).

Both the annual average rainfall rate and the periodic distribution and variance of rainfall can affect the river dynamics. The rainstorm frequency, the concentrated rainfall in the season, the flood peak arising from snowmelt, and the dry-wet alternation change the effective runoff duration (e.g., Alavinia et al., 2019). The spatial variation of rainfall is also an important factor. Concentrated rainfall on the windward slope can enhance the spatial gradient of the flow and erosion in the drainage basin and influence the form of the river channel slope, the competition of tributaries, and the adjustment of the channel network structure (Han et al., 2015). On the contrary, a more uniform distribution of rainfall may lead to more dispersed downcutting and transport, and the response of the river channel may be closer to the overall consistent slow adjustment.

The sediment supply is influenced by climate, thereby regulating the erosion efficiency and channel morphology of rivers (Mohamadi & Kavian, 2015). Intense slope erosion and landslide activity can transport a large amount of particles into the river channel. Rivers are prone to sedimentation or diversion. Intermittent sediment transport may lead to periodic uplift of riverbeds and filling of river valleys. Erosion occurs again when water flow increases or sediment supply decreases, forming river terraces. Sediments have a dual impact on bedrock erosion (Turowski et al., 2007). Moderate particle volume can improve erosion, while excessive coverage can inhibit it. Changes in surface vegetation cover can also affect erosion. Vegetation reduction usually enhances slope runoff and sand supply efficiency and increases flood peak and suspended sediment flux (Roering et al., 2002). Conversely, vegetation restoration tends to stabilize slopes, reduce sediment supply, and change the threshold for river transition from erosion to accumulation. In summary, climate plays an important role in erosion, sediment transport, and sedimentation. Therefore, climate can alter the rate and direction of landscape evolution, as well as its final morphology.

1.1.3 Interactions Between Tectonics, Climate, and Erosion

One of the important understandings in modern geomorphology is that tectonics, climate, and erosion are not independent of each other. Erosion connects the two forces into a coupled system. Tectonics determines the topographic relief and potential energy gradient. Climate determines precipitation (including rain, snow, and other forms of water) and effective erosion events. Erosion transforms these boundary conditions into material flux and landscape adjustments, which in turn alter the environment of climatic and tectonic processes (Figure 1.5).

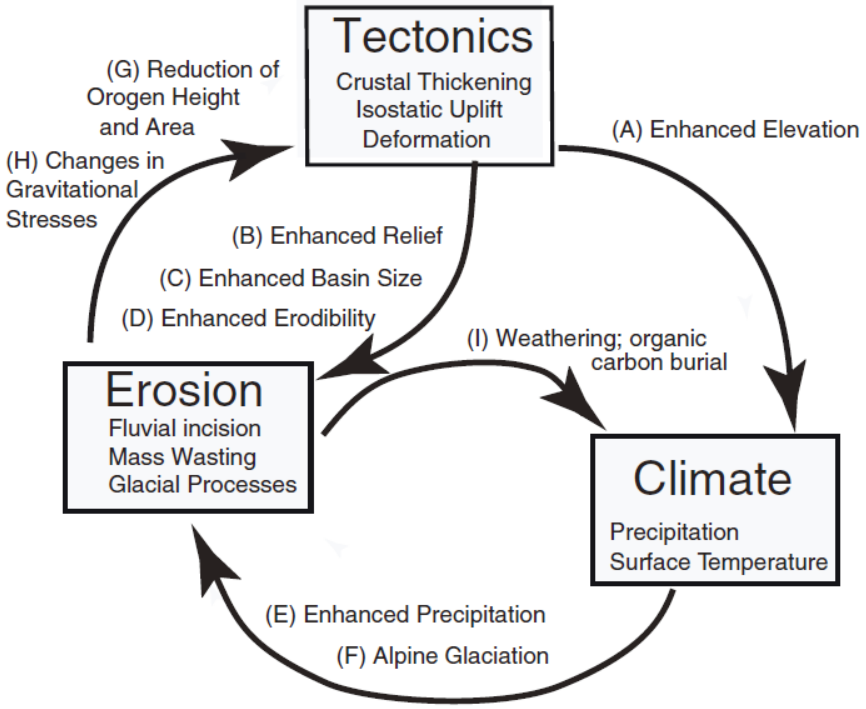

Figure 1.5. Schematic diagram illustrating feedbacks between tectonics, climate, and erosion. Adapted from Willett et al. (2006).

A common type of feedback is "tectonics → climate → erosion". The uplift of mountains and plateaus forms topographic barriers and influences atmospheric circulation, thereby reshaping the spatial distribution of rainfall. The rainfall rate on the windward slope increases, while the leeward slope forms a rain shadow in the arid area (Han et al., 2015). Erosion, therefore, shows strong spatial heterogeneity. Rivers on windward slopes are more prone to deepening, and slope surfaces are more prone to instability. The leeward slope may be dominated by intermittent floods and wind-induced processes. The uplift of the Himalaya and Tibetan Plateau is believed to have strengthened the Asian monsoon and formed a large-scale aridification pattern in its northern leeward region (Tada et al., 2016). Spatially variant erosion driven by climate shapes asymmetric mountain ranges and river network patterns.

Another feedback type that consistently receives attention is "climate → erosion → tectonics". When heavy rainfall, glacier cutting, or headwater erosion increases the erosion rate in a given area, surface materials are removed quickly. The load on the crust decreases accordingly. The lithosphere undergoes rebound and uplift through isostatic response, thereby enhancing the landscape roughness and possibly further maintaining or enhancing local erosion (Tucker & Slingerland, 1994; Kelin X. Whipple, 2009). This mechanism is more easily identified in mountain ranges with highly concentrated rainfall. Observations in the Southern Alps of New Zealand indicate a high spatial overlap between the maximum rainfall zone and the fastest tectonic uplift (Jiao et al., 2017). The overlap provides support for the positive feedback that climate-induced intensified erosion can promote further mountain uplift. In this type of system, erosion may become an active factor regulating the distribution of uplift and mountain morphology.

The coupling effect does not necessarily mean that the landscape always maintains a strict steady state, but it often drives the system towards a dynamic equilibrium. When deviating from equilibrium, the slope of the river channel, the steepness of the channel, the position of the divide, and the sediment flux will be adjusted until a new steady state is established.

1.1.4 Landscape Responses Across Spatial and Temporal Scales

The response of geomorphic systems to the coupling of tectonics and climate shows significant multi-scale characteristics. Different spatial scales correspond to different dominant processes and observable signals. Different time windows determine whether the system presents an "event response", "phased adjustment", or "long-term average state". Therefore, interpreting landscapes requires a discussion of the range of scales.

In space, the response can extend from regional orogenic belts to individual slopes. At the scale of orogenic belts, the long-term competition between tectonic uplift and climate erosion is mainly reflected in macroscopic characteristics such as average elevation and mountain range orientation (Champagnac et al., 2012). At the drainage basin scale, signals are more commonly identified through quantifiable geomorphic indices, such as channel steepness index, area elevation integration, drainage scale (length and area), and channel density (Figure 1.6) (DiBiase et al., 2010). These indicators can link landscapes with process intensity to identify the impact of tectonic uplift and climate change (Kelin X. Whipple, 2004). At the smaller slope scale, the movement of block-like materials gradually becomes dominated by gravity. The frequency, spatial distribution, and causes of landslides, folds, and other geological processes are highly sensitive to rainfall, rock strength, and slope thresholds. These small-scale processes can rapidly alter local topography (Ahmed et al., 2019; Tanyaş et al., 2018).

In terms of time scale, the scale of geomorphic response varies from a few days to several million years. On a very short time scale, catastrophic rainfall and floods can cause instantaneous erosion, river

adjustments, and bank collapse of river channels (Snyder et al., 2003). On a medium time scale, the impact of glacial-interglacial cycles can adjust erosion and sedimentation patterns through glacier advance and retreat (Wickert, 2016). At longer geological time scales (on the order of millions of years), the morphology of orogenic belts is controlled by a long-term balance between uplift and erosion, and macroscopic geomorphological features can be relatively stable and slowly evolving (Willett & Brandon, 2002).

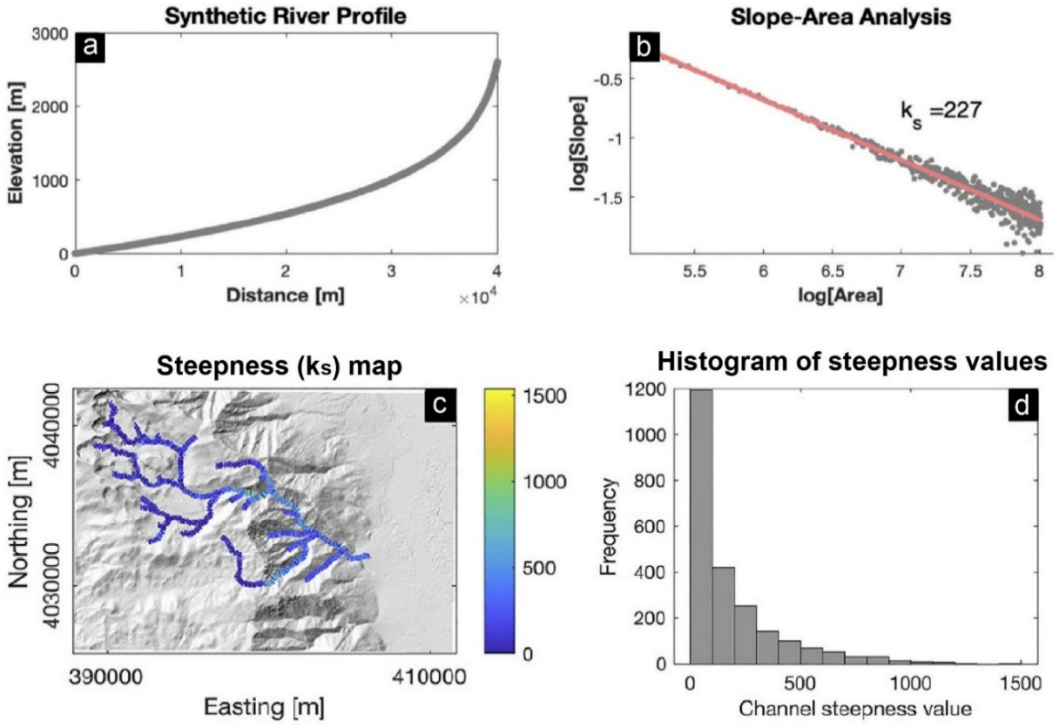

Figure 1.6. (a) Synthetic river profile; (b) Slope and area data extracted from the synthetic profile; (c) Channel steepness map; (d) Histogram of channel steepness values. Modified from Smith et al. (2022).

1.1.5 Morphology and Formation Mechanisms of Drainage Basins.

A drainage basin is a landscape unit bounded by a divide. Surface runoff from rainfall and groundwater ultimately converges into the same river system (Figure 1.7). The drainage basin is one of the fundamental scales for studying the water cycle and landscape evolution. Most drainage basins have a branched river network structure, consisting of main streams and tributaries. Along the longitudinal profile, the drainage basin usually includes three zones: upstream erosion, midstream transport, and downstream deposition. Overall, a drainage basin is a typical source-to-sink system (Sømme et al., 2009).

The formation and evolution of drainage basins are mainly driven by hydrodynamic processes. Rainfall converges due to gravity, usually undergoing a transition from sheet flow, rill flow to stable river flow, and completing erosion, transport, and deposition at different locations (Moore & Burch, 2010). The

intensity and spatial distribution of these processes are jointly controlled by tectonics and climate. Regional uplift can raise the erosion base level and enhance the river incision. In contrast, subsidence often increases accommodation space, which may lead to the siltation, oscillation, or diversion of rivers (Guerrero et al., 2008). Structural features such as faults and folds also constrain the river direction, promoting their distribution along structural zones and forming drainage patterns with structural control features such as trellis patterns (P.R. Bierman & D.R. Montgomery, 2019).

Climate can affect runoff and erosion efficiency through rainfall rate and duration. Humid areas are more prone to sustained runoff, denser river networks, and more continuous erosion and material transport. The runoff in arid areas is mostly intermittent, with common shallow and wide temporary channels and event transport (Pelletier & DeLong, 2004; Tucker & Slingerland, 1997). Therefore, the morphology of the drainage basin and the river network records the surface process response under the long-term coupling effect of tectonic uplift and climate change.

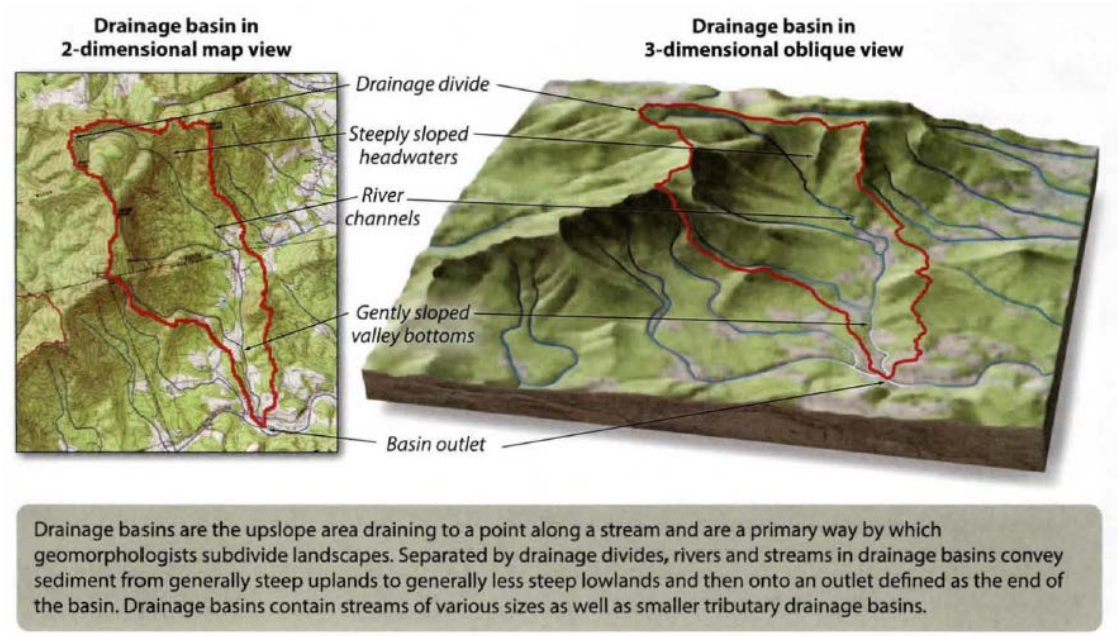

Figure 1.7. Conceptual diagram of a drainage basin showing key geomorphic elements, including the drainage divide, channels, headwaters, and outlet. Adapted from P. R. Bierman and D. R. Montgomery (2019).

1.2 Modelling Surface Processes

The formation of landscape involves a gap in time between what we see today and the geological timescales over which landscapes appear. Field observations of landscape, coupled with thermochronology, provide valuable constraints on rates of uplift and erosion. However, many constraints provide either a snapshot in time or a whole integrated history. Landscape Evolution Models (LEMs) are therefore proving a helpful toolkit to test hypotheses about the dynamic interactions

between tectonics, climate, and surface processes (Chen et al., 2014; Tucker & Hancock, 2010). In this section, I review the history of LEMs, the physical laws, and the specific numerical framework I used in the study.

1.2.1 A Brief History of Landscape Evolution Models

The theory of landscape evolution originated in the late 19th century. William Morris Davis proposed the theory of the "Cycle of Erosion" ("Davisian Cycle") (Davis, 1899). He divided landscape evolution into three stages: youth, maturity, and old age. The "Cycle of Erosion" theory has long dominated qualitative research in geomorphology.

In the mid-20th century, the focus of geomorphological research shifted to quantitative analysis methods based on physical processes. Horton (1945) used hydrophysical methods to propose a mathematical description of river systems and basins for the first time. Strahler (1952) then suggested that the area-altitude curves of a drainage basin can be described by a three-variable equation. The shape and integral values of the curves reflect stages of basin evolution. Studies of river profiles argued that the rate of transport of erosion products in a drainage basin depends on the initial topography, time, and geological conditions (J. T. Hack, 1957). A series of studies based on mathematical and physical methods has laid the theoretical foundation for process geomorphology, enabling geomorphological research to shift from description to mechanism analysis and from qualitative inference to quantitative modeling.

In the 1970s and 1990s, the increases in computing power facilitated the development of numerical landscape evolution models (LEMs). Computers enable researchers to go beyond simple mathematical analytical solutions and achieve numerical simulations of three-dimensional landscapes. Early models, such as the Ahnert model, mainly simulated the evolution of slopes under different weathering conditions (Ahnert, 1987). Later models began to use grid systems to simulate river downcutting and flow processes (e.g., Howard, 1994; Willgoose et al., 2008). These tools enable researchers to simulate landscape dynamics and surface erosion on geological timescales.

With the development of other Earth process models, new coupled models link surface processes with deep Earth dynamics and atmospheric circulation. Contemporary models such as Landlab, SSSPAM, and Badlands are able to do simulations with complex grids and constrained perturbations (Hobley et al., 2017; Salles & Hardiman, 2016; Welivitiya et al., 2019). They can not only simulate a single landscape, but also reproduce the complete evolution of the "source-to-sink" system, which enables the simulation of the overall evolution of basins and mountains.

1.2.2 Contemporary Landscape Evolution Models

Today's LEMs continue to expand in scope and capabilities. The development of models tends to be modular, open-source, and capable of simulating the interactions among multiple surface processes.

The emergence of modular modeling frameworks is an important development. Landlab was proposed by Hobley et al. (2017) and further developed by Barnhart et al. (2020a). Landlab is a Python package that allows users to build custom landscape evolution models. The package includes various components that can be used to simulate a wide range of processes, including water flow paths, hillslope diffusion, sediment transport, and vegetation dynamics. Its modular design provides a foundation for the development of subsequent new modules, offering greater flexibility for different studies.

On a spatial scale, the LEMs have expanded from individual drainage basins and mountain scales to continental and global scales. The eSCAPE model uses parallel computation to simulate source-to-sink sediment transport from continents to adjacent marine basins at regional-to-global scales for the first time (Salles, 2019). Based on the concept of global simulation, the goSPL model further integrates large-scale plate tectonics, mantle dynamics, and paleoclimate boundary conditions, enabling simulations of long-term landscape evolution and sedimentation at global scales (Salles et al., 2020). Advances in numerical methods and high-performance computing have made it increasingly feasible to explore landscape evolution on a spherical grid over hundreds of millions of years.

Another important development direction of LEMs is the incorporation of biological and soil-forming processes into models. Although vegetation and soil are found everywhere on the surface, their influence was often not fully considered in early LEMs. The roles of vegetation and soil are often simplified by modulating effective erosion parameters. Soil-Landscape Evolution Models (SLEMs) have been developed to simulate the co-evolution of soil, landscape, and hydrological systems (van der Meij et al., 2018). For example, the LORICA model couples landscape evolution with dynamic soil profiles and pedogenic processes to simulate soil development and landscape change (Temme & Vanwalleghem, 2016). The SSSPAM model can calculate erosion and deposition, as well as the particle size grading in soil profiles (Welivitiya et al., 2019; Welivitiya et al., 2016). Contemporary LEMs are therefore no longer limited to morphological simulation of the landscape.

Early LEMs focused on forward simulations, and contemporary LEMs can be used to estimate parameters and predict later landscape development under real-world scenarios. Inversion-based methods are increasingly utilizing modern topographic data to estimate poorly constrained process parameters and landscape evolution history. For example, Barnhart et al. (2020b, 2020c) demonstrated how topographic inversion and optimization methods can be used to evaluate the structure of LEMs and estimate process rates from modern topography.

Taken together, these advances show that contemporary LEMs are becoming increasingly diverse in terms of architecture and application. Each model has its own strengths, and the choice of model depends on the scientific problem to be solved.

1.2.3 Governing Equations: Fluvial Incision and Hillslope Diffusion

Numerical landscape models typically follow the principle of mass conservation. Landscape evolution in the models is primarily driven by tectonic uplift (*U*) and erosion/deposition processes (*E*).

$$\frac{\partial z}{\partial t} = U - E \tag{1}$$

Where *z* is the surface elevation, and *t* is the evolution time. *E* is typically decomposed into two primary geomorphic components: fluvial incision (advective transport) and hillslope transport (diffusive transport).

In bedrock landscapes, river incision is most commonly approximated using the Stream Power Incision Model (SPIM). This semi-empirical law assumes that the erosion rate is proportional to the energy expenditure of the water flow acting on the channel bed. The stream power law can be written as:

$$E_{fluvial} = KA^m S^n \tag{2}$$

Where:

- *K* is the erodibility coefficient, which is influenced by lithology, hydraulic condition, climate, and channel geometry (Kelin X. Whipple, 2004).
- *A* is the upstream drainage area. While physically-based models ideally solve the Saint-Venant equations for water height θ and velocity, the use of the drainage area (*A*) approximates these values under assumptions of steady-state uniform rainfall (Chen et al., 2014).
- *S* is the local channel slope (∇z).
- *m* and *n* are positive constants that depend on the dominant erosion mechanism (e.g., plucking vs. abrasion) and basin hydrology (Kelin X. Whipple & Tucker, 1999).

On hillslopes, sediment transport is often modelled as a linear diffusion process, representing the creep of soil due to biogenic perturbation, freeze-thaw cycles, and rain splash. The hillslope transportation is described by:

$$E_{hillslope} = -\nabla \cdot q_s \tag{3}$$

Where the sediment flux q_s is linearly related to the topographic slope:

$$q_s = -D\nabla z \tag{4}$$

Where *D* is the hillslope diffusion coefficient (m^2/yr). The diffusion equation is the combination of the two equations:

$$\frac{\partial z}{\partial t} = D\nabla^2 z \tag{5}$$

The linear diffusion function is usually used in low-relief landscapes. For the area with steep slopes, nonlinear diffusion laws are required because landslide probability increases as slopes approach a critical angle of stability (Roering et al., 2002; Roering et al., 1999).

1.2.4 Common Approaches: Analytical, Analogue, and Numerical

The commonly used methods for studying landscape evolution can be roughly classified into three categories: analytical methods, analogy (physical) experiments, and numerical modeling (Tucker & Hancock, 2010). The differences among the three are mainly reflected in their level of abstraction, controllability, repeatability, and ability to handle spatial heterogeneity and transient processes. Analytical methods are used to establish the relationship between mechanism intuition and scale. Physical experiments are used to directly observe process coupling and nonlinear responses. Numerical models are used to test different tectonic and climate scenarios under controllable conditions.

(1) Analytical

The analytical method is based on control equations (such as river incision, slope diffusion, etc.), and obtains analytical or semi-analytical solutions through mathematical derivation. They are particularly adept at answering mechanism questions of 'what if' and providing scale relationships between key parameters. For instance, with the stream power framework, the relation between the steady-state longitudinal profiles and concavity, steepness, and uplift rate could be obtained (Kelin X. Whipple & Tucker, 1999). The analytical method is easy to apply and provides a theoretical framework for model design and interpretation of results. It is also often used to estimate system response time and identify which parameter combinations are theoretically indistinguishable. The analytical method has limitations. To ensure solvability, the analytical method usually needs to be simplified. When transient forcing, complex boundary conditions, and lithological spatial heterogeneity are involved, analytical solutions are often insufficient for direct application (Willgoose, 2005).

(2) Analogue / Physical

Analogic experiments compress the surface process down to the laboratory. Typical experimental devices are rain-simulation sandboxes. Researchers can observe the formation of river channels, divide migration, and deposition following the change in uplift and rainfall.

Physical experiments provide intuitive process evidence. For example, Bonnet and Crave (2003) experiment demonstrates how landscape and erosion responses can undergo different stages of

adjustment over time under the combined effects of tectonics and climate change, which is insightful for distinguishing landscape signals driven by tectonics and climate. The shortcomings of physical experiments lie in scaling and similarity (Paola et al., 2009). Natural systems usually operate on large scales. Physical experiments cannot satisfy all dynamic-similarity conditions simultaneously (Reynolds number, Froude number, particle-scale effects, etc.). Therefore, it is appropriate to get mechanisms and trends in experimental results rather than reproduce natural systems point-by-point.

(3) Numerical

Numerical modeling applies control equations to iteratively solve for the variables of the landscape elevation at each time step (Chen et al., 2014). Its strength lies in its ability to concurrently incorporate boundary conditions for spatial and temporal heterogeneity, such as spatially varying rainfall and lithology, and variable uplift rates. Compared to analytical methods, numerical models are easier to simulate complex scenarios. Compared to physical experiments, numerical experiments are easier to replicate, and conditions are easier to control. Numerical modeling also has apparent limitations. The model results are sensitive to parameter values and grid resolution and need to be verified against observations. Model evaluation and uncertainty quantification have therefore become key steps (Paola et al., 2009).

1.2.5 Introduction to Badlands

The numerical model used in this thesis is Badlands (Basin and Landscape Dynamics). Badlands is an open-source, Python-driven numerical model for simulating sediment transport, landscape dynamics, and basin stratigraphic evolution in geologic time (Salles et al., 2018; Salles & Hardiman, 2016). Badlands provides a programmable, flexible tool for investigating Earth surface processes at regional to continental scales over timescales of thousands to millions of years. Badlands utilizes a Triangular Irregular Network (TIN) to construct the model surface. TIN allows spatial resolution to vary during the modeling process, making the results comparable in resolution to the input. Badlands is a source-to-sink model. The material is eroded upstream, transported through river channels, and ultimately reaches drainage basins or oceans for deposition. Key functions include:

- Efficient Flow Routing: Utilizing a Single-Flow-Direction (SFD) algorithm based on the *O(n)* method of Braun and Willett (2013).
- Parallelisation: The framework is designed for distributed memory environments (MPI), allowing for the simulation of high-resolution landscapes over large spatiotemporal scales.
- Multiple Incision Regimes: Both detachment-limited erosion and transport-limited and hybrid (tool-and-cover) incision laws are supported, allowing for more complex river dynamics.
- Marine Processes: The model simulates marine dynamics, including wave-induced longshore drift and carbonate reef growth based on fuzzy logic rules (Salles et al., 2018).

- Flexural Isostasy: Coupling surface mass redistribution with an elastic plate model that supports a laterally heterogeneous lithosphere.

1.3 Scope of Thesis

In this thesis, I use Badlands to model landscape evolution on geological time scales (10-50 Ma) under climatic and tectonic forcing. The main purpose is to gain a deeper understanding of how to determine and distinguish the climatic and tectonic signals preserved in river and basin features, providing a reference for interpreting landscape evolution from modern observations.

In Chapters 2 and 3, I design and test ideal numerical experiments under varying parameter values. Chapter 2 discusses the impact of changes in uplift rate and rainfall rate on landscape evolution under spatially uniform rainfall patterns. Spatially variable rainfall is considered in Chapter 3 based on the experiments in Chapter 2. Chapter 3 further discusses the response of the landscape to orographic rainfall. Through quantitative analysis of changes in river profiles, divide migration, and basin asymmetry, I have demonstrated that transient landscapes preserve diagnostic signals to distinguish climatic and tectonic forcing.

Chapter 4 introduces the actual topography (modern DEM) and explores the uplift history of the Andean Plateau (Altiplano) based on the findings from the previous chapters. I test five uplift scenarios and three fold setups proposed by previous researchers, and compare the simulated drainage patterns and landscape features with current observations. The results show that the stepwise uplift accompanied by the shortening of the fold and thrust belt is the most suitable for explaining the uplift history of the Altiplano.

Chapter 5 summarizes the research results of Chapters 2-4 and proposes future research directions. Chapter 6 summarizes the main conclusions regarding the preservation and interpretation of tectonic and climate signals in landscapes.

2 Article 1

Rainfall and Tectonic Forcing Lead to Contrasting Headwater Slope Evolutions

Yinbing Zhu[1], Patrice Rey[1], Tristan Salles[1]

[1]School of Geosciences, University of Sydney, Sydney, NSW, 2006, Australia

Earth Surf. Dynam., 13, 1249–1261, 2025
https://doi.org/10.5194/esurf-13-1249-2025

Earth Surface Dynamics
Open Access
EGU

Rainfall and tectonic forcing lead to contrasting headwater slope evolutions

Yinbing Zhu, Patrice Rey, and Tristan Salles

School of Geosciences, University of Sydney, Sydney, NSW, 2006, Australia

Correspondence: Patrice Rey (patrice.rey@sydney.edu.au)

Received: 3 April 2025 – Discussion started: 23 April 2025
Revised: 22 August 2025 – Accepted: 16 September 2025 – Published: 24 November 2025

Abstract. Landscapes evolve through the coupled effects of tectonics and surface processes. Previous studies have shown that uplift rate changes generate upstream-migrating erosion waves, altering downstream slopes while upstream slopes remain constant until the wave arrives. However, the distinctive differences between landscape responses to uplift versus climatic changes, particularly rainfall rate changes, remain incompletely described. This study uses a numerical model to investigate landscape responses to changes in both rainfall and uplift rates. Results show that, unlike the simple upstream-migrating erosion waves from uplift rate changes, rainfall rate changes generate more complex responses. Specifically, rainfall rate changes cause transient slope change reversals at the headwaters due to differential erosion between the divide and its adjacent areas, a pattern not observed in uplift-induced evolution. These reversals are more pronounced when hillslope diffusion plays a dominant role. While both rainfall and tectonic forcing drive landscape change, they produce recognizably different signatures in river profiles. If these distinctive signatures can be identified from river profiles or inferred from erosion rate measurements, they can help disentangle climatic and tectonic influences on landscape evolution.

1 Introduction

Whilst tectonic and geodynamic forces generate longer wavelength topography, Earth's surface processes powered by climate dissect the Earth's surface, creating high-frequency topographic features that contribute to the reconfiguration of drainage patterns and the re-routing of sediments from source to sink (e.g., Allen, 2008; Wobus et al., 2006a; Whipple et al., 2013; Martinsen et al., 2022; Seybold et al., 2021). Whether or not climatic and tectonic disturbances impact landscape evolution differently has been debated for decades (e.g., Kirby and Whipple, 2012; Whipple, 2009; Bonnet and Crave, 2003; Whittaker, 2012). Previous research has focused on various landscape features, such as river channels, drainage divides, and alluvial fans, to understand whether they respond differently to tectonic and climatic disturbances (e.g., Leonard and Whipple, 2021; Mao et al., 2021; Shi et al., 2021; Willett et al., 2014). Rivers, in particular, have been found to respond strongly to climatic and tectonic disturbances, making them a valuable feature for studying how landscapes evolve (e.g., Molin et al., 2023; Quye-Sawyer et al., 2021; D'Arcy and Whittaker, 2014). Here, we investigate via numerical experiments how river channels respond to rainfall and uplift, paying particular attention to the role of hillslope diffusion, which is often overlooked in favour of river incision processes. We show that river channels respond slightly differently to tectonic and rainfall-driven changes when hillslope diffusion is considered. After changes in uplift rate, the channel slope at the headwaters records a monotonic increase (uplift rate increase) or decrease (uplift rate decrease). In contrast, after changes in rainfall rate, the channel slope records a non-monotonic adjustment, which becomes more pronounced as the surface diffusion coefficient increases. We suggest that changes in rainfall rate cause a transient spatial variation in erosion rate around the divide area due to the interaction between hillslope diffusion and river incision. This difference has the potential to distinguish between tectonic and climatic influences on landscape evolution.

1.1 River incision vs hillslope diffusion

Several numerical models have been proposed to quantify river incision processes (e.g., Dietrich et al., 2003; Howard and Kerby, 1983; Perron et al., 2008). The most commonly used is the detachment-limited stream power model, which assumes that sediments are instantly flushed from the channel and that the bedrock erosion rate E depends on the channel slope S, drainage area A, and precipitation P:

$$E = k_{\mathrm{d}}(PA)^m S^n \tag{1}$$

where m and n are positive constant exponents, and k_{d} is a coefficient describing the erodibility of the channel bed and reflects the combined impacts on the erosion of climate, lithology, bedload, and other potential parameters (Kirby and Whipple, 2012; Smith et al., 2022; Whipple and Tucker, 1999). Equation (1) simplifies the impact of climate on erosion by focusing only on mean rainfall rate. However, real landscapes respond to climate change not only through shifts in mean precipitation but also through (i) the distribution of storm magnitudes, (ii) the phase of precipitation (snow vs. rain) that controls the timing of snowmelt runoff (Meira Neto et al., 2020), and (iii) the dominant runoff-generation mechanism (Uhlenbrook et al., 2005). Moreover, incision in channels is often controlled by erosion thresholds (DiBiase and Whipple, 2011) and may be further moderated by vegetation–evapotranspiration feedbacks (Yetemen et al., 2019). While these factors are critical for site-specific predictions, Eq. (1) is used here to isolate the first-order impact of a change in fluvial erosion efficiency on landscape form, providing a baseline for understanding these more complex interactions.

Following the principle of conservation of mass, the rate of surface elevation change ($\partial z/\partial t$) is determined by the difference between the uplift rate U and erosion rate:

$$\frac{\partial z}{\partial t} = U - E \tag{2}$$

As rivers incise, the sloping ground at their flanks increases, driving hillslope diffusion, which describes the downward transport of creeping soil (Fernandes and Dietrich, 1997; Dietrich et al., 2003). Models indicate that the convexity of the hillslope profile is influenced by hillslope processes and the rate of incision at the hillslope base (e.g., Armstrong, 1987; Ahnert, 1987). Hence, river incision and hillslope diffusion are coupled and evolve simultaneously. A simple model describing the process of hillslope diffusion assumes that the flux of soil along hillslopes is linearly related to the hillslope gradient (e.g., Culling, 1963, 1960; Salles and Duclaux, 2014; Tucker and Hancock, 2010):

$$\frac{\partial z}{\partial t} = k_{\mathrm{hl}} \nabla^2 z \tag{3}$$

where k_{hl} is the hillslope diffusion coefficient, which integrates climate, lithology, soil conditions, and biotic influences (Dietrich and Perron, 2006; Hurst et al., 2013; Robl et al., 2017). Hillslope diffusion is the result of a combination of multiple near-surface processes: (i) rainsplash and sheet-flow creep driven by raindrop impact and overland flow (Guy et al., 1987; Meyer et al., 1975; Young and Wiersma, 1973), (ii) soil creep produced by cyclical wetting-drying, shrink–swell, and freeze–thaw strains (Anderson and Anderson, 2010), (iii) bioturbation by burrowing animals and tree throw that mix and move regolith (Gabet et al., 2003; Roering et al., 2010), and (iv) small shallow landslides that act diffusively when averaged over long timescales (Martin, 2000).

Climate controls the relative efficiency of these mechanisms. Mean annual precipitation and storm magnitudes regulate rainsplash fluxes and influence vegetation density, which in turn affects soil creep (Istanbulluoglu and Bras, 2006). Freeze–thaw frequency, governed by temperature and moisture, dictates the rate of frost creep and solifluction in high-altitude or high-latitude settings (Hales and Roering, 2007). Hillslope diffusion gradually transports soil and sediment downslope due to gravity and reshapes substantially the landscape over time (e.g., Litwin et al., 2025; Perron et al., 2008; Roering, 2008). It has been shown that hillslope diffusion strongly influences drainage density and valley spacing (Perron et al., 2008; Sweeney et al., 2015; Tucker and Bras, 1998). Additionally, the sediment and soil transported from hillslopes impact river incision by either acting as tools for erosion or forming a protective cover that shields the underlying bedrock from further erosion (Sklar and Dietrich, 2001).

While much research has focused on river channel evolution (e.g., Kirby and Whipple, 2012; Wobus et al., 2010), few have explored whether and how river channels respond differently to tectonic and climatic changes when hillslope diffusion is included. This knowledge gap exists in part because there is not yet a comprehensive theory describing how the hillslope diffusion coefficient changes with climate. Before addressing this issue, the following paragraph clarifies the notions of steady-state and transient landscapes.

1.2 Steady state vs. transient landscapes

Computer-generated landscapes evolving under controlled tectonic and climatic conditions provide a robust framework for better understanding the formation and evolution of natural landscapes (e.g., Chen et al., 2014; Pan et al., 2021; Salles and Hardiman, 2016; Schwanghart and Scherler, 2014). These models show that a landscape reaches a steady state when the uplift rate equals the erosion rate. When the uplift rate changes, landscapes are in a transient state of disequilibrium and evolve to reach a new steady state (e.g., Leonard and Whipple, 2021; Miller et al., 2012; O'Hara et al., 2019). Steady-state and transient landscapes show a sharp contrast in the morphology of river profiles. When a river channel has reached a steady state, its longitudinal elevation profile is usually smooth and concave-up (Fig. 1a). In contrast, under uniform lithology, knickpoints

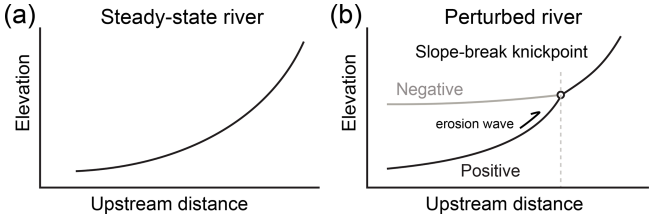

Figure 1. Channel profiles with different morphology. **(a)** A steady-state river profile. **(b)** Transient river profiles with a negative or positive slope-break knickpoint.

Table 1. Diffusion coefficient, erodibility, and initial Pe of four models.

Model	Diffusion coefficient k_{hl} ($m^2\,yr^{-1}$)	Erodibility k_d ($1\,yr^{-1}$)	Initial Pe (Rainfall = $2\,m\,yr^{-1}$)
M1	0	2.3×10^{-6}	∞ (no diffusion)
M2	1	2.3×10^{-6}	5204
M3	2	2.3×10^{-6}	2602
M4	2	4.6×10^{-6}	5204

form in transient river channels (Wobus et al., 2006b; Lague, 2014; Neely et al., 2017; Whipple et al., 2013). A knickpoint is a location where there is an abrupt change in the channel slope (Fig. 1b). A positive knickpoint forms where the slope suddenly increases downstream, while a negative knickpoint forms where the slope decreases abruptly. A mobile positive knickpoint indicates an increase in uplift rate and/or a decrease in erosion efficiency (induced by a decrease in rainfall rate, for example), while a mobile negative knickpoint indicates the opposite conditions (Baldwin et al., 2003). Both types of knickpoints typically form at the river mouth and migrate upstream toward the headwaters.

A migrating knickpoint separates the channel into two segments, upstream and downstream segments. It has been proposed that regardless of whether the transient change is driven by tectonics or climate, the elevation of the upstream segment changes while its slope remains constant (Whipple, 2001). After the downstream segment reaches a steady state, its channel elevation and slope have changed (e.g., Whipple, 2001; Whipple and Tucker, 1999).

2 Methodology and model setup

To investigate landscape evolution under climatic or tectonic changes, as well as varying erodibility and hillslope diffusion, we use the long-term surface evolution model Badlands (Basin and Landscape Dynamics) (Salles, 2016; Salles and Hardiman, 2016). Badlands can be used to simulate landscape development via the mobilisation of sediments through hillslope diffusion and stream-power incision. Our model assumes that hillslope sediment transport rates are linearly proportional to the slope gradient. Any material delivered to a channel cell from adjacent hillslopes increases the elevation of the cell. The river then erodes this new surface as if it were bedrock, without distinguishing it from the underlying substrate. Here, we explore landscape responses to changes in rainfall or uplift, and we disregard isostatic re-adjustment. In particular, we focus on contrasts in average elevation, surface roughness, and river profiles.

Our initial landscape models are mapped over a $40\,km \times 80\,km$ grid with a uniform initial elevation of 10 m and a spatial resolution of $400\,m \times 400\,m$. We acknowledge that our 400 m grid spacing is larger than hillslope lengths in many natural landscapes. However, a sensitivity test at a finer 200 m resolution confirmed that our primary findings are robust and not an artifact of the chosen grid size (Figs. S1 and S2 in the Supplement). We design four initial models with varying hillslope diffusion and erodibility coefficients (Table 1). The diffusion coefficient is set to 0 in model M1, meaning the landscape evolution is purely driven by riverine processes with an erodibility coefficient of $2.3 \times 10^{-6}\,yr^{-1}$. We set the diffusion coefficient to $1\,m^2\,yr^{-1}$ in model M2 and $2\,m^2\,yr^{-1}$ in model M3. Finally, in our last model M4, the erodibility is doubled to $4.6 \times 10^{-6}\,yr^{-1}$. In all cases, the stream-power law uses $m = 0.5$ and $n = 1.0$.

For each model, we compute the dimensionless parameter Pe to combine two a priori independent parameters (the diffusion coefficient k_{hl} and the erodibility k_d) into a single dimensionless measure of process competition (Bonetti et al., 2020; Perron et al., 2008; Perron et al., 2009):

$$\mathrm{Pe} = \frac{k_d P^m l^{2m+1}}{k_{hl}} \tag{4}$$

Pe is analogous to a Péclet number, which is the ratio of a diffusion timescale to an advection timescale (Perron et al., 2008). Low Pe values indicate diffusion-dominated systems, while high values indicate advection-dominated systems. We take the characteristic horizontal length scale l to be 40 km, representative of the real landscape. Based on our parameter values, model M3 has the lowest Pe, indicating that diffusion is more dominant in this model than in the others. Furthermore, models M2 and M4 share the same Pe because their parameters for k_{hl} and k_d are both doubled in M4 relative to M2, keeping their ratio constant.

Our four models are submitted to a combination of uniform uplift at a rate of $300\,m\,Myr^{-1}$ and background rainfall at a rate of $2\,m\,yr^{-1}$ until they reach a steady-state equilibrium, where mean elevation and river profiles no longer change (Montgomery, 2001; Willett and Brandon, 2002). This first stage lasts for 25 Myr (Fig. 2), after which all models reach a steady state.

In the second stage, which also lasts 25 Myr, each model is subjected to a perturbation while the other forcing remains constant. We either:

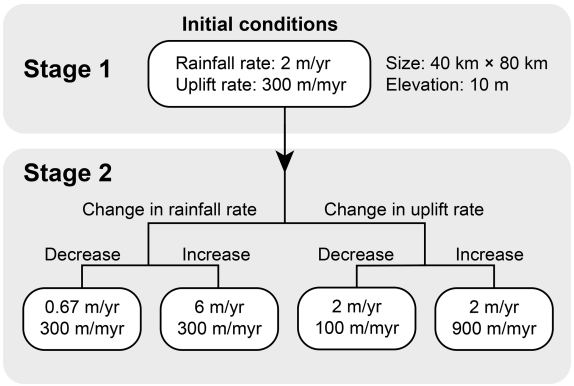

Figure 2. Each of our four initial models (M1 to M4) experiences four different two-stage landscape evolutions controlled by changes in rainfall or uplift. Stage 1: An initial flat landscape is uplifted under an uplift rate of $300\,\mathrm{m\,Myr^{-1}}$ and a rainfall rate of $2\,\mathrm{m\,yr^{-1}}$ until a steady-state landscape is reached. Stage 2: Changes in rainfall or uplift rate.

Table 2. Pe for Stage 2 rainfall-change scenarios.

Model	Pe (Rainfall = $0.67\,\mathrm{m\,yr^{-1}}$)	Pe (Rainfall = $6\,\mathrm{m\,yr^{-1}}$)
M2	3004	9014
M3	1502	4507
M4	3004	9014

- Increase rainfall to $6\,\mathrm{m\,yr^{-1}}$ or decrease it to $0.67\,\mathrm{m\,yr^{-1}}$, while keeping uplift fixed at $300\,\mathrm{m\,Myr^{-1}}$, or
- Increase uplift to $900\,\mathrm{m\,Myr^{-1}}$ or decrease it to $100\,\mathrm{m\,Myr^{-1}}$, while keeping rainfall fixed at $2\,\mathrm{m\,yr^{-1}}$.

This design yields 16 individual experiments (Fig. 2), allowing us to assess landscape responses to changes in rainfall and uplift rates separately. A key consequence of our experimental design is that a change in rainfall rate directly changes the advection timescale associated with river incision. Thus, this changes Pe and alters the fundamental balance between advective and diffusive processes, as shown in Stage 2 (Table 2).

3 Results

3.1 Comparison of final, steady-state landscapes

To quantitatively compare landscape responses across our experiments, we compute two metrics: mean landscape elevation and surface roughness. Mean landscape elevation serves as an integrated measure of the overall erosional state of the landscape, reflecting the cumulative effect of tectonic uplift, channel incision, and hillslope processes on topographic development. Surface roughness quantifies the local topographic variability resulting from the competing effects of processes that create and destroy relief (Doane et al., 2024). We calculate roughness as the difference between the maximum and minimum elevation values within a defined neighborhood surrounding each central pixel using the "roughness" algorithm of GDAL in QGIS (Wilson et al., 2007).

Our results show that the mean landscape elevation and surface roughness increase following a decrease in rainfall rate or an increase in uplift rate, and decrease following an increase in rainfall rate or a decrease in uplift rate. Regardless of rainfall or uplift changes, the absence of hillslope diffusion in M1 ($k_{\mathrm{hl}} = 0$) leads to the largest surface roughness (Fig. 3a). When hillslope diffusion is included, the landscapes in models M2, M3, and M4 are smoother than those in model M1 (Fig. 3b–d). For models M2 and M4, doubling both the diffusion and erosion coefficients reduces both the mean elevation and the mean surface roughness by a factor of ~ 2. For models M2 and M3, doubling only the diffusion coefficient reduces the surface roughness by $\sim 15\%$ and increases the mean elevation by $\sim 20\%$. For models M3 and M4, doubling the erosion coefficient alone reduces the mean elevation by a factor of more than 2.

Stronger diffusion smooths local slopes but also increases the flux of material into valleys. In our detachment-limited model, any material added to the channel from hillslopes is treated as bedrock, meaning the river must incise through it with the same efficiency as the underlying rock. To maintain equilibrium with a constant uplift rate, the river must therefore steepen to gain the power needed to erode both the uplifted bedrock and the additional material load (Litwin et al., 2025). This behavior represents an amplification of the channel gradient response, as the channel must become steeper than if the hillslope material were treated as easily erodible sediment. As stronger diffusion widens valley spacing and forces channels to steepen, the total relief and mean elevation of landscapes increase.

3.2 Impact on river channel response

To explore channel responses to changes in rainfall or uplift rates under various ratios of hillslope diffusion to erodibility, we analyze the trunk stream of the western basin, including the evolution of erosion and deposition, as well as the evolution of the longitudinal channel profile. Although we present results only from the western basin, we have verified that both drainage basins exhibit similar evolutions.

3.2.1 Null-case control (Model M1, $k_{\mathrm{hl}} = 0$)

To isolate the impact of hillslope diffusion, we first present the results from model M1, which has a diffusion coefficient of zero and serves as our null case (Fig. 4). This model il-

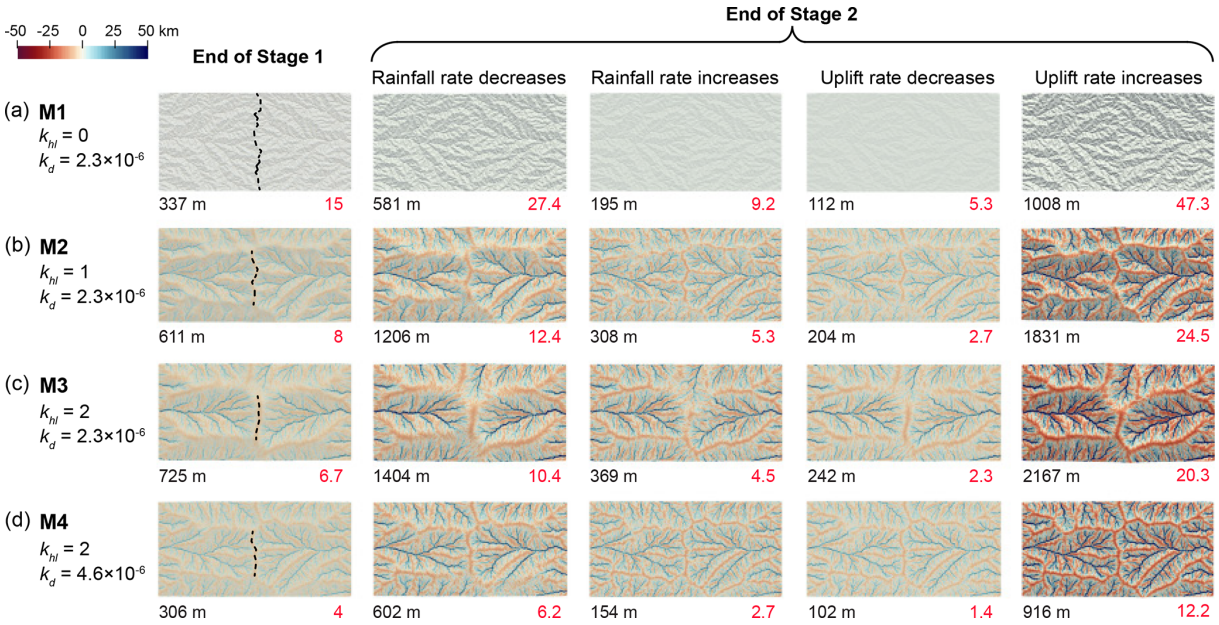

Figure 3. Hillshade maps showing cumulative erosion and deposition resulting from hillslope diffusion at the end of Stage 1 and the end of Stage 2 for models M1 **(a)**, M2 **(b)**, M3 **(c)**, and M4 **(d)**. Each model differs in hillslope diffusion coefficients (k_{hl}) and erodibility values (k_d). Blue areas indicate deposition, while red areas represent erosion. Color bar values indicate cumulative depositional (positive) and erosional (negative) amounts (km). Numbers below each map display the mean elevation (black) and roughness (red). Dashed lines on maps at the end of Stage 1 denote the divides. The divides in Stage 2 are similar to those in Stage 1 and are not marked in this stage.

lustrates the baseline landscape response when driven purely by riverine processes, showing the development of a standard migrating knickpoint. By establishing this null case, we can then clearly distinguish the critical role of hillslope diffusion in landscape evolution in models M2, M3, and M4.

In the absence of hillslope diffusion, when the rainfall rate decreases or the uplift rate increases, the trunk stream rises gradually, and the slope increases from the river mouth. A positive knickpoint and an erosion wave develop at the river mouth and migrate upstream (Fig. 4a and d). The downstream channel reaches a steady state first, with no further changes in elevation or slope. Conversely, when the rainfall rate increases or the uplift rate decreases, the channel's elevation and slope decrease. A negative knickpoint and an erosion wave develop at the river mouth and migrate upstream (Fig. 4b and c). Once the erosion wave reaches the headwaters, the knickpoint disappears, and the entire channel returns to a new steady state. Notably, within 1–2 Myr of the change in rainfall or uplift rates, the channel elevation at the headwaters changes, but the slope remains nearly constant (Figs. 5a1–a3 and 6a1–a3). As the erosion wave approaches the headwaters, the channel slope increases or decreases monotonically and eventually stabilizes.

3.2.2 Diffusion-enabled models (M2–M4)

In contrast, when hillslope diffusion is present (models M2, M3, and M4), we observe major differences in the evolution of headwater channel slope following changes in uplift and rainfall rates. An increase in uplift rate leads to a monotonic slope increase in the headwaters (Fig. 5b1–b3, c1–c3, and d1–d3). In contrast, a decrease in rainfall rate triggers a "transient slope change reversal", a phenomenon we define as a non-monotonic adjustment where the headwater channel slope initially changes in the opposite direction of its final steady state. This is observed as a transient slope decrease followed by a subsequent, long-term increase (Fig. 6b1–b3, c1–c3, and d1–d3). The opposite pattern occurs when the rainfall rate increases: a temporary slope increase is followed by a decrease. We do not find a distinct threshold for the initiation of the transient slope change reversal; rather, it is present whenever hillslope diffusion is active (Pe $< \infty$). The primary control on the reversal is its magnitude and persistence, which vary continuously with Pe. Our results show that landscapes with lower Pe values, where hillslope diffusion is more dominant relative to channel incision, exhibit more pronounced and persistent reversals. For example, model M3, which has the lowest Pe, shows a reversal that persists longer and extends over a longer channel segment compared to other models (Fig. 6c1–c3). Although models M2 and M4 share the same Pe value, the larger k_{hl} and k_d values of model M4 halve both the diffusion and advection timescales relative to model M2. Consequently, the transient slope change reversal persists longer in model M2 in time, even though the non-dimensional dynamics are identical (Fig. 6b3 and d3).

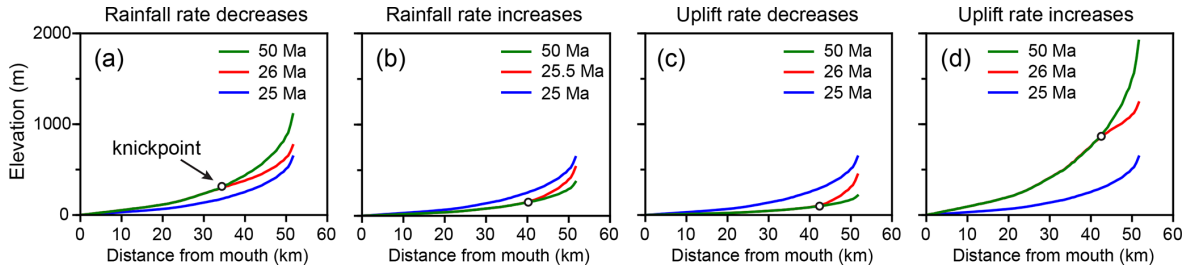

Figure 4. Longitudinal profiles of the trunk stream after changes in rainfall or uplift rates in model M1 (no hillslope diffusion). The changes occur at 25 Ma, affecting the steady state trunk stream in blue.

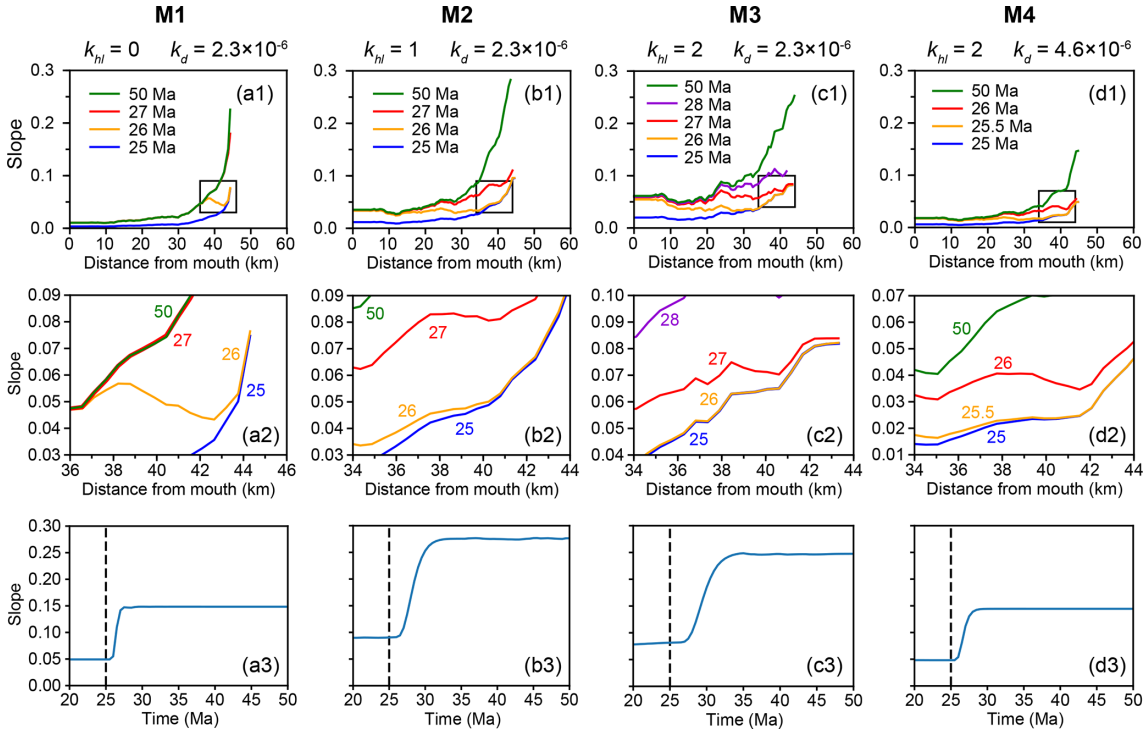

Figure 5. Evolution of trunk stream slope following an increase in uplift rate. **(a1–d1)** Longitudinal slope profiles of the trunk stream at selected time steps (colored lines), with each subplot corresponding to a model (M1–M4). Black rectangles indicate the headwater regions. **(a2–d2)** Enlarged views of the headwater areas, corresponding to the boxed regions in panels **(a1)**–**(d1)**. **(a3–d3)** Temporal evolution of the mean channel slope in the upper ∼ 800 m of the trunk stream, capturing the dynamic slope response across model runs. Dashed vertical lines mark the timing of the uplift rate increase (25 Ma).

4 Discussion

4.1 Mechanism of transient slope change reversal

To better understand the cause of the transient slope change reversal, we calculate the erosion rate for each grid cell 1 Myr after the disturbance and extract the erosion rate along the trunk stream for all models (Fig. 7). The transient slope change reversal is driven by differential erosion rates between the divide and adjacent areas.

In model M1, the erosion rates of the divide and its adjacent areas remain homogeneous following changes in rainfall and uplift rates (Fig. 7a3). Similarly, in models M2, M3, and M4, an increase or decrease in uplift rate results in consistent erosion rates between the divide and adjacent areas (red and orange profiles in Fig. 7b3, c3, and d3). The surface uplift rate is defined as the difference between the uplift and erosion rates. Given the spatial uniformity of uplift rates, equal erosion rates at the divide and its adjacent areas result in identical surface uplift rates, preventing transient slope change reversals (black and red profiles in Fig. 8).

In contrast, following a decrease in rainfall rate in models M2, M3, and M4, the erosion rate of the divide exceeds that of adjacent downstream areas (green profiles in Fig. 7b3, c3, and d3). This difference in erosion rate directly causes the

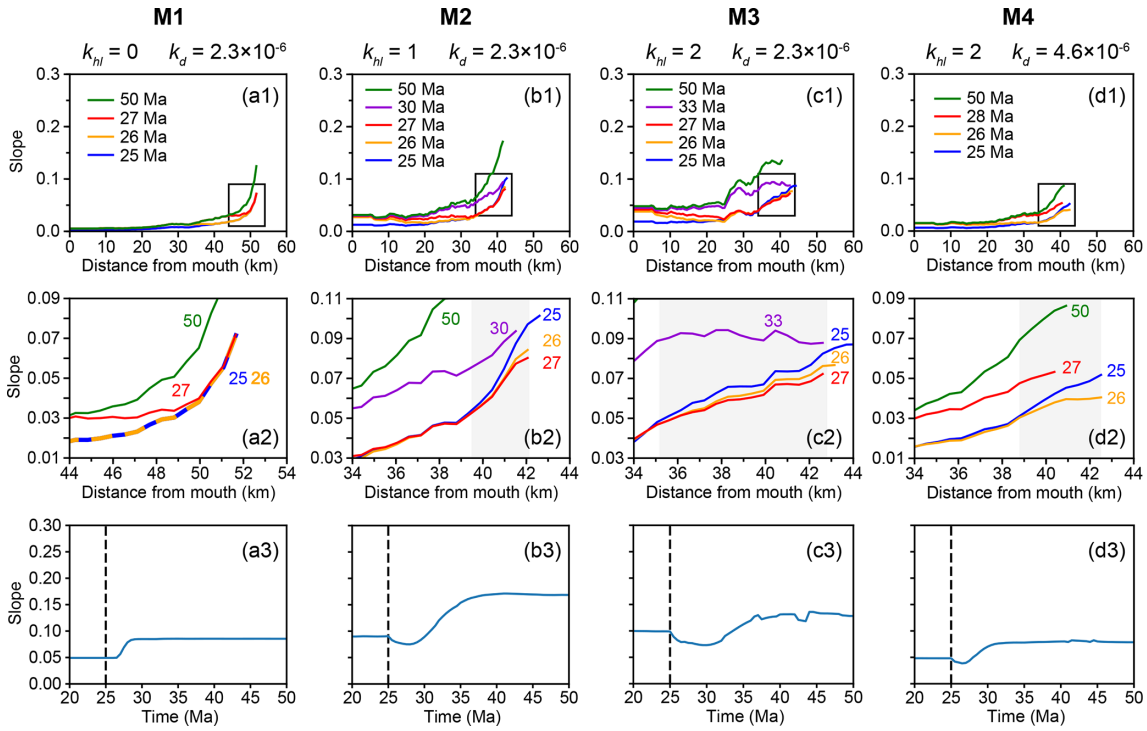

Figure 6. Evolution of trunk stream slope following a decrease in rainfall rate. **(a1–d1)** Longitudinal slope profiles of the trunk stream at selected time steps (colored lines), with each subplot corresponding to a model (M1–M4). Black rectangles indicate the headwater regions. **(a2–d2)** Enlarged views of the headwater areas, corresponding to the boxed regions in panels **(a1)**–**(d1)**. Grey bands indicate the regions where the transient slope change reversal occurs. **(a3–d3)** Temporal evolution of the mean channel slope in the upper ∼ 800 m of the trunk stream, capturing the dynamic slope response across model runs. Dashed vertical lines mark the timing of the rainfall rate decrease (25 Ma).

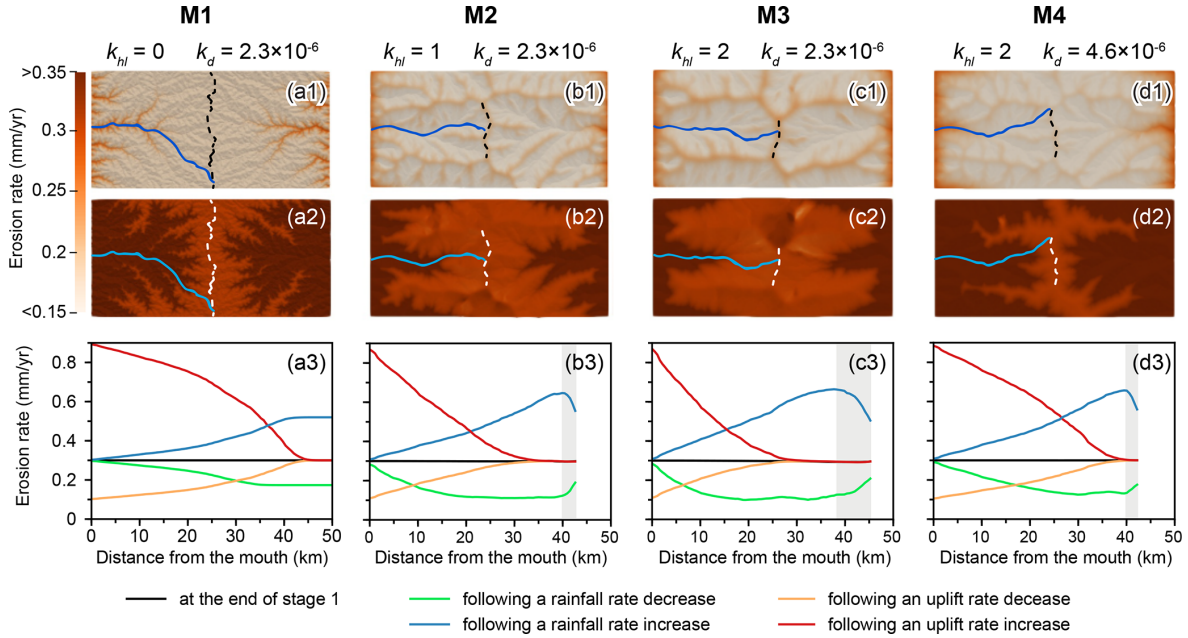

Figure 7. Erosion rates (mm yr^{-1}) per grid cell, calculated over 1 Myr following **(a1–d1)** a decrease in rainfall rate and **(a2–d2)** an increase in uplift rate. Blue lines in panels **(a1)**–**(d1)** and **(a2)**–**(d2)** represent trunk streams, and dashed lines mark divides. **(a3–d3)** Longitudinal erosion profiles along trunk streams, with grey bands indicating the regions where the transient slope change reversal occurs.

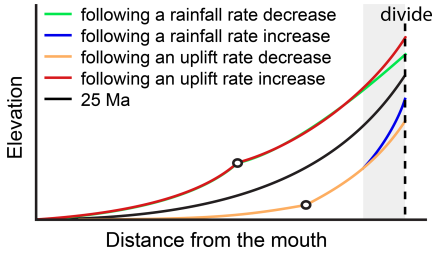

Figure 8. Schematic diagram of the longitudinal profile of the channel in a steady state (black line) or a transient state after changes in rainfall or uplift rate. The grey band indicates the region where the transient slope change reversal occurs.

surface uplift rate of the divide to be lower than that of adjacent downstream areas, resulting in a temporary decrease in the channel slope at the divide and, therefore, triggering a transient slope change reversal (green profile in Fig. 8). Conversely, following an increase in rainfall rate, the erosion rate of the divide is lower than in adjacent areas (blue profiles in Fig. 7b3, c3, and d3), causing a temporary slope increase at the divide and again triggering a transient slope change reversal (blue profile in Fig. 8). These findings suggest that rainfall changes distinctly influence divide erosion patterns, with spatial contrasts in erosion rate playing a key role in driving transient slope responses.

The transient slope change reversal is driven by a disequilibrium between the hillslope diffusion timescale and the channel advection (incision) timescale. Pe quantifies the ratio of these two timescales. Following a change in rainfall rate, the advection timescale, which is inversely related to incision efficiency, adjusts almost instantaneously. In contrast, the diffusion timescale, governed by topography, does not (Clubb et al., 2019). This abrupt shift in their ratio (i.e., the change in Pe) creates a lag and drives the transient behavior at the headwaters. For instance, following a decrease in rainfall rate, the advection timescale lengthens (river incision becomes less efficient) due to lower discharge (Mitchell, 2020; Montgomery et al., 2000). However, sediment continues to diffuse from divides to channels at a rate set by the pre-existing topography (i.e., the diffusion timescale is initially unchanged). This imbalance causes the rate of sediment supply from hillslopes at the headwaters to exceed the rate of sediment removal by rivers, reducing the channel slope temporarily and causing a transient slope change reversal. As the channel adjusts and the erosion wave migrates upstream, this reversal gradually disappears.

In contrast, a change in uplift rate uniformly raises the entire landscape without immediately affecting the efficiency of diffusion and incision. Because both the divide and its adjacent areas experience similar erosion conditions under constant discharge, no transient slope reversal occurs.

Notably, a lower Pe value amplifies the imbalance between sediment supply from hillslopes and removal by rivers. This enlarges the zone where divide erosion rates differ from downstream areas. Therefore, the transient slope change reversal persists over a longer channel segment and for a longer duration, as observed in model M3 (Fig. 6c2 and c3). In contrast, increasing Pe enhances river incision, which reduces the relative influence of diffusion. This leads to a shorter channel segment experiencing transient slope change reversal and a shorter duration of the transient response in model M4 (Fig. 6d2 and d3).

In summary, the transient slope change reversal results from the competition between incision and diffusion following a change in rainfall. This reversal disappears as the erosion wave gradually approaches the divide area, and the landscape returns to a steady state where the erosion rate is spatially uniform.

4.2 Field and analytical approaches for detecting transient reversals

Transient slope change reversals could be identified using slope-area analysis or χ analysis. Both methods rely on the stream power model, which describes the relationship between channel slope and drainage area as a power function (Flint, 1974). For a river channel in a steady state, plotting log slope against log area yields a straight line. However, in cases of transient slope change reversals, this relationship may deviate from linearity. While slope-area analysis can be sensitive to data noise (e.g., DEM inaccuracies), χ analysis reduces this influence through an integral approach (Royden and Taylor Perron, 2013; Perron and Royden, 2013). For steady-state rivers, χ should also correlate linearly with elevation, whereas nonlinear χ-elevation relationships may indicate transient slope change reversals. In our models, a decrease in rainfall rate produces a localized flattening at high χ (headwaters), directly reflecting the transient slope-change reversal (Fig. 9). By contrast, in uplift-driven transients the χ-elevation profile bows downward at low χ, while the high-χ (headwater) segment remains straight and is simply translated upward. However, χ-elevation analysis has limitations: it requires a steady-state baseline profile to distinguish different types of disturbances. Therefore, χ-elevation is best used in concert with additional information, such as independent erosion-rate measurements, to robustly identify and attribute transient slope-change reversals.

Transient slope change reversals could also be identified by investigating the erosion rate. One approach to quantify erosion rates is using cosmogenic nuclides, particularly radionuclides like ^{10}Be and ^{26}Al (e.g., Balco et al., 2008; Gosse and Phillips, 2001; Lal, 1991; Muzikar, 2009). These nuclides are produced in surface minerals by cosmic ray interactions, with production rates decreasing exponentially with depth due to cosmic ray attenuation (Dunai, 2010; Lal, 1991). Cosmogenic nuclide concentrations increase as a surface remains exposed to cosmic rays (Ivy-Ochs and Kober, 2008). In contrast, in rapidly eroding areas, nuclide concen-

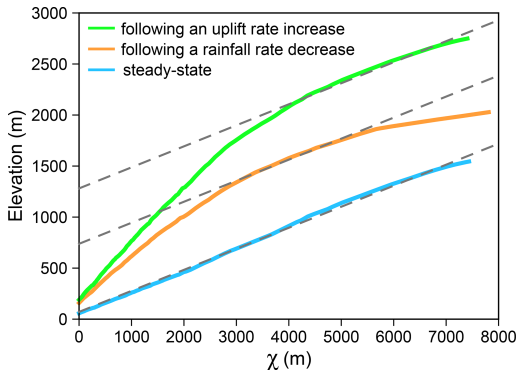

Figure 9. χ-elevation profiles of trunk streams in model M3 under three conditions: following an uplift rate increase (green), following a rainfall rate decrease (orange), and steady-state (light blue). The three grey dashed lines are parallel reference trends. χ-elevation profiles are calculated using a reference concavity index (θ_{ref}) of 0.4.

trations remain low due to the continuous removal of surface materials.

By mapping nuclide concentrations, spatial patterns in erosion rates could be linked to rainfall or uplift changes. For instance, if the erosion rate is relatively uniform around the divide area, it may suggest a transient response driven by tectonic events. Conversely, if nuclide data indicate that erosion rates are larger at the divide relative to downstream areas, then recent drainage reorganization may be related to a decrease in rainfall rate. Thus, cosmogenic nuclide measurements provide a valuable tool to distinguish between climatic and tectonic drivers of landscape change.

4.3 Model limitations

In this study, we aim to explore the first-order impact of hillslope diffusion and river incision on landscape and consider a landscape evolving under the action of hillslope diffusion and river incision only. While the linear diffusion model is a common starting point, we acknowledge that it does not capture nonlinear processes, such as those driven by shallow landslides, which can become significant on steeper slopes (e.g., Jiménez-Hornero et al., 2005; Martin, 2000; Roering et al., 1999). Furthermore, our model does not account for potential feedback between climate and the diffusion coefficient itself. In natural settings, the hillslope diffusion coefficient can vary with climatic conditions via processes such as frost-crack weathering, and near-surface processes such as soil saturation, and root growth (Braun, 2018; Perron, 2017; Bogaard and Greco, 2015; Andersen et al., 2015; Gabet and Mudd, 2010; Gabet, 2000). Considering this feedback could introduce additional complexity. For instance, an increase in rainfall rate could increase the hillslope diffusion coefficient through higher soil moisture (Perron, 2017), potentially amplifying the transient slope change reversal. Conversely, a decrease in rainfall rate could decrease the hillslope diffusion coefficient and dampen the reversal. Future work could explore the parameter space where these feedbacks become significant.

In addition, our use of a detachment-limited stream power model simplifies the complexities of sediment flux. The "transient slope change reversal" we observe is fundamentally a result of a disequilibrium between hillslope sediment supply and the channel's transport capacity following a change in rainfall. A more complex model incorporating sediment transport dynamics (a "transport-limited" or "mixed" model) would likely modulate the magnitude and duration of this reversal.

5 Conclusion

Changes in rainfall and uplift rates induce different responses in the channel slope at the headwaters, with hillslope diffusion playing a crucial role in mediating these processes. When the rainfall rate changes, hillslope diffusion interacts with river incision to generate transient spatial variations in erosion around the divide area, leading to transient slope change reversals at the headwaters. In contrast, changes in uplift rates result in spatially uniform erosion across the divide area, preventing such reversals. Identifying these reversals from river profiles or erosion rate estimates at different locations could help determine the driving force behind landscape adjustments. A high hillslope diffusion coefficient increases both the duration and spatial extent of these reversals along the river profile. In contrast, higher erodibility enhances river incision and diminishes the role of diffusion, reducing these reversal effects.

Our findings provide new insights into how rainfall and tectonic forcing reshape landscapes over time. By investigating the interaction between diffusion and incision, we show that the transient variations in channel profiles, particularly near the divide, provide potential markers for interpreting past landscape evolution and deciphering the complex interplay between tectonic uplift and climatic variability.

Code and data availability. Version 2.2.0 of Badlands used for the landscape and sedimentary evolution modeling is preserved at https://doi.org/10.5281/zenodo.1069573 (Salles and Howson, 2017), available via GNU General Public License v3.0 and developed openly at https://github.com/badlands-model/badlands (last access: 20 September 2025).

Supplement. The supplement related to this article is available online at https://doi.org/10.5194/esurf-13-1249-2025-supplement.

Author contributions. YZ designed and ran the simulations, analyzed the results, and wrote the manuscript. PR contributed to the

result analysis and manuscript revision. TS developed the model code and contributed to the manuscript revision.

Competing interests. The contact author has declared that none of the authors has any competing interests.

Disclaimer. Publisher's note: Copernicus Publications remains neutral with regard to jurisdictional claims made in the text, published maps, institutional affiliations, or any other geographical representation in this paper. While Copernicus Publications makes every effort to include appropriate place names, the final responsibility lies with the authors. Views expressed in the text are those of the authors and do not necessarily reflect the views of the publisher.

Acknowledgements. We thank the three anonymous reviewers and the associate editor Simon Mudd for their constructive comments and suggestions, which helped to improve this manuscript.

Financial support. This research has been supported by the China Scholarship Council (grant no. 202006400009) and the University of Sydney (Top-up PhD scholarship).

Review statement. This paper was edited by Simon Mudd and reviewed by three anonymous referees.

References

Ahnert, F.: Approaches to dynamic equilibrium in theoretical simulations of slope development, Earth Surface Processes and Landforms, 12, 3–15, https://doi.org/10.1002/esp.3290120103, 1987.

Allen, P. A.: Time scales of tectonic landscapes and their sediment routing systems, Geological Society, London, Special Publications, 296, 7–28, https://doi.org/10.1144/sp296.2, 2008.

Andersen, J. L., Egholm, D. L., Knudsen, M. F., Jansen, J. D., and Nielsen, S. B.: The periglacial engine of mountain erosion – Part 1: Rates of frost cracking and frost creep, Earth Surf. Dynam., 3, 447–462, https://doi.org/10.5194/esurf-3-447-2015, 2015.

Anderson, R. S. and Anderson, S. P.: Geomorphology: the mechanics and chemistry of landscapes, Cambridge University Press, https://doi.org/10.1017/CBO9780511794827, 2010.

Armstrong, A. C.: Slopes, boundary conditions, and the development of convexo-concave forms – some numerical experiments, Earth Surface Processes and Landforms, 12, 17–30, https://doi.org/10.1002/esp.3290120104, 1987.

Balco, G., Stone, J. O., Lifton, N. A., and Dunai, T. J.: A complete and easily accessible means of calculating surface exposure ages or erosion rates from 10Be and 26Al measurements, Quaternary Geochronology, 3, 174–195, https://doi.org/10.1016/j.quageo.2007.12.001, 2008.

Baldwin, J. A., Whipple, K. X., and Tucker, G. E.: Implications of the shear stress river incision model for the timescale of postorogenic decay of topography, Journal of Geophysical Research: Solid Earth, 108, https://doi.org/10.1029/2001jb000550, 2003.

Bogaard, T. A. and Greco, R.: Landslide hydrology: from hydrology to pore pressure, WIREs Water, 3, 439–459, https://doi.org/10.1002/wat2.1126, 2015.

Bonetti, S., Hooshyar, M., Camporeale, C., and Porporato, A.: Channelization cascade in landscape evolution, Proceedings of the National Academy of Sciences, 117, 1375–1382, https://doi.org/10.1073/pnas.1911817117, 2020.

Bonnet, S. and Crave, A.: Landscape response to climate change: Insights from experimental modeling and implications for tectonic versus climatic uplift of topography, Geology, 31, 123, https://doi.org/10.1130/0091-7613(2003)031<0123:lrtcci>2.0.co;2, 2003.

Braun, J.: A review of numerical modeling studies of passive margin escarpments leading to a new analytical expression for the rate of escarpment migration velocity, Gondwana Research, 53, 209–224, https://doi.org/10.1016/j.gr.2017.04.012, 2018.

Chen, A., Darbon, J., and Morel, J.-M.: Landscape evolution models: A review of their fundamental equations, Geomorphology, 219, 68–86, https://doi.org/10.1016/j.geomorph.2014.04.037, 2014.

Clubb, F. J., Mudd, S. M., Hurst, M. D., and Grieve, S. W. D.: Differences in channel and hillslope geometry record a migrating uplift wave at the Mendocino triple junction, California, USA, Geology, 48, 184–188, https://doi.org/10.1130/g46939.1, 2019.

Culling, W. E. H.: Analytical Theory of Erosion, The Journal of Geology, 68, 336–344, https://doi.org/10.1086/626663, 1960.

Culling, W. E. H.: Soil Creep and the Development of Hillside Slopes, The Journal of Geology, 71, 127–161, https://doi.org/10.1086/626891, 1963.

D'Arcy, M. and Whittaker, A. C.: Geomorphic constraints on landscape sensitivity to climate in tectonically active areas, Geomorphology, 204, 366–381, https://doi.org/10.1016/j.geomorph.2013.08.019, 2014.

DiBiase, R. A. and Whipple, K. X.: The influence of erosion thresholds and runoff variability on the relationships among topography, climate, and erosion rate, Journal of Geophysical Research, 116, https://doi.org/10.1029/2011jf002095, 2011.

Dietrich, W. E. and Perron, J. T.: The search for a topographic signature of life, Nature, 439, 411–418, https://doi.org/10.1038/nature04452, 2006.

Dietrich, W. E., Bellugi, D. G., Sklar, L. S., Stock, J. D., Heimsath, A. M., and Roering, J. J.: Geomorphic Transport Laws for Predicting Landscape form and Dynamics, in: Prediction in Geomorphology, 103–132, https://doi.org/10.1029/135GM09, 2003.

Doane, T. H., Gearon, J. H., Martin, H. K., Yanites, B. J., and Edmonds, D. A.: Topographic Roughness as an Emergent Property of Geomorphic Processes and Events, AGU Advances, 5, https://doi.org/10.1029/2024av001264, 2024.

Dunai, T. J.: Cosmogenic nuclides: principles, concepts and applications in the earth surface sciences, Cambridge University Press, https://doi.org/10.1017/CBO9780511804519, 2010.

Fernandes, N. F. and Dietrich, W. E.: Hillslope evolution by diffusive processes: The timescale for equilibrium adjustments, Water Resources Research, 33, 1307–1318, https://doi.org/10.1029/97wr00534, 1997.

Flint, J.-J.: Stream gradient as a function of order, magnitude, and discharge, Water Resources Research, 10, 969–973, https://doi.org/10.1029/WR010i005p00969, 1974.

Gabet, E. J.: Gopher bioturbation: field evidence for non-linear hillslope diffusion, Earth Surface Processes and Landforms, 25, 1419–1428, 2000.

Gabet, E. J. and Mudd, S. M.: Bedrock erosion by root fracture and tree throw: A coupled biogeomorphic model to explore the humped soil production function and the persistence of hillslope soils, Journal of Geophysical Research: Earth Surface, 115, https://doi.org/10.1029/2009jf001526, 2010.

Gabet, E. J., Reichman, O. J., and Seabloom, E. W.: The Effects of Bioturbation on Soil Processes and Sediment Transport, Annual Review of Earth and Planetary Sciences, 31, 249–273, https://doi.org/10.1146/annurev.earth.31.100901.141314, 2003.

Gosse, J. C. and Phillips, F. M.: Terrestrial in situ cosmogenic nuclides: theory and application, Quaternary Science Reviews, 20, 1475–1560, https://doi.org/10.1016/s0277-3791(00)00171-2, 2001.

Guy, B., Dickinson, W., and Rudra, R.: The roles of rainfall and runoff in the sediment transport capacity of interrill flow, Transactions of the ASAE, 30, 1378–1386, 1987.

Hales, T. C. and Roering, J. J.: Climatic controls on frost cracking and implications for the evolution of bedrock landscapes, Journal of Geophysical Research: Earth Surface, 112, https://doi.org/10.1029/2006jf000616, 2007.

Howard, A. D. and Kerby, G.: Channel changes in badlands, Geological Society of America Bulletin, 94, 739–752, https://doi.org/10.1130/0016-7606(1983)94<739:CCIB>2.0.CO;2, 1983.

Hurst, M. D., Mudd, S. M., Attal, M., and Hilley, G.: Hillslopes record the growth and decay of landscapes, Science, 341, 868–871, https://doi.org/10.1126/science.1241791, 2013.

Istanbulluoglu, E. and Bras, R. L.: On the dynamics of soil moisture, vegetation, and erosion: Implications of climate variability and change, Water Resources Research, 42, https://doi.org/10.1029/2005wr004113, 2006.

Ivy-Ochs, S. and Kober, F.: Surface exposure dating with cosmogenic nuclides, E&G Quaternary Sci. J., 57, 179–209, https://doi.org/10.3285/eg.57.1-2.7, 2008.

Jiménez-Hornero, F. J., Laguna, A., and Giráldez, J. V.: Evaluation of linear and nonlinear sediment transport equations using hillslope morphology, Catena, 64, 272–280, https://doi.org/10.1016/j.catena.2005.09.001, 2005.

Kirby, E. and Whipple, K. X.: Expression of active tectonics in erosional landscapes, Journal of Structural Geology, 44, 54–75, https://doi.org/10.1016/j.jsg.2012.07.009, 2012.

Lague, D.: The stream power river incision model: evidence, theory and beyond, Earth Surface Processes and Landforms, 39, 38–61, https://doi.org/10.1002/esp.3462, 2014.

Lal, D.: Cosmic ray labeling of erosion surfaces: in situ nuclide production rates and erosion models, Earth and Planetary Science Letters, 104, 424–439, https://doi.org/10.1016/0012-821x(91)90220-c, 1991.

Leonard, J. S. and Whipple, K. X.: Influence of Spatial Rainfall Gradients on River Longitudinal Profiles and the Topographic Expression of Spatially and Temporally Variable Climates in Mountain Landscapes, Journal of Geophysical Research: Earth Surface, 126, https://doi.org/10.1029/2021jf006183, 2021.

Litwin, D. G., Malatesta, L. C., and Sklar, L. S.: Hillslope diffusion and channel steepness in landscape evolution models, Earth Surf. Dynam., 13, 277–293, https://doi.org/10.5194/esurf-13-277-2025, 2025.

Mao, Y., Li, Y., Yan, B., Wang, X., Jia, D., and Chen, Y.: Response of Surface Erosion to Crustal Shortening and its Influence on Tectonic Evolution in Fold-and-Thrust Belts: Implications From Sandbox Modeling on Tectonic Geomorphology, Tectonics, 40, https://doi.org/10.1029/2020tc006515, 2021.

Martin, Y.: Modelling hillslope evolution: linear and non-linear transport relations, Geomorphology, 34, 1–21, https://doi.org/10.1016/s0169-555x(99)00127-0, 2000.

Martinsen, O. J., Sømme, T. O., Thurmond, J. B., Helland-Hansen, W., and Lunt, I.: Source-to-sink systems on passive margins: theory and practice with an example from the Norwegian continental margin, Geological Society, London, Petroleum Geology Conference Series, 7, 913–920, https://doi.org/10.1144/0070913, 2022.

Meira Neto, A. A., Niu, G.-Y., Roy, T., Tyler, S., and Troch, P. A.: Interactions between snow cover and evaporation lead to higher sensitivity of streamflow to temperature, Communications Earth & Environment, 1, https://doi.org/10.1038/s43247-020-00056-9, 2020.

Meyer, L. D., Foster, G. R., and Römkens, M. J. M.: Source of soil eroded by water from upland slopes, in: Present and prospective technology for predicting sediment yields and sources, USDA-ARS, U.S. Gov. Print. Office, Washington, DC, 177–189, 1975.

Miller, S. R., Baldwin, S. L., and Fitzgerald, P. G.: Transient fluvial incision and active surface uplift in the Woodlark Rift of eastern Papua New Guinea, Lithosphere, 4, 131–149, https://doi.org/10.1130/l135.1, 2012.

Mitchell, S. B.: Sediment transport and Marine Protected Areas, in: Marine Protected Areas, 587–598, https://doi.org/10.1016/b978-0-08-102698-4.00030-7, 2020.

Molin, P., Sembroni, A., Ballato, P., and Faccenna, C.: The uplift of an early stage collisional plateau unraveled by fluvial network analysis and river longitudinal profile inversion: The case of the Eastern Anatolian Plateau, Tectonics, 42, e2022TC007737, https://doi.org/10.1029/2022tc007737, 2023.

Montgomery, D. R.: Slope Distributions, Threshold Hillslopes, and Steady-state Topography, American Journal of Science, 301, 432–454, https://doi.org/10.2475/ajs.301.4-5.432, 2001.

Montgomery, D. R., Zabowski, D., Ugolini, F. C., Hallberg, R. O., and Spaltenstein, H.: 8 – Soils, Watershed Processes, and Marine Sediments, in: International Geophysics, edited by: Jacobson, M. C., Charlson, R. J., Rodhe, H., and Orians, G. H., Academic Press, 159–iv, https://doi.org/10.1016/S0074-6142(00)80114-X, 2000.

Muzikar, P.: Inferring exposure ages and erosion rates from cosmogenic nuclides: A probabilistic formulation, Quaternary Geochronology, 4, 124–129, https://doi.org/10.1016/j.quageo.2008.11.005, 2009.

Neely, A. B., Bookhagen, B., and Burbank, D. W.: An automated knickzone selection algorithm (KZ-Picker) to analyze transient landscapes: Calibration and validation, Journal of Geophysical Research: Earth Surface, 122, 1236–1261, https://doi.org/10.1002/2017jf004250, 2017.

O'Hara, D., Karlstrom, L., and Roering, J. J.: Distributed landscape response to localized uplift and the fragility of steady states, Earth and Planetary Science Letters, 506, 243–254, https://doi.org/10.1016/j.epsl.2018.11.006, 2019.

Pan, B., Cai, S., and Geng, H.: Numerical simulation of landscape evolution and mountain uplift history constrain—A case study from the youthful stage mountains around the central Hexi Corridor, NE Tibetan Plateau, Science China Earth Sciences, 64, 412–424, https://doi.org/10.1007/s11430-020-9716-6, 2021.

Perron, J. T.: Climate and the Pace of Erosional Landscape Evolution, Annual Review of Earth and Planetary Sciences, 45, 561–591, https://doi.org/10.1146/annurev-earth-060614-105405, 2017.

Perron, J. T. and Royden, L.: An integral approach to bedrock river profile analysis, Earth Surface Processes and Landforms, 38, 570–576, https://doi.org/10.1002/esp.3302, 2013.

Perron, J. T., Dietrich, W. E., and Kirchner, J. W.: Controls on the spacing of first-order valleys, Journal of Geophysical Research, 113, https://doi.org/10.1029/2007jf000977, 2008.

Perron, J. T., Kirchner, J. W., and Dietrich, W. E.: Formation of evenly spaced ridges and valleys, Nature, 460, 502–505, https://doi.org/10.1038/nature08174, 2009.

Quye-Sawyer, J., Whittaker, A. C., Roberts, G. G., and Rood, D. H.: Fault Throw and Regional Uplift Histories From Drainage Analysis: Evolution of Southern Italy, Tectonics, 40, https://doi.org/10.1029/2020tc006076, 2021.

Robl, J., Hergarten, S., and Prasicek, G.: The topographic state of fluvially conditioned mountain ranges, Earth-Science Reviews, 168, 190–217, https://doi.org/10.1016/j.earscirev.2017.03.007, 2017.

Roering, J. J.: How well can hillslope evolution models "explain" topography? Simulating soil transport and production with high-resolution topographic data, Geological Society of America Bulletin, 120, 1248–1262, https://doi.org/10.1130/b26283.1, 2008.

Roering, J. J., Kirchner, J. W., and Dietrich, W. E.: Evidence for nonlinear, diffusive sediment transport on hillslopes and implications for landscape morphology, Water Resources Research, 35, 853–870, https://doi.org/10.1029/1998wr900090, 1999.

Roering, J. J., Marshall, J., Booth, A. M., Mort, M., and Jin, Q.: Evidence for biotic controls on topography and soil production, Earth and Planetary Science Letters, 298, 183–190, https://doi.org/10.1016/j.epsl.2010.07.040, 2010.

Royden, L. and Taylor Perron, J.: Solutions of the stream power equation and application to the evolution of river longitudinal profiles, Journal of Geophysical Research: Earth Surface, 118, 497–518, https://doi.org/10.1002/jgrf.20031, 2013.

Salles, T.: Badlands: A parallel basin and landscape dynamics model, SoftwareX, 5, 195–202, https://doi.org/10.1016/j.softx.2016.08.005, 2016.

Salles, T. and Duclaux, G.: Combined hillslope diffusion and sediment transport simulation applied to landscape dynamics modelling, Earth Surface Processes and Landforms, 40, 823–839, https://doi.org/10.1002/esp.3674, 2014.

Salles, T. and Hardiman, L.: Badlands: An open-source, flexible and parallel framework to study landscape dynamics, Computers & Geosciences, 91, 77–89, https://doi.org/10.1016/j.cageo.2016.03.011, 2016.

Salles, T. and Howson, I.: badlands-model/pyBadlands: stable release version 2.0.0 (v2.0.0), Zenodo [code], https://doi.org/10.5281/zenodo.1069573, 2017.

Schwanghart, W. and Scherler, D.: Short Communication: TopoToolbox 2 – MATLAB-based software for topographic analysis and modeling in Earth surface sciences, Earth Surf. Dynam., 2, 1–7, https://doi.org/10.5194/esurf-2-1-2014, 2014.

Seybold, H., Berghuijs, W. R., Prancevic, J. P., and Kirchner, J. W.: Global dominance of tectonics over climate in shaping river longitudinal profiles, Nature Geoscience, 14, 503–507, https://doi.org/10.1038/s41561-021-00720-5, 2021.

Shi, F., Tan, X., Zhou, C., and Liu, Y.: Impact of asymmetric uplift on mountain asymmetry: Analytical solution, numerical modeling, and natural examples, Geomorphology, 389, https://doi.org/10.1016/j.geomorph.2021.107862, 2021.

Sklar, L. S. and Dietrich, W. E.: Sediment and rock strength controls on river incision into bedrock, Geology, 29, https://doi.org/10.1130/0091-7613(2001)029<1087:Sarsco>2.0.Co;2, 2001.

Smith, A. G. G., Fox, M., Schwanghart, W., and Carter, A.: Comparing methods for calculating channel steepness index, Earth-Science Reviews, 227, https://doi.org/10.1016/j.earscirev.2022.103970, 2022.

Sweeney, K. E., Roering, J. J., and Ellis, C.: Experimental evidence for hillslope control of landscape scale, Science, 349, 51–53, https://doi.org/10.1126/science.aab0017, 2015.

Tucker, G. E. and Bras, R. L.: Hillslope processes, drainage density, and landscape morphology, Water Resources Research, 34, 2751–2764, https://doi.org/10.1029/98wr01474, 1998.

Tucker, G. E. and Hancock, G. R.: Modelling landscape evolution, Earth Surface Processes and Landforms, 35, 28–50, https://doi.org/10.1002/esp.1952, 2010.

Uhlenbrook, S., Didszun, J., and Leibundgut, C.: Runoff generation processes on hillslopes and their susceptibility to global change, Global Change and Mountain Regions: An Overview of Current Knowledge, 297–307, https://doi.org/10.1007/1-4020-3508-X_30, 2005.

Whipple, K. X.: Fluvial Landscape Response Time: How Plausible Is Steady-State Denudation?, American Journal of Science, 301, 313–325, https://doi.org/10.2475/ajs.301.4-5.313, 2001.

Whipple, K. X.: The influence of climate on the tectonic evolution of mountain belts, Nature Geoscience, 2, 97–104, https://doi.org/10.1038/ngeo413, 2009.

Whipple, K. X. and Tucker, G. E.: Dynamics of the stream-power river incision model: Implications for height limits of mountain ranges, landscape response timescales, and research needs, Journal of Geophysical Research: Solid Earth, 104, 17661–17674, https://doi.org/10.1029/1999jb900120, 1999.

Whipple, K. X., DiBiase, R. A., and Crosby, B. T.: 9.28 Bedrock Rivers, in: Treatise on Geomorphology, edited by: Shroder, J. and Wohl, E., Academic Press, San Diego, CA, 550–573, https://doi.org/10.1016/b978-0-12-374739-6.00254-2, 2013.

Whittaker, A. C.: How do landscapes record tectonics and climate?, Lithosphere, 4, 160–164, https://doi.org/10.1130/rf.L003.1, 2012.

Willett, S. D. and Brandon, M. T.: On steady states in mountain belts, Geology, 30, 175, https://doi.org/10.1130/0091-7613(2002)030<0175:ossimb>2.0.co;2, 2002.

Willett, S. D., McCoy, S. W., Perron, J. T., Goren, L., and Chen, C. Y.: Dynamic reorganization of river basins, Science, 343, 1248765, https://doi.org/10.1126/science.1248765, 2014.

Wilson, M. F. J., O'Connell, B., Brown, C., Guinan, J. C., and Grehan, A. J.: Multiscale Terrain Analysis of Multibeam Bathymetry Data for Habitat Mapping

on the Continental Slope, Marine Geodesy, 30, 3–35, https://doi.org/10.1080/01490410701295962, 2007.

Wobus, C., Whipple, K. X., Kirby, E., Snyder, N. P., Johnson, J., Spyropolou, K., Crosby, B., and Sheehan, D.: Tectonics from topography: Procedures, promise, and pitfalls, Geol. Soc. Am. Spec. Pap., 398, 55–74, https://doi.org/10.1130/2006.2398(04), 2006a.

Wobus, C. W., Crosby, B. T., and Whipple, K. X.: Hanging valleys in fluvial systems: Controls on occurrence and implications for landscape evolution, Journal of Geophysical Research, 111, https://doi.org/10.1029/2005jf000406, 2006b.

Wobus, C. W., Tucker, G. E., and Anderson, R. S.: Does climate change create distinctive patterns of landscape incision?, Journal of Geophysical Research: Earth Surface, 115, https://doi.org/10.1029/2009jf001562, 2010.

Yetemen, O., Saco, P. M., and Istanbulluoglu, E.: Ecohydrology controls the geomorphic response to climate change, Geophysical Research Letters, 46, 8852–8861, 2019.

Young, R. A. and Wiersma, J.: The role of rainfall impact in soil detachment and transport, Water Resources Research, 9, 1629–1636, 1973.

3 Article 2

Diagnostic Signals of Rainfall and Tectonic Uplift: Insights from Divide Migration and Landscape Relaxation Times

Yinbing Zhu[1], Patrice Rey[1], Tristan Salles[1]

[1]School of Geosciences, University of Sydney, Sydney, NSW, 2006, Australia

A version of this chapter has been submitted to the journal *Australian Journal of Earth Sciences*. It is prepared in the *Australian Journal of Earth Sciences* journal format.

Abstract

Distinguishing between the relative contributions of climatic and tectonic forcing to landscape evolution remains a fundamental challenge in geomorphology. Using landscape evolution models, we investigate how the drainage basin responds differently to changes in rainfall versus uplift rates under both uniform and orographic rainfall conditions. Our results identify diagnostic signals that may distinguish these forcing mechanisms. Following a change in rainfall rate, the headwater slope adjusts rapidly because the erosion efficiency changes instantaneously across the landscape. In contrast, following a change in uplift rate, headwater slopes remain constant until the upstream-migrating erosion waves arrive. The relaxation time required for the landscape to recover from changes in rainfall and uplift rates differs markedly. The landscape adjusts more rapidly to increased rainfall rate than to decreased rainfall rate. In contrast, changes in the uplift rate produce comparable relaxation times. Under orographic rainfall conditions, divide migration is more sensitive to changes in rainfall rate than to changes in uplift rate. An increase in rainfall rate drives divide migration towards the windward side, whereas a decrease in rainfall rate drives it towards the leeward side. The mean steady-state elevation shows a linear relationship with the uplift rate but a negative power-law relationship with rainfall rate. Compared to humid regions, landscapes in arid environments are more sensitive to changes in rainfall. Differences in landscape response to changes in tectonic and climatic forcing serve as valuable diagnostic signals. They provide testable criteria for interpreting landscape features in the natural environment and deciphering the relative contributions of tectonic versus climatic forcing.

Key Points:

- Headwater channel slopes change rapidly following rainfall perturbations but remain fixed following uplift changes until erosion waves arrive.
- Divide migration under orographic rainfall is 2.4-16 times more sensitive to rainfall rate changes than to uplift rate changes, with contrasting migration directions revealing distinct forcing mechanisms.

- Mean steady-state elevation scales linearly with uplift rate but follows a negative power-law with rainfall rate, indicating landscapes are most sensitive to rainfall changes in arid to semi-arid conditions.

Keywords: diagnostic signal; landscape evolution; numerical modelling; orographic rainfall; tectonic uplift; divide migration

Introduction

The Earth's surface records the interplay between climatic and tectonic forcing. (Allen, 2008; Seybold et al., 2021; Whipple et al., 2013). However, interpreting whether the observed landscape changes are caused by climatic or tectonic forcing remains a challenge (Kirby & Whipple, 2012; Whittaker, 2012). Although both processes shape the landscape, the response of the landscape to the two differs, which can be reflected in features such as drainage network geometry, channel morphology, and drainage divide locations (Leonard & Whipple, 2021; Willett et al., 2014).

Traditional methods for analyzing the competition focus on river characteristics, such as the steepness index and knickpoint migration (Wobus et al., 2006). However, studies have shown that the dynamics of drainage divide under spatially varying rainfall (such as topographic rainfall) may provide further assistance (Forte & Whipple, 2018; He et al., 2021; Zavala et al., 2020). When rainfall changes spatially, the resulting erosion asymmetry can drive sustained divide migration, and its magnitude and direction may reveal the nature of forcing mechanisms.

Here, we use numerical landscape evolution experiments to isolate the effects of rainfall and uplift perturbations. We implement uniform and spatially varying rainfall scenarios to quantify how perturbation intensity and type influence divide migration and channel adjustment. Our results show that divide migration under orographic rainfall is 2.4–16 times more sensitive to rainfall changes than to uplift changes of equivalent magnitude. Furthermore, an increase in rainfall rate drives divide migration against the prevailing wind direction. The difference in migration direction of the divide is absent in uplift-driven scenarios. In addition, we analyze differential landscape response to

perturbations by examining headwater channel slope evolution and landscape relaxation times, providing independent criteria for distinguishing between rainfall and tectonic forcing in naturally transient landscapes.

Methods

Steady-state and transient landscapes have contrasting characteristics in river channel morphology. River channels in steady-state show downstream decreases in channel slope with increasing drainage area, described by power-law scaling relationships (e.g., Flint, 1974; Hack, 1957; Snyder et al., 2000):

$$S = k_s A^{-\theta} \qquad (1)$$

Where S is the channel slope, k_s is the channel steepness index, A is the upstream drainage area, and θ is the concavity index. The normalized channel steepness index k_{sn} quantifies the relationship using a reference concavity value θ_{ref}, facilitating comparisons across basins with different drainage areas (Wobus et al., 2006). The logarithm of Equation 1 delivers a linear relationship between $log(S)$ and $log(A)$:

$$log(S) = log(k_{sn}) - \theta_{ref} log(A) \qquad (2)$$

In a $log(S)$-$log(A)$ space, steady-state channels plot as a single, continuous trend. Transient landscapes depart from these steady-state relationships, developing knickpoints or knickzones that separate the unchanged upstream channel from the adjusted downstream channel (Crosby & Whipple, 2006; Lague, 2014). These features appear as discontinuities in slope-area plots. Knickpoints and knickzones are thought to reflect landscape responses to perturbations in uplift rate, erosion efficiency, or both (Whipple et al., 2013). We quantify these features using slope-area analysis, in which departures from single power-law scaling indicate a transient state (Gailleton et al., 2019).

Model configuration and experimental design

Our experimental design builds upon the modelling framework detailed in Zhu et al. (2025), which investigates headwater channel slope evolution under varying hillslope diffusion coefficients. Here, we extend that analysis to quantify drainage divide migration and landscape relaxation timescales under orographic rainfall conditions. We simulate landscape evolution using Badlands (Salles et al., 2018; Salles & Hardiman, 2016), a finite-volume landscape evolution model that couples fluvial incision via stream power erosion with hillslope sediment transport via linear diffusion. Our model domain spans 40 km × 80 km at 400 m resolution and is initialized as a flat surface with a uniform elevation of 10 m (Table 1 and Figure 1). The stream power incision model relates erosion rate E to drainage area A, channel slope (S), and upstream averaged rainfall rate (P):

$$E = KP^m A^m S^n \qquad (3)$$

where K is the erodibility coefficient of the bedrock, m and n are positive constant exponents (Han et al., 2015; Kirby & Whipple, 2012; Smith et al., 2022; Whipple & Tucker, 1999).

Table 1. Common parameters used in Badlands models

Parameter	Value	Unit
Size of the model domain	40 × 80	km
Size of the cell (d_x, d_y)	400, 400	m
Initial elevation	10	m
Time step (d_t)	0.5	Ma
Total duration	100	Ma
m (drainage area exponent)	0.5	-
n (slope exponent)	1	-
Erodibility (k_d)	2.3×10^{-6}	1/yr
Surface diffusion coefficient (k_h)	1.0	m^2/yr
Easterly wind velocity (orographic rainfall)	4	m/s

Each experiment consists of two evolutionary stages (Figure 1). In the first stage, the uniform uplift rate is 300 m/Myr, and the background rainfall rate is 2 m/yr. The landscape evolves under these constant boundary conditions for 50 Ma. This stage ensures that the landscape reaches a dynamic

equilibrium at the end of the stage, i.e., a stable mean elevation where erosion balances uplift (Montgomery, 2001; Willett & Brandon, 2002). At the beginning of the second stage (50 Ma), perturbations are applied. The evolution continues for another 50 Ma, allowing the landscape to adjust to the new boundary conditions and reach a new equilibrium state.

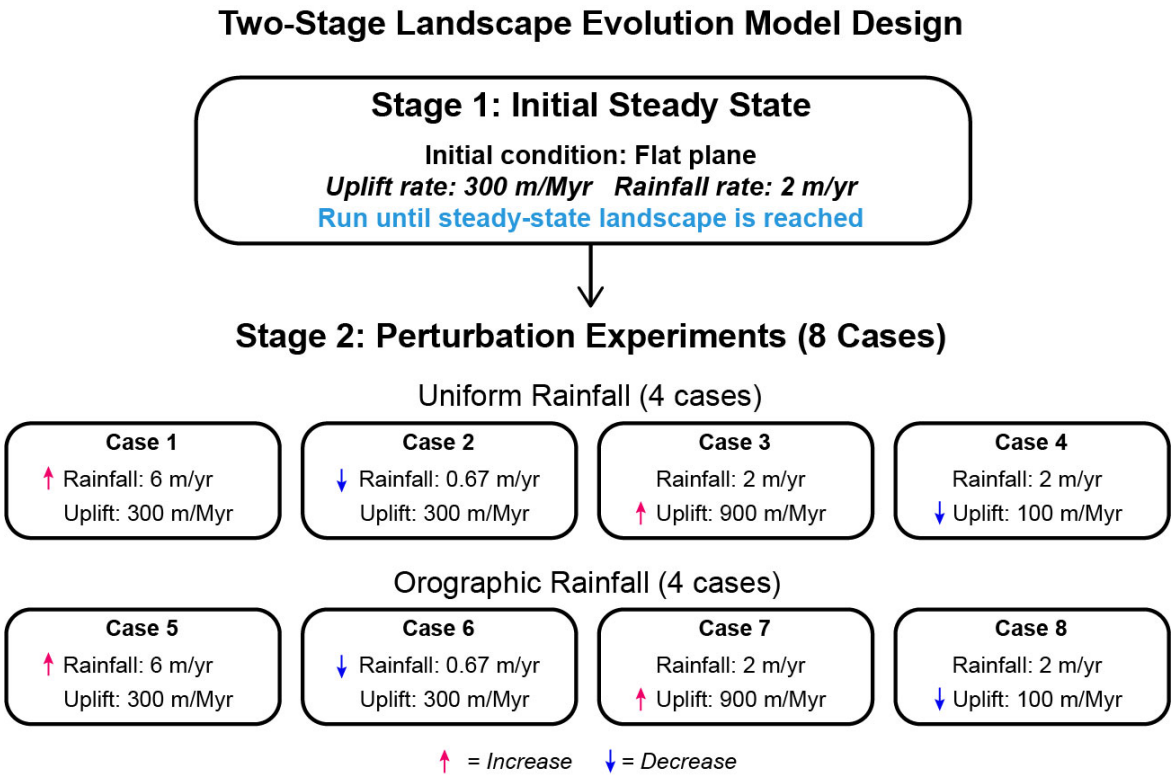

Figure 1. Two-stage landscape evolution controlled by changes in rainfall or uplift. Stage 1: An initial flat surface evolves under constant forcing (300 m/Myr uplift, 2 m/yr rainfall) until reaching steady-state equilibrium. Stage 2: Perturbations applied at 50 Ma alter either rainfall rate or uplift rate while the other forcing remains constant. Eight experiments result from combining four perturbation types with two rainfall regimes (uniform vs. orographic).

We have tested four perturbation scenarios at the transition between Stage 1 and 2: (1) rainfall rate increases to 6 m/yr, (2) rainfall rate decreases to 0.67 m/yr, (3) uplift rate increases to 900 m/Myr, and (4) uplift rate decreases to 100 m/Myr. The proportional perturbation magnitudes (threefold increase and decrease) allow for a direct comparison of response variation. Each scenario is tested under both uniform rainfall and orographic rainfall conditions, resulting in 8 different cases (Figure 1). To

simulate orographic rainfall, we apply an easterly wind to the uniform model to represent the effect of moist air rising over mountains, producing stronger rainfall on the windward slope and creating a rain shadow on the leeward slope. The resulting rainfall gradient across the divide provides climate asymmetry for studying its impact on river channel adjustment and divide migration. The experimental design isolates the effects of rainfall and uplift perturbations.

Analysis procedures

Badlands outputs are interpolated from the TIN to 30 m-resolution digital elevation models (DEMs) for analysis. Although the input resolution is 400 m, we have verified that a finer 30 m output resolution better preserves channel network details without introducing artifacts (Deng et al., 2007; Goulden et al., 2014).

We use TopoToolbox to analyze DEMs. TopoToolbox is a MATLAB-based library that can extract drainage networks, calculate slope-area relationships, and compute channel steepness indices, among other functions (Schwanghart & Kuhn, 2010; Schwanghart & Scherler, 2014).

To identify knickzones in slope-area space, we design a two-step automated procedure. First, we cluster slope-area data points using the DBSCAN algorithm (scikit-learn library; Pedregosa et al., 2011), which groups spatially proximate points without requiring pre-specification of cluster numbers. Second, we perform segmented linear regression on each cluster using Equation 2 to extract k_{sn} values for each channel segment. This automated procedure reduces subjectivity compared to manual knickzone selection while maintaining reproducibility of the 16 experiments. Drainage divide positions are tracked through time. We extract the position of the main drainage divide along a central transect. The divide migration rate is calculated as the temporal derivative of the divide position.

We quantify landscape relaxation time as the interval required for the mean landscape elevation to stabilize within 1% of its final steady-state value following the 50 Ma perturbation. The relaxation time provides a characteristic timescale for landscape adjustment.

Our analysis focuses on the eastern drainage basin. In orographic rainfall scenarios, the eastern drainage basin corresponds to the windward slope. Compared to the leeward slope, the windward slope receives more rainfall under orographic enhancement. The orographic effects of rainfall forcing are expected to be most pronounced. Therefore, the windward slope is an ideal area to identify climate signals associated with orographic effects. Under uniform rainfall conditions, we have verified that eastern and western basins evolve identically. Therefore, focusing on either the eastern or western basin has no impact on the results.

Results

Steady-state morphology

At the end of Stage 1, the landscape reaches dynamic equilibrium where mean elevation stabilizes and erosion balances uplift. We present results for the eastern drainage basin in each case to compare the effects of orographic rainfall on the windward basin.

Under uniform rainfall conditions (2 m/yr background rainfall, 300 m/Myr uplift), the mean elevation of the steady-state landscape is 600 m (Table 2). The drainage divide develops near the center of the landscape (Figure 2a). The k_{sn} map shows relatively homogeneous channel steepness values across the drainage basin, with only minor spatial variations (Figure 2a). The slope-area relationship for the trunk stream shows a clear power-law form. Although automatic clustering identifies five distinct segments (Figure 2b), their regression lines are nearly parallel. The gaps between clusters in the slope-area plot (e.g., the gap between $log(A)$ = 8.3 and 8.5 in Figure 2b) reflect the sudden increase in upstream drainage area when tributaries converge into the trunk stream. The data points near the basin outlet have a high degree of dispersion (lower-right part in Figure 2b). It is due to the exaggeration of the low slope in the double logarithmic coordinate system, rather than the true knickpoint (Mudd et al., 2018; Smith et al., 2022).

Table 2. Steady-state landscape attributes (mean elevation and channel k_{sn}) and relaxation time of different cases

Rainfall condition	Case	Mean elevation (m)	Mean k_{sn}	Relaxation time (Myr)
Uniform rainfall	End of Stage 1 (50 Ma)	600	94	
	Case 1: Increase in rainfall rate	303	42	3
	Case 2: Decrease in rainfall rate	1187	212	11
	Case 3: Increase in uplift rate	1802	279	7
	Case 4: Decrease in uplift rate	200	32	6
Orographic rainfall	End of Stage 1 (50 Ma)	631	85	
	Case 5: Increase in rainfall rate	336	47	6.5
	Case 6: Decrease in rainfall rate	1055	154	39
	Case 7: Increase in uplift rate	1887	268	13
	Case 8: Decrease in uplift rate	209	29	7.5

Note. Relaxation time is the time required for the landscape to reach a steady state.

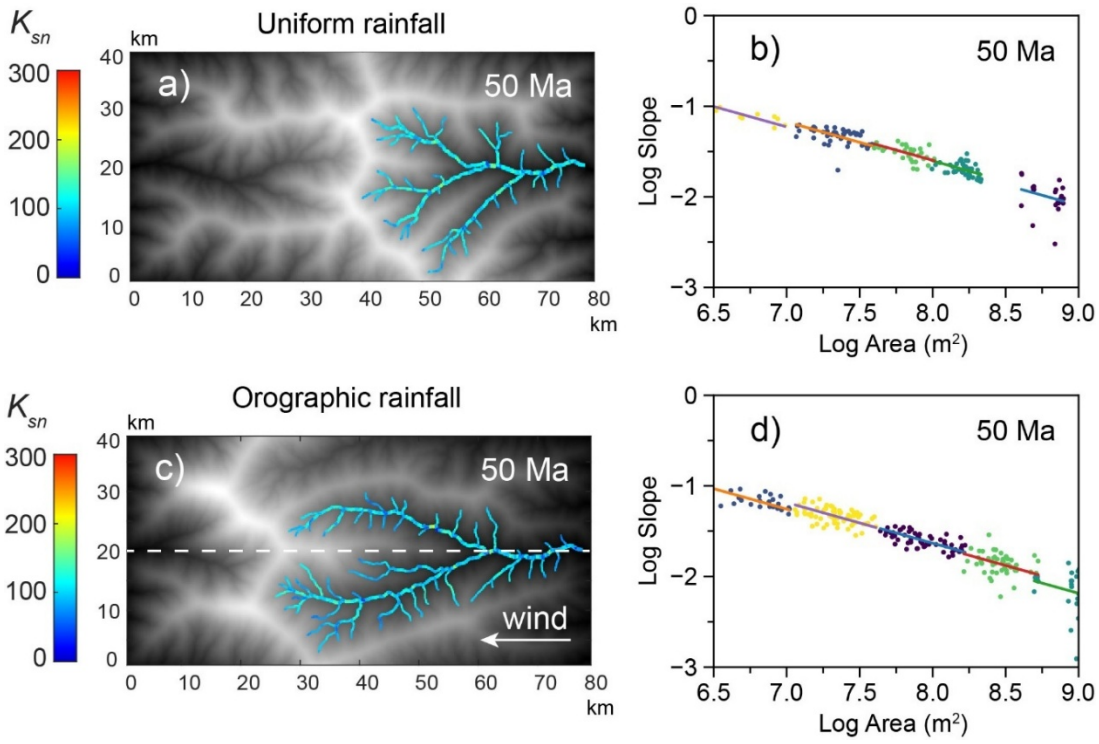

Figure 2. k_{sn} maps (a and c) and clustered slope-area plots (b and d) of the largest drainage basin at the end of Stage 1. The dashed line in (c) indicates the location of the cross section in Figure 5.

When the easterly wind is applied in the model, orographic rainfall forms and changes the landscape. Orographic rainfall leads to the divide gradually migrating westward (downwind) in the first stage, forming an asymmetric stable landscape (Figure 2c). The landscape eventually reaches a steady state where the divide position no longer changes.

Although the background rainfall and uplift rates are the same, the mean elevation under orographic rainfall conditions (631 meters) is about 5% higher than that under uniform rainfall conditions (600 meters, Table 2). The slope-area analysis confirms the steady state, and the segmentation identified by the clustering algorithm is similar to that under uniform rainfall conditions (Figure 2d).

Transient response to rainfall

Changes in rainfall rate trigger landscape adjustments that differ between uniform and orographic rainfall conditions. Under uniform rainfall, following an increase in rainfall rate from 2 to 6 m/yr at 50 Ma, the mean landscape elevation decreases from 600 to 303 m, while k_{sn} decreases from 94 to 42 (Table 2). The landscape reaches a new steady state within three Myrs, the fastest transient response among all perturbation cases. Channel slope decreases rapidly at the river mouth (Figure 3a). The headwater channel slope shows a slight transient increase within the first 1-2 Myrs before decreasing toward its final steady-state value (Figure 3b). Negative knickzones form at the river mouth and migrate upstream. The k_{sn} map at 51 Ma shows spatial variation. Downstream values decrease while headwater values almost remain constant (Figure 3c). By 100 Ma, the landscape reaches a steady state with relatively uniform lower k_{sn} values across the drainage network (Figure 3d). The slope-area plot at 51 Ma shows clear negative knickzones as downward steps toward the river mouth (Figure 3e). Multiple regression lines are required to capture the segmented profile. k_{sn} values decrease from headwaters to the mouth. At 100 Ma, all data points collapse onto a single regression line except for those near the river mouth, which form a downward step (Figure 3f). Because there is no sharp change in value on the k_{sn} map at 100 Ma, the downward step is due to the exaggeration effect.

A decrease in rainfall rate from 2 to 0.67 m/yr produces opposite effects. Mean elevation increases from 600 to 1187 m, and k_{sn} rises from 94 to 212 (Table 2). The landscape reaches a steady state after 11 Myrs, almost four times as long as in the rainfall increase case. Channel slope increases at the river mouth but decreases subtly at the headwaters during the initial transient phase (Figure 3g and h). Positive knickzones form at the river mouth and migrate upstream. The k_{sn} map at 51 Ma shows modest increases expressed as small upward steps in the slope-area plot (Figure 3i and k). Within the same 1-Myr interval, these changes are less evident than the negative knickzones following rainfall increase. By 100 Ma, the landscape is steady with uniformly increased k_{sn} values (Figure 3j and l).

Under orographic rainfall, a rainfall rate increase from 2 to 6 m/yr reduces the mean elevation from 631 to 336 m and decreases k_{sn} from 85 to 47 (Table 2). The landscape reaches a steady state after 6.5 Myrs, more than twice as long as in the uniform rainfall case. Negative knickzones form at the river mouth and migrate upstream (Figure 3a). The headwater channel slope shows a subtle response at 51 Ma (Figure 3b). The spatial evolution of k_{sn} (Figure 3c and d) and the downward steps of negative knickzones (Figure 3e and f) follow patterns generally similar to those under uniform rainfall.

Reducing rainfall from 2 to 0.67 m/yr under orographic conditions increases mean elevation from 631 to 1055 m and raises k_{sn} from 85 to 154 (Table 2). The landscape reaches a steady state after 39 Myrs, the longest among all cases. The channel response (Figure 3g and h), k_{sn} spatial patterns (Figure 3i and j), and knickzone characteristics (Figure 3k and l) are similar to those under uniform rainfall.

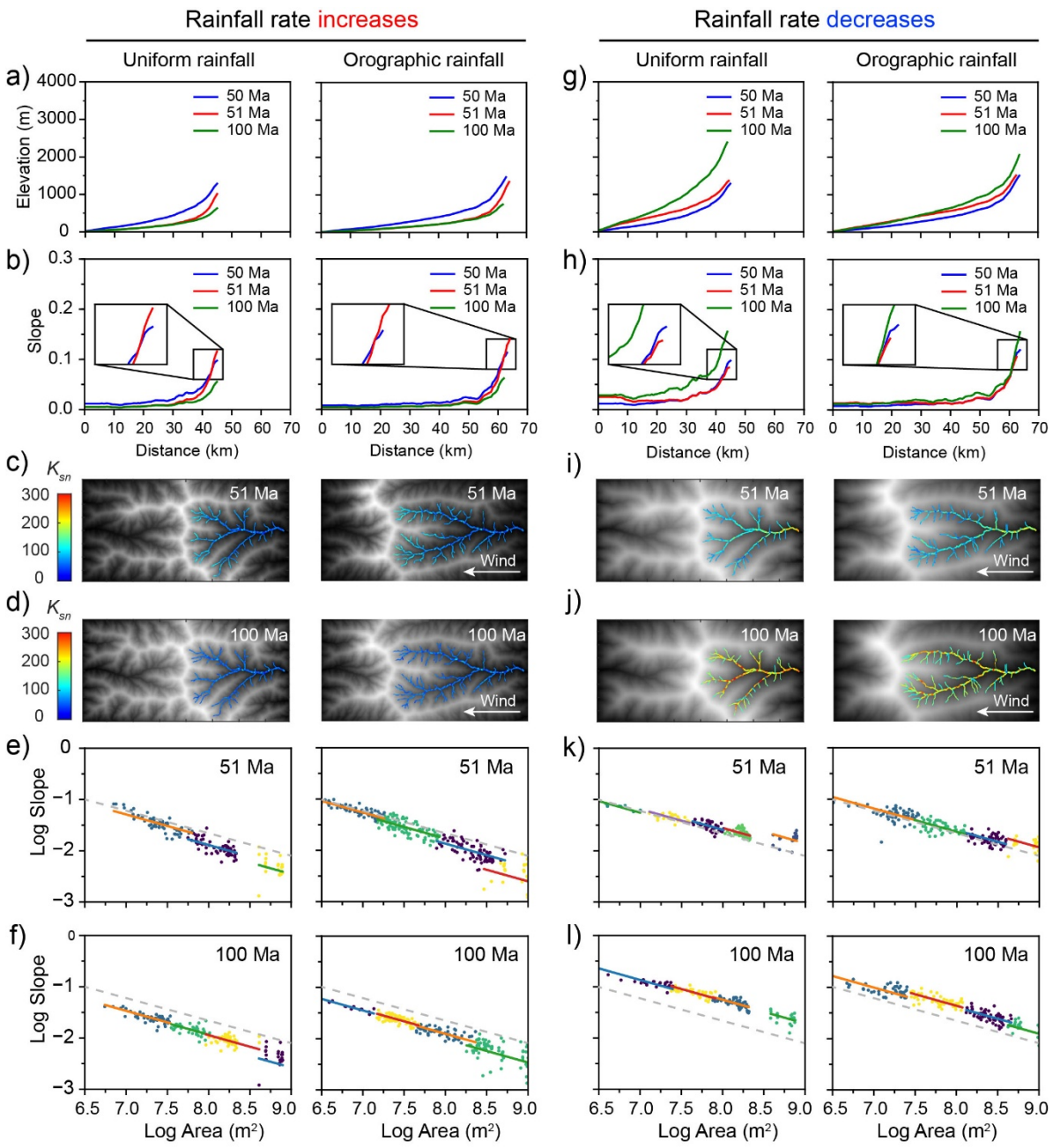

Figure 3. Changes in landscape after changes in rainfall rate. Longitudinal profiles (a and g) and slope profiles (b and h) of the trunk stream of the largest drainage basin. k_{sn} maps of the largest drainage basin at 51 Ma (c and i) and 100 Ma (d and j). Clustered slope-area plots of channels in the largest drainage basin at 51 Ma (e and k) and 100 Ma (f and l). Gray dashed lines in (e, f, k, and l) indicate the regression line at 100 Ma.

Transient response to uplift

The response of the landscape to changes in uplift rate differs from its response to changes in rainfall rate. Under uniform rainfall, increasing uplift rate from 300 to 900 m/Myr at 50 Ma raises mean elevation from 600 to 1802 m and increases k_{sn} from 94 to 279 (Table 2). The landscape reaches a steady state within seven Myrs. Initial slope adjustments concentrate at the river mouth, with headwater slope remaining fixed during early transient phases (Figure 4a and b). Positive knickzones form at the river mouth and migrate upstream (Figure 4a). The k_{sn} map at 51 Ma shows increased values in downstream channels. In comparison, headwater values remain near their pre-perturbation state (Figure 4c). By 100 Ma, a uniform channel steepness has formed across the drainage network (Figure 4d). The slope-area plot at 51 Ma shows positive knickzones as upward steps toward the river mouth (Figure 4e). By 100 Ma, all regression lines converge to the same line (Figure 4f).

Decreasing the uplift rate from 300 to 100 m/Myr reduces the mean elevation from 600 to 200 m and lowers k_{sn} from 94 to 32 (Table 2). The landscape reaches a steady state after six Myrs, slightly shorter than the uplift increase case. Channel slope decreases at the river mouth but remains unchanged at the headwater during the initial transient phase (Figure 4g and h). Negative knickzones form and migrate upstream (Figure 4g). The k_{sn} spatial evolution (Figure 4i and j) and slope-area adjustments (Figure 4k and l) correspond to those of the uplift increase case but in the opposite direction.

Under orographic rainfall, increasing the uplift rate from 300 to 900 m/Myr raises the mean elevation from 631 to 1887 m and increases k_{sn} from 85 to 268 (Table 2). The landscape reaches a steady state after 13 Myrs, which is longer than the seven Myrs required under uniform rainfall. Channel profiles (Figure 4g and h), k_{sn} spatial patterns (Figure 4i and j), and slope-area evolution (Figure 4k and l) are generally similar to those under uniform rainfall.

Reducing the uplift rate from 300 to 100 m/Myr under orographic rainfall decreases the mean elevation from 631 to 209 m and lowers k_{sn} from 85 to 29 (Table 2). The landscape reaches a steady

state after 7.5 Myrs. Channel profiles (Figure 4g and h), k_{sn} spatial patterns (Figure 4i and j), and slope-area evolution (Figure 4k and l) are generally similar to those under uniform rainfall.

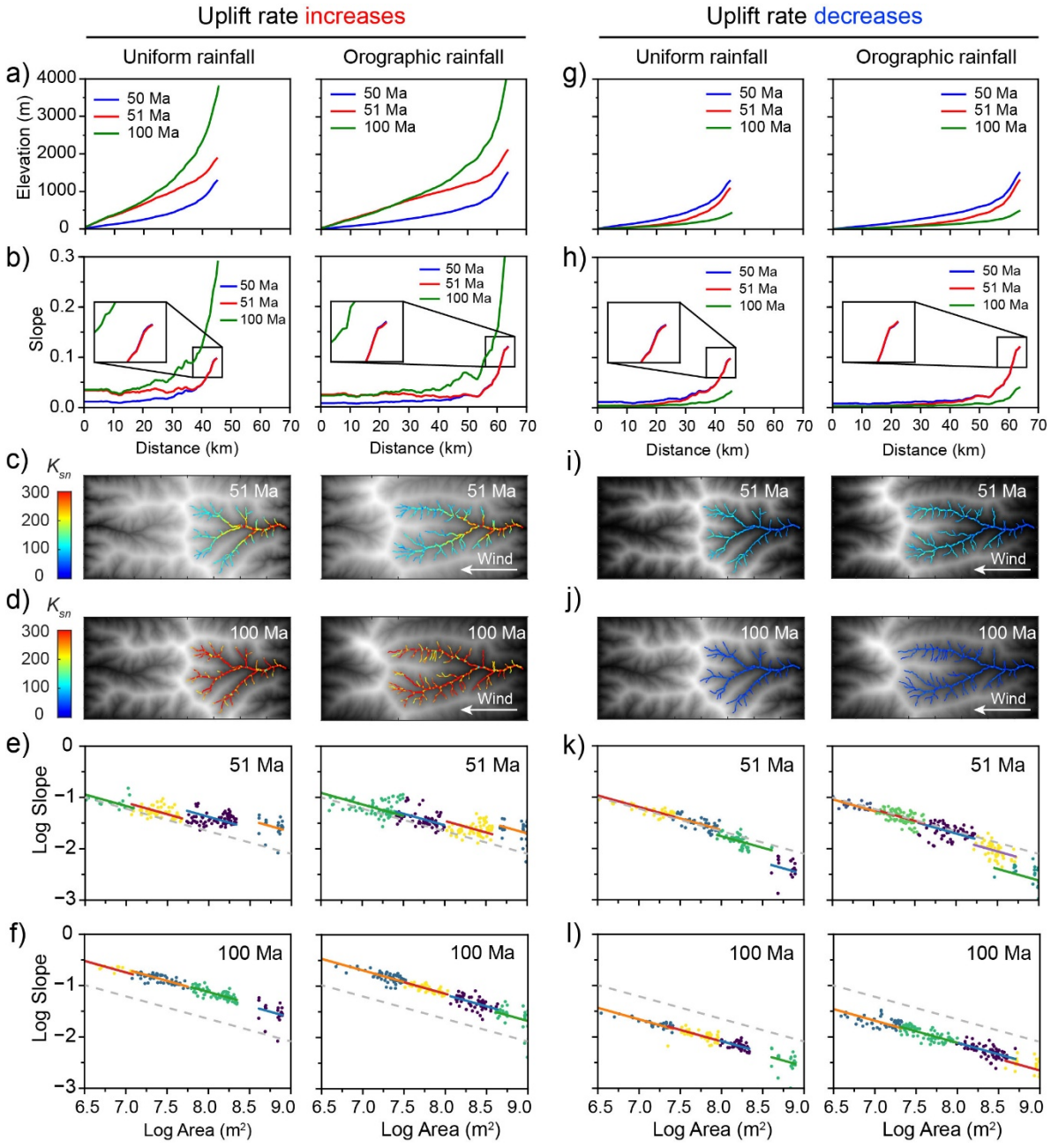

Figure 4. Changes in landscape after changes in uplift rate. Longitudinal profiles (a and g) and slope profiles (b and h) of the trunk stream of the largest drainage basin. k_{sn} maps of the largest drainage basin at 51 Ma (c and i) and 100 Ma (d and j). Clustered slope-area plots of channels in the largest drainage basin at 51 Ma (e and k) and 100 Ma (f and l). Gray dashed lines in (e, f, k, and l) indicate the regression line at 100 Ma.

Divide migration under orographic rainfall

Under uniform rainfall, the drainage divide remains stationary, regardless of changes in rainfall rate or uplift rate. In contrast, under orographic rainfall, both rainfall and uplift changes trigger divide migration with varying magnitudes and directions (Figure 5).

Following the threefold increase in rainfall rate at 50 Ma, the divide migrates windward (eastward) rapidly (Figure 5a). Total divide migration reaches 2.7 km over 6.5 Myrs (Figure 5b). Following the threefold decrease in rainfall rate at 50 Ma, the divide initially does not react immediately. After ~8 Myrs, it begins migrating leeward (westward) (Figure 5c). This migration process undergoes two pauses, each lasting ~5 Myrs. Finally, it moves 6.4 km leeward after 39 Myrs (Figure 5d).

Following the threefold increase in uplift rate at 50 Ma, the divide first migrates ~0.6 km windward, then gradually reverses direction and migrates leeward (Figure 5e). The divide stabilizes 1.1 km leeward of its 50 Ma position after 13 Myrs (Figure 5f). The threefold decrease in the uplift rate results in a minor migration of the divide. The divide first migrates ~1.2 km leeward, then reverses direction and migrates windward (Figure 5g). The divide stabilizes 0.4 km leeward of its 50 Ma position after 7.5 Myrs (Figure 5h).

Changes in rainfall rate produce 2.7–6.4 km of shift with opposite directions (windward for increase, leeward for decrease), while uplift rate changes result in 0.4–1.1 km of predominantly leeward migration.

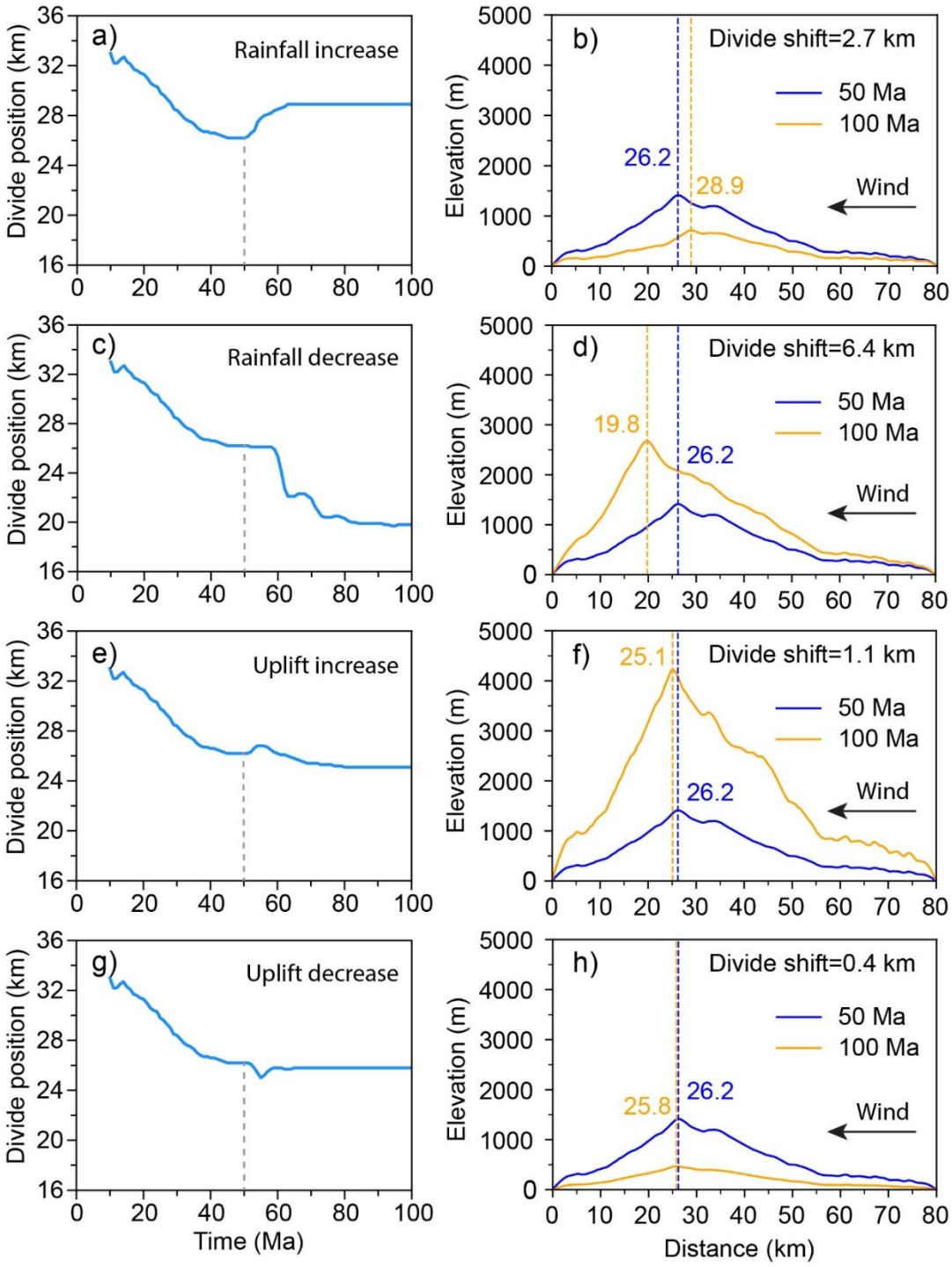

Figure 5. Divide position and corresponding cross sections of landscapes under orographic rainfall. (a, c, e, g) Divide position through time. Dashed lines mark 50 Ma, after which rainfall or rock uplift rates change. (b, d, f, h) West-east cross sections in the middle of the landscape showing divide positions at 50 Ma (blue dashed) and 100 Ma (orange dashed). The location of the cross section is shown in Figure 2.

Discussion

Diagnostic differences and dynamic asymmetry of landscape response

The study results indicate a significant difference in the response of the landscape to rainfall and uplift changes. The difference arises from the different ways in which rainfall and uplift forcing affect surface erosion processes and signal propagation.

Headwater slope behavior as a diagnostic signal

One effective indicator for distinguishing between these two types of forcing is the investigation of changes in channel slope at the headwaters. This difference reflects how rainfall and uplift, respectively, alter the erosion field across the entire drainage basin. Rainfall change acts as a distributed forcing. When the rainfall rate changes, its effects are instantaneous throughout the drainage basin. This perturbation primarily works by altering the capacity of river incision. The increased rainfall rate immediately enhances the erosion efficiency of the river flow (Ferrier et al., 2013). However, the rate at which hillslope transport sediment to the channel is mainly controlled by topographic slope (Pelletier, 2008) and remains constant initially. Thus, the rate at which sediment is incised down the channel temporarily exceeds the rate of sediment supply from the hillslope. This imbalance intensifies channel downcutting, thereby immediately triggering a temporary increase in channel slope at the headwaters (Zhu et al., 2025).

In contrast, changes in the uplift rate are a perturbation to the base (Snyder et al., 2002). It first changes the erosion base level at the river mouth, thereby effectively influencing the model boundary. Therefore, the erosion response begins at the river mouth and gradually migrates upstream in the form of an erosion wave. The erosion rate at the headwaters remains unchanged until the erosion wave arrives. Consequently, in the initial stage after the uplift rate change, the slope of the channel at the headwaters remains constant. This constant slope serves as an important diagnostic signal that the perturbation is due to tectonic uplift.

Knickzone characteristics and relaxation time asymmetries

Migrating knickzones form under both rainfall and uplift perturbations, but their characteristics differ. Negative knickzones form following rainfall rate increase or uplift rate decrease, while positive knickzones form following rainfall rate decrease or uplift rate increase.

In addition, the relaxation times required to eliminate knickzones and reestablish uniform k_{sn}values differ for rainfall-induced and uplift-induced changes. Under uniform rainfall, the landscape adjusts to rainfall increases in only 3 Myrs but requires 11 Myrs to adjust to rainfall decreases, a 3.7-fold difference (Table 2). Under orographic rainfall, this difference is even more significant: 6.5 Myrs for rainfall increases versus 39 Myrs for rainfall decreases, a sixfold difference. In contrast, uplift increases and decreases produce comparable relaxation times (a 1.2-fold under uniform rainfall and 1.7-fold under orographic rainfall). This difference in rainfall-induced relaxation times arises from the nonlinear (power-law) dependence of erosion on rainfall rate. In the stream power law (Equation 3), the exponent m typically ranges from 0.4 to 0.6 (Kirby & Whipple, 2012; Whipple & Tucker, 1999), and m = 0.5 in our model (Table 1). A threefold change in rainfall rate amplifies erosion efficiency by a factor of $3^{0.5} \approx 1.7$. The landscape adjusts faster when erosion efficiency increases because higher erosion rates more rapidly eliminate the topographic disequilibrium.

In contrast, uplift-induced relaxation times do not show such a large difference because the uplift rate does not directly participate in the governing equations. The same threefold change in uplift rate (either increase or decrease) creates approximately proportional changes in the topographic disequilibrium.

The extended relaxation times under orographic rainfall (compared to uniform rainfall) for both forcing types result from the spatially heterogeneous erosion rates across the divide. The landscape not only adjusts channel profiles but also reestablishes the erosion balance between windward and leeward slopes.

Steady-state scaling relationships: Linear versus power-law

The mean steady-state elevation scales differently with rainfall rate versus uplift rate. Under uniform rainfall conditions, the mean elevation is linearly related to the uplift rate (Figure 6a). In contrast, the mean elevation shows a negative power-law relationship with rainfall rate (Figure 6b). This difference in scaling relationship indicates an important diagnostic feature: the landscape is disproportionately sensitive to changes in rainfall rate under arid-to-semiarid conditions. The same absolute change in rainfall rate (e.g., ±1 m/yr) has a larger proportional effect on erosion rates when background rainfall is low than when it is high. This power-law scaling is consistent with results from laboratory physical modelling (Figure 6c) (Bonnet & Crave, 2006). The distinct non-linearity in rainfall response allows us to disentangle climatic forcing from the linear signal of tectonic uplift, particularly in arid environments. These linear and power-law relationships are preserved under orographic rainfall conditions, although differences in absolute elevation exist at the same background rainfall rate (Table 2).

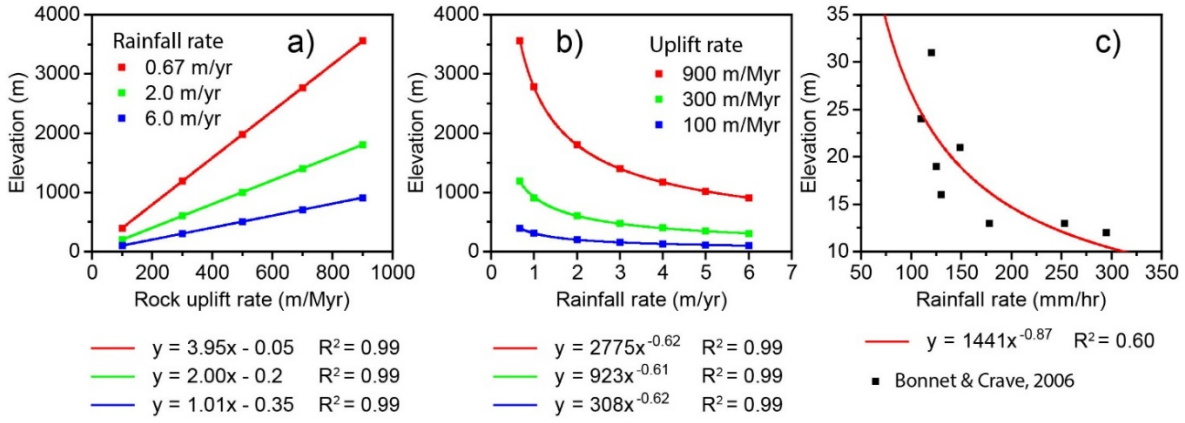

Figure 6. Mean steady-state elevation against different rainfall and uplift rates. (a) Mean steady-state elevation against rock uplift rate under uniform rainfall conditions of 0.67 m/yr, 2 m/yr, and 6 m/yr. (b) Mean steady-state elevation against uniform rainfall rate when uplift rate is 100 m/Myr, 300 m/Myr, and 900 m/Myr. (c) Mean steady-state elevation of landscapes against rainfall rate, modified from Bonnet and Crave (2006).

Mechanisms of divide migration under orographic rainfall

Under orographic rainfall, although the magnitude of rainfall rate change is the same (threefold), divide migration is more sensitive to rainfall rate changes than to uplift rate changes. The fundamental driver of divide migration under orographic rainfall is the asymmetry in erosion rates across the divide, which in turn is controlled by the spatial gradient in rainfall rate (Roe, 2005). Under steady-state conditions at 50 Ma, orographic rainfall results in a difference in rainfall rate on either side of the divide (1.75 m/yr on the windward side and 0.84 m/yr on the leeward side; Figures 7a and 8). Despite the asymmetrical rainfall, the erosion rates on both sides remained balanced (Willett et al., 2001).

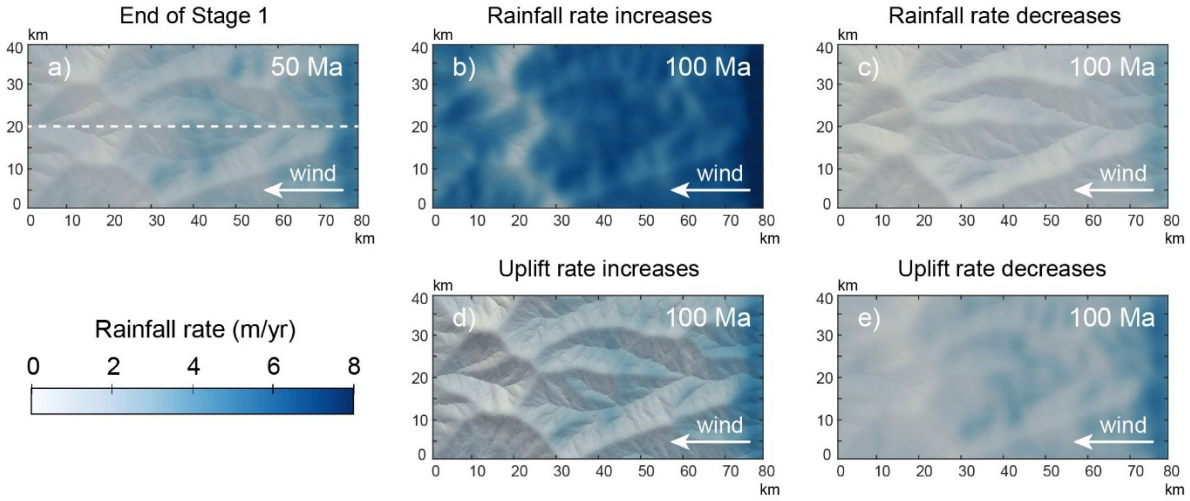

Figure 7. Rainfall maps under different conditions. (a) Rainfall field at the end of Stage 1. The dashed lines represent the cross-sectional location of each rainfall rate profile in Figure 8. (b) and (c) show the rainfall fields after the rainfall rate increases and decreases, respectively. (d) and (e) show the rainfall fields after the uplift rate increases and decreases, respectively.

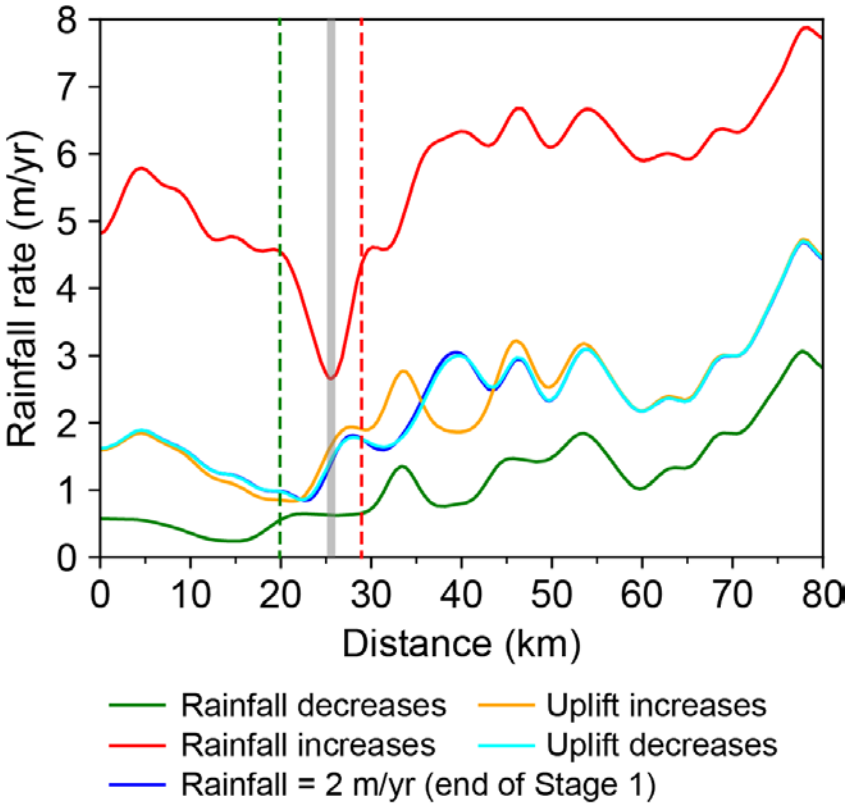

Figure 8. Rainfall rate along the cross section in Figure 7. The red dashed line indicates the divide position at 100 Ma after the rainfall rate increases. The green dashed line indicates the divide position at 100 Ma after the rainfall rate decreases. The grey region represents the range of the divide position at the end of Stage 1 (50 Ma) and at 100 Ma after changes in the uplift rate.

Rainfall-induced divide migration

Divide migration velocity scales with the difference in erosion rates on either side (Forte & Whipple, 2018). When the rainfall rate increases threefold, both sides of the divide receive more rainfall, thereby increasing erosion rates (Figure 7b). The windward side experiences a larger absolute increase in rainfall rate (from 1.75 to 4.6 m/yr, a 2.85 m/yr increase, versus 0.84 to 2.7 m/yr, a 1.86 m/yr increase on the leeward side; Figure 8), and the erosion rate difference amplifies. The amplified discharge and stream power on the windward side accelerate erosion and cause the divide to migrate windward (eastward). Once the new steady state is achieved, erosion rates on both sides equalize, and the divide stabilizes.

In contrast, when the rainfall rate decreases threefold, the orographic effect weakens (Figure 7c). The absolute rainfall rate difference across the divide has narrowed to only 0.38 m/yr (windward 0.62 m/yr, leeward 0.24 m/yr; Figure 8). In such low-rainfall conditions, the weakened orographic contrast reduces the erosion rate difference between windward and leeward sides. However, according to the power-law erosion function (Equation 3), under such relatively arid conditions, even small changes in rainfall rate can translate into large differences in erosion rates. The divide migrates extensively leeward as the drainage network reorganizes to the new low-rainfall equilibrium.

Uplift-induced divide migration

When the uplift rate changes, the orographic rainfall gradient changes only slightly (Figure 7d and e). When the uplift rate increases from 300 to 900 m/Myr, the landscape steepens and elevates. However, the difference in rainfall rate across the divide remains relatively constant, at approximately 0.9-1.0 m/yr (Figure 8). Similarly, when uplift decreases, the difference in rainfall rate also changes slightly. If the difference in rainfall rate does not change significantly, the imbalance in erosion rate driving drainage divide migration is limited. The small amount of divide movement in uplift scenarios (0.4-1.1 km) happens because the landscape temporarily adjusts its shape, and the rainfall pattern responds slightly to the new topography. However, this does not create the major shift in erosion patterns that causes the much larger divide migration (2.7-6.4 km) in rainfall scenarios.

Limitations

Although our model results show contrasting landscape responses to rainfall and uplift changes, challenges remain in applying them to natural landscapes. The transient change in headwater slope during rainfall-driven landscape evolution is subtle. Our model does not account for factors such as lithology and sediment supply variations, and the weak slope signals in river channels may be masked in nature (e.g., Hurst et al., 2013; Korup & Schlunegger, 2009; Shan et al., 2019). High-resolution topographic data, dense cosmogenic nuclide sampling to detect differential erosion patterns, and careful site selection (focusing on homogeneous lithologies and simple channel networks) may be

necessary to detect these signals. In addition, we use a detachment-limited stream power model for simulation. However, in many natural landscapes, erosion is limited by sediment transport capacity. This is particularly common in low-gradient river channels, where channel morphology and slope are mainly controlled by the sediment supply from upstream (Whipple & Tucker, 2002). Despite these limitations, our model still provides insights into the mechanisms by which different forcings shape landscapes.

Conclusions

Our study suggests that the landscape responds to changes in rainfall and uplift in different ways. This understanding helps analyze climate and tectonic signals in geological records. By comparing the transient and steady-state responses of the landscape to changes in rainfall and uplift rates, we have drawn the following four main conclusions:

First, the slope of the headwater river channel is an important signal for distinguishing rainfall forcing from uplift forcing. Because rainfall is a distributed change, it immediately triggers an adjustment in the erosion capacity of the entire drainage basin, resulting in a temporary change in channel slope at the headwaters. In contrast, tectonic uplift is a boundary change that migrates upstream in the form of erosion waves. Therefore, before the erosion wave arrives, the slope at the headwaters remains constant, which is a characteristic of tectonic activity.

Second, the response time of the landscape to changes in rainfall rate and uplift rate varies. Due to the non-linear (power-law) relationship between rainfall rate and erosion efficiency, the landscape recovers more quickly from an increase in rainfall rate than from a decrease, particularly under orographic rainfall conditions. In contrast, the response times to changes in uplift rate are broadly similar, indicating that the duration of the transient state may help distinguish rainfall forcing from uplift forcing.

Third, divide migration is sensitive to changes in rainfall rate under orographic rainfall conditions, but relatively insensitive to changes in uplift rate. We find that changes in rainfall rate alter the gradient in

erosion rate across the divide, driving large-scale migration. In contrast, although changes in uplift rate affect local rainfall rates, the rainfall-rate gradient across the divide remains largely unchanged. Therefore, the distance of the divide migration is limited. Large-scale divide migration is more likely a signal of climate change rather than tectonic activity.

Finally, in the steady state, the mean elevation of the landscape is linearly related to the uplift rate, whereas it shows a negative power-law relationship with the rainfall rate. The non-linear relationship indicates the significant sensitivity of the landscape in arid and semi-arid regions to climate change. Although our model simplifies the response of the landscape, it demonstrates how landscapes record climate and tectonic history and the underlying mechanisms involved.

Acknowledgements

The first author gratefully acknowledges the financial support from the China Scholarship Council (CSC) and the School of Geosciences at the University of Sydney.

Disclosure statement

No potential conflict of interest was reported by the authors.

ORCID

Yinbing Zhu[1] (https://orcid.org/0000-0002-4115-3308)

Patrice F. Rey[1] (https://orcid.org/0000-0002-1767-8593)

Tristan Salles[1] (https://orcid.org/0000-0001-6095-7689)

Data Availability Statement

Version 2.2.0 of Badlands used for the landscape and sedimentary evolution modeling is preserved at https:// doi.org/10.5281/zenodo.1069573 (Salles & Howson, 2017), available via GNU General Public License v3.0 and developed openly at https://github.com/badlands-model/badlands. The TopoToolbox v2.3.1 library is available at https://topotoolbox.wordpress.com/ download/.

References

Allen, P. A. (2008). Time scales of tectonic landscapes and their sediment routing systems. *Geological Society, London, Special Publications, 296*(1), 7-28. https://doi.org/10.1144/sp296.2

Bonnet, S., & Crave, A. (2006). Macroscale dynamics of experimental landscapes. *Geological Society, London, Special Publications, 253*(1), 327-339. https://doi.org/10.1144/GSL.SP.2006.253.01.17

Crosby, B. T., & Whipple, K. X. (2006). Knickpoint initiation and distribution within fluvial networks: 236 waterfalls in the Waipaoa River, North Island, New Zealand. *Geomorphology, 82*(1-2), 16-38. https://doi.org/10.1016/j.geomorph.2005.08.023

Deng, Y., Wilson, J. P., & Bauer, B. O. (2007). DEM resolution dependencies of terrain attributes across a landscape. *International Journal of Geographical Information Science, 21*(2), 187-213. https://doi.org/10.1080/13658810600894364

Ferrier, K. L., Huppert, K. L., & Perron, J. T. (2013). Climatic control of bedrock river incision. *Nature, 496*(7444), 206-209. https://doi.org/10.1038/nature11982

Flint, J.-J. (1974). Stream gradient as a function of order, magnitude, and discharge. *Water Resources Research, 10*(5), 969-973. https://doi.org/10.1029/WR010i005p00969

Forte, A. M., & Whipple, K. X. (2018). Criteria and tools for determining drainage divide stability. *Earth and Planetary Science Letters*, *493*, 102-117. https://doi.org/10.1016/j.epsl.2018.04.026

Gailleton, B., Mudd, S. M., Clubb, F. J., Peifer, D., & Hurst, M. D. (2019). A segmentation approach for the reproducible extraction and quantification of knickpoints from river long profiles. *Earth Surface Dynamics*, *7*(1), 211-230. https://doi.org/10.5194/esurf-7-211-2019

Goulden, T., Hopkinson, C., Jamieson, R., & Sterling, S. (2014). Sensitivity of watershed attributes to spatial resolution and interpolation method of LiDAR DEMs in three distinct landscapes. *Water Resources Research*, *50*(3), 1908-1927. https://doi.org/10.1002/2013wr013846

Hack, J. T. (1957). Studies of longitudinal stream profiles in Virginia and Maryland. https://doi.org/10.3133/pp294B

Han, J., Gasparini, N. M., & Johnson, J. P. L. (2015). Measuring the imprint of orographic rainfall gradients on the morphology of steady - state numerical fluvial landscapes. *Earth Surface Processes and Landforms*, *40*(10), 1334-1350. https://doi.org/10.1002/esp.3723

He, C., Yang, C. J., Turowski, J. M., Rao, G., Roda-Boluda, D. C., & Yuan, X. P. (2021). Constraining tectonic uplift and advection from the main drainage divide of a mountain belt. *Nat Commun*, *12*(1), 544. https://doi.org/10.1038/s41467-020-20748-2

Hurst, M. D., Mudd, S. M., Yoo, K., Attal, M., & Walcott, R. (2013). Influence of lithology on hillslope morphology and response to tectonic forcing in the northern Sierra Nevada of California. *Journal of Geophysical Research: Earth Surface*, *118*(2), 832-851. https://doi.org/10.1002/jgrf.20049

Kirby, E., & Whipple, K. X. (2012). Expression of active tectonics in erosional landscapes. *Journal of Structural Geology*, *44*, 54-75. https://doi.org/10.1016/j.jsg.2012.07.009

Korup, O., & Schlunegger, F. (2009). Rock-type control on erosion-induced uplift, eastern Swiss Alps. *Earth and Planetary Science Letters*, *278*(3-4), 278-285. https://doi.org/10.1016/j.epsl.2008.12.012

Lague, D. (2014). The stream power river incision model: evidence, theory and beyond. *Earth Surface Processes and Landforms*, *39*(1), 38-61. https://doi.org/10.1002/esp.3462

Leonard, J. S., & Whipple, K. X. (2021). Influence of Spatial Rainfall Gradients on River Longitudinal Profiles and the Topographic Expression of Spatially and Temporally Variable Climates in Mountain Landscapes. *Journal of Geophysical Research: Earth Surface*, *126*(12). https://doi.org/10.1029/2021jf006183

Montgomery, D. R. (2001). Slope Distributions, Threshold Hillslopes, and Steady-state Topography. *American Journal of Science*, *301*(4-5), 432-454. https://doi.org/10.2475/ajs.301.4-5.432

Mudd, S. M., Clubb, F. J., Gailleton, B., & Hurst, M. D. (2018). How concave are river channels? *Earth Surface Dynamics*, *6*(2), 505-523. https://doi.org/10.5194/esurf-6-505-2018

Pedregosa, F., Varoquaux, G., Gramfort, A., Michel, V., Thirion, B., Grisel, O., Blondel, M., Prettenhofer, P., Weiss, R., & Dubourg, V. (2011). Scikit-learn: Machine learning in Python. *the Journal of machine Learning research*, *12*, 2825-2830.

Pelletier, J. D. (2008). The diffusion equation. In *Quantitative Modeling of Earth Surface Processes* (pp. 30-65). Cambridge University Press. https://doi.org/10.1017/cbo9780511813849.003

Roe, G. H. (2005). Orographic Precipitation. *Annual Review of Earth and Planetary Sciences*, *33*(1), 645-671. https://doi.org/10.1146/annurev.earth.33.092203.122541

Salles, T., Ding, X., & Brocard, G. (2018). pyBadlands: A framework to simulate sediment transport, landscape dynamics and basin stratigraphic evolution through space and time. *PLoS One*, *13*(4), e0195557. https://doi.org/10.1371/journal.pone.0195557

Salles, T., & Hardiman, L. (2016). Badlands: An open-source, flexible and parallel framework to study landscape dynamics. *Computers & Geosciences*, *91*, 77-89. https://doi.org/10.1016/j.cageo.2016.03.011

Schwanghart, W., & Kuhn, N. J. (2010). TopoToolbox: A set of Matlab functions for topographic analysis. *Environmental Modelling & Software*, *25*(6), 770-781. https://doi.org/10.1016/j.envsoft.2009.12.002

Schwanghart, W., & Scherler, D. (2014). TopoToolbox 2 – MATLAB-based software for topographic analysis and modeling in Earth surface sciences. *Earth Surface Dynamics*, *2*(1), 1-7. https://doi.org/10.5194/esurf-2-1-2014

Seybold, H., Berghuijs, W. R., Prancevic, J. P., & Kirchner, J. W. (2021). Global dominance of tectonics over climate in shaping river longitudinal profiles. *Nature Geoscience*, *14*(7), 503-507. https://doi.org/10.1038/s41561-021-00720-5

Shan, L., Yang, X., & Zhu, Q. (2019). Effects of DEM resolutions on LS and hillslope erosion estimation in a burnt landscape. *Soil Research, 57*(7). https://doi.org/10.1071/sr19043

Smith, A. G. G., Fox, M., Schwanghart, W., & Carter, A. (2022). Comparing methods for calculating channel steepness index. *Earth-Science Reviews*, *227*. https://doi.org/10.1016/j.earscirev.2022.103970

Snyder, N. P., Whipple, K. X., Tucker, G. E., & Merritts, D. J. (2000). Landscape response to tectonic forcing: Digital elevation model analysis of stream profiles in the Mendocino triple junction region, northern California. *Geological Society of America Bulletin*, *112*(8), 1250-1263. https://doi.org/10.1130/0016-7606(2000)112<1250:lrttfd>2.0.co;2

Snyder, N. P., Whipple, K. X., Tucker, G. E., & Merritts, D. J. (2002). Interactions between onshore bedrock-channel incision and nearshore wave-base erosion forced by eustasy and tectonics. *Basin Research*, *14*(2), 105-127. https://doi.org/10.1046/j.1365-2117.2002.00169.x

Whipple, K. X., DiBiase, R. A., & Crosby, B. T. (2013). 9.28 Bedrock Rivers. In J. Shroder, Wohl, E. (Ed.), *Treatise on Geomorphology* (Vol. 9, Fluvial Geomorphology, pp. 550-573). Academic Press. https://doi.org/10.1016/b978-0-12-374739-6.00254-2

Whipple, K. X., & Tucker, G. E. (1999). Dynamics of the stream-power river incision model: Implications for height limits of mountain ranges, landscape response timescales, and research needs. *Journal of Geophysical Research: Solid Earth*, *104*(B8), 17661-17674. https://doi.org/10.1029/1999jb900120

Whipple, K. X., & Tucker, G. E. (2002). Implications of sediment-flux-dependent river incision models for landscape evolution. *Journal of Geophysical Research*, *107*(B2). https://doi.org/10.1029/2000jb000044

Whittaker, A. C. (2012). How do landscapes record tectonics and climate? *Lithosphere*, *4*(2), 160-164. https://doi.org/10.1130/rf.L003.1

Willett, S. D., & Brandon, M. T. (2002). On steady states in mountain belts. *Geology*, *30*(2), 175. https://doi.org/10.1130/0091-7613(2002)030<0175:ossimb>2.0.co;2

Willett, S. D., McCoy, S. W., Perron, J. T., Goren, L., & Chen, C. Y. (2014). Dynamic reorganization of river basins. *Science*, *343*(6175), 1248765. https://doi.org/10.1126/science.1248765

Willett, S. D., Slingerland, R., & Hovius, N. (2001). Uplift, Shortening, and Steady State Topography in Active Mountain Belts. *American Journal of Science*, *301*(4-5), 455-485. https://doi.org/10.2475/ajs.301.4-5.455

Wobus, C., Whipple, K. X., Kirby, E., Snyder, N. P., Johnson, J., Spyropolou, K., Crosby, B., & Sheehan, D. (2006). Tectonics from topography: Procedures, promise, and pitfalls. *Tectonics, Climate, and Landscape Evolution*, *398*, 55-74. https://doi.org/10.1130/2006.2398(04)

Zavala, V., Carretier, S., & Bonnet, S. (2020). Influence of orographic precipitation on the topographic and erosional evolution of mountain ranges. *Basin Research*, *32*(6), 1574-1599. https://doi.org/10.1111/bre.12443

Zhu, Y., Rey, P., & Salles, T. (2025). Rainfall and tectonic forcing lead to contrasting headwater slope evolutions. *Earth Surf. Dynam.*, *13*(6), 1249-1261. https://doi.org/10.5194/esurf-13-1249-2025

4 Article 3

Evaluating Central Andean Altiplano uplift histories with numerical model: a quantitative comparison of fold setups and uplift scenarios

Yinbing Zhu[1], Patrice Rey[1], Tristan Salles[1]

[1]School of Geosciences, University of Sydney, Sydney, NSW, 2006, Australia

A version of this chapter has been prepared for submission to journal *Earth Surface Processes and Landforms*. It is prepared in the *Earth Surface Processes and Landforms* journal format.

Abstract

The uplift history of the Altiplano in the Central Andes and its coupling mechanism with landscape evolution have long been controversial. To quantitatively evaluate the shaping effect of different tectonic uplift scenarios on landscapes, we use the landscape evolution model combined with the Earth Mover's Distance (EMD) analysis method to systematically test the combined effects of five Altiplano uplift scenarios (earlier rapid, rapid, slow and steady, stepwise, and uniform and slow) and three fold setups (no folds, vertical folds, fold shortening).

By comparing the modeling results with the normalized channel steepness index (k_{sn}) and knickpoint distribution, our study suggests that the uplift of the Altiplano is controlled by the shortening of the fold-thrust belt and low-magnitude uplift pulses in the Late Miocene. The results show that Fold Shortening (FS), which includes horizontal shortening components, most accurately reproduces the observed N-S tributary pattern and the spatial distribution of knickpoints, indicating that the horizontal movement of the fold-thrust belt plays a key role in the evolution of bedrock channels.

In the uplift scenario, the combination of stepwise uplift (SW) and fold shortening yields the highest similarity (lowest EMD value) with the modern landscape, supporting the view that the Altiplano has experienced an uplift pulse since the Late Miocene. In addition, simulations indicate that rapid and large-magnitude uplift can generate strong landscape signals that may mask the influence of local tectonic activity. Slow and steady uplift is difficult to maintain the current high-altitude characteristics of the eastern Central Andes.

This study not only provides validation for the pulse uplift hypothesis in the Altiplano but also demonstrates the potential of combining tectonic kinematics with surface processes in analyzing the evolution of orogenic belts.

Keywords: Altiplano uplift, landscape, channel steepness index, knickpoint, Earth Mover's Distance, fold shortening

1. INTRODUCTION

The Andes have been one of the most popular areas for studying plate subduction and mountain building. The average altitude of the plateau (Altiplano) in the Central Andes reaches ~3.7 km, and some areas exceed 4.5 km. Although many studies have examined the uplift of the Altiplano, its uplift history remains controversial. The focus of the controversy is whether the Altiplano has experienced rapid uplift. Studies supporting the rapid uplift scenario suggest that the central Altiplano experienced a rapid pulse of ~2.5 ± 1 km of surface uplift between 10 and 6 Ma (e.g., Ghosh et al., 2006; Garzione et al., 2006; Garzione et al., 2008). In addition, the uplift of the southern Altiplano is earlier than that of the central Altiplano. Its paleoelevation rapidly increased ~2.6 ± 0.7 km between 16 and 9 Ma (Garzione et al., 2014). In contrast, other studies suggest that the Altiplano may have risen slowly and steadily since before the Miocene, or it may have experienced a small pulse of uplift between ~10 and ~6 Ma (Insel et al., 2012; Ehlers and Poulsen, 2009; Fiorella et al., 2015). Combining stable isotopes, paleobotany, paleoclimate, and other geological evidence, previous studies suggest that the paleoelevation of the Altiplano was less than ~2 km by the late Oligocene (e.g., Kar et al., 2016; Insel et al., 2012; Hoke and Garzione, 2008; Garzione et al., 2008; Garzione et al., 2006; Garzione et al., 2017; Fiorella et al., 2015; Gregory-Wodzicki, 2000). Some studies further restrict it to about ~1.1-1.5 km (Leier et al., 2013; Garzione et al., 2014; Lamb and Hoke, 1997). According to different hypotheses and the corresponding supporting evidence, Table 1 and Figure 1 summarize five hypothesized uplift scenarios of the Altiplano.

Table 1. Summary of Altiplano uplift scenarios used in this study

Uplift scenario	Time-Elevation Pairs (Ma-km)				Notes
Slow and steady (SS)	25-1.1	0-3.7			Linear trend (Insel et al., 2012)
Stepwise (SW)	25-2.0	10-2.0	6-3.1	0-3.7	High initial elevation, then stepwise rise (Insel et al., 2012)
Uniform and slow (US)	25-1.5	11.5-2.2	6-3.7	0-3.7	Slow uplift and reached modern elevation by 6 Ma (Fiorella et al., 2015)
Earlier rapid (ER)	25-1.1	16-1.1	13-3.0	9-3.7 0-3.7	Rapid uplift after 16 Ma (Garzione et al., 2014)
Rapid uplift (RU)	25-1.1	10-1.2	6-3.7	0-3.7	Rapid uplift after 10 Ma (Garzione et al., 2008)

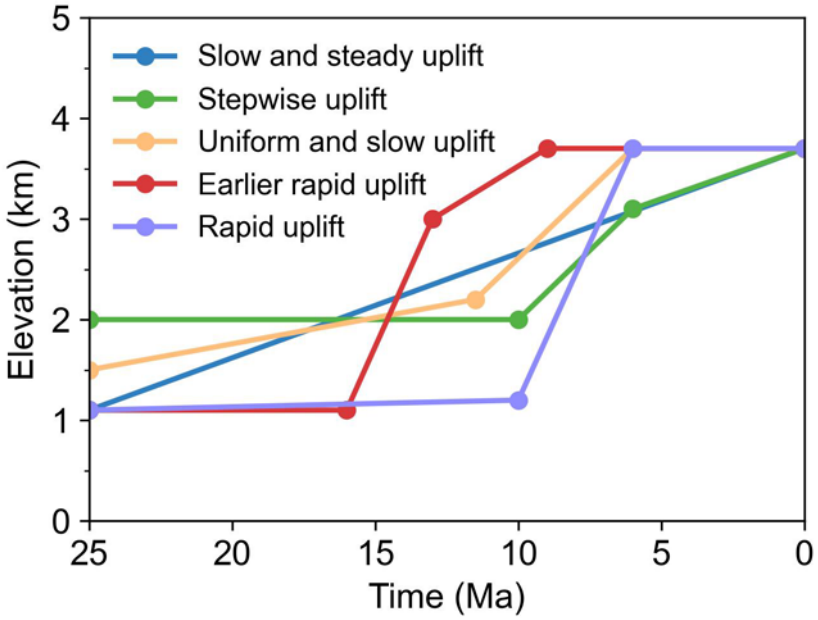

Figure 1. Five hypothesized uplift scenarios of the Altiplano. Data points correspond to Time-Elevation Pairs in Table 1.

The uplift of the Altiplano blocked the moisture-rich northeasterly winds blowing from the Amazon Basin (Insel et al., 2012; Poulsen et al., 2010; Ehlers and Poulsen, 2009). This moisture is lifted over the mountain range, resulting in an increased rainfall rate on the eastern flank and a rainshadow on the western flank (Evenstar et al., 2023; Ehlers and Poulsen, 2009; Houston and Hartley, 2003). The rainfall rate on the eastern flank of the Altiplano reaches the range of 500 to 4000 mm/yr (Figure 2a) (Bookhagen and Strecker, 2008).

Paleoclimate modelling that considers the sensitivity of oxygen isotopes to climate suggests that rainfall rate is positively correlated with Altiplano elevation (Insel et al., 2012; Garzione et al., 2017). In contrast, the rainfall rate of the Atacama Desert to the west of the Altiplano has decreased due to the uplift of the Altiplano (Rech et al., 2006; Houston and Hartley, 2003). The Atacama Desert had a semi-arid climate during the early Miocene (24-20 Ma) (Rech et al., 2019). With the uplift of the Altiplano, a rainshadow effect initiated by 15 Ma and reached a level that transformed the climate to extreme hyperaridity by 12-10 Ma (Rech et al., 2019; Rech et al., 2006; Jordan et al., 2014). The modern rainfall rate in the Atacama Desert is ~20 mm/yr (Strecker et al., 2007).

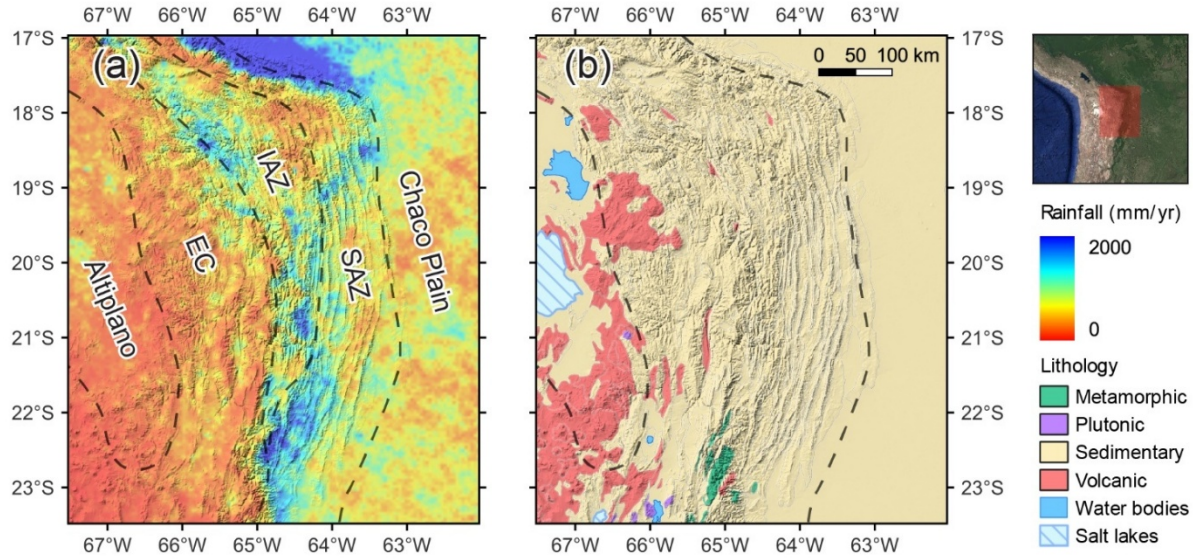

Figure 2. (a) Rainfall rate map (TRMM 2B31) and (b) Lithology map of the Altiplano and its eastern flank. EC = Eastern Cordillera; IAZ = Interandean zone; SAZ = Subandean zone.

Despite extensive studies, the uplift history of the Altiplano remains contentious. One approach that has not yet been explored in depth is landscape analysis. Different uplift scenarios should produce distinct landscape signatures in topographic characteristics. Landscape evolution models provide a powerful tool to test competing uplift hypotheses by simulating topographic development under different uplift scenarios and comparing model outputs with observed landscapes. In this study, we use landscape evolution models to simulate the five hypothesized uplift scenarios (Table 1, Figure 1) for the Central Andes. We extract topographic metrics, drainage patterns, and river profiles from both the simulated landscapes and the DEM of the modern Andes. By comparing these landscape features between model results and observations, we aim to determine which uplift scenarios produce landscape signatures consistent with the current Andes landscape.

2. METHODOLOGY AND METHODS

2.1 Experimental Design

Before the simulation, we first consider the lithology of the study area. The lithology in the Central Andes varies spatially (Figure 2b). The Western Cordillera has been affected by extensive volcanic activities and is largely covered by andesitic and rhyolitic rocks (Gómez et al., 2019). The Altiplano is a transition area where both sedimentary and volcanic rocks and associated sediments are exposed. To its east, in the Eastern Cordillera, the Interandean Zone, and the Subandean Zone, the lithology is almost entirely sedimentary rocks. The drainage basins in our study area are all located on the eastern flank of the Altiplano. Therefore, the

lithology is assumed to be spatially homogeneous, i.e., the erosion coefficient (erodibility) is constant.

In addition to lithology, initial topography, tectonic events, and rainfall are also important. We design and test three fold setups in the model to evaluate each of the five hypothesized uplift scenarios (Table 1).

To provide a clear conceptual framework of the model setups, the integrated 3D configuration of tectonic forcing (vertical uplift and horizontal shortening) and climatic condition (orographic rainfall) used in this study is schematically illustrated in Figure 3.

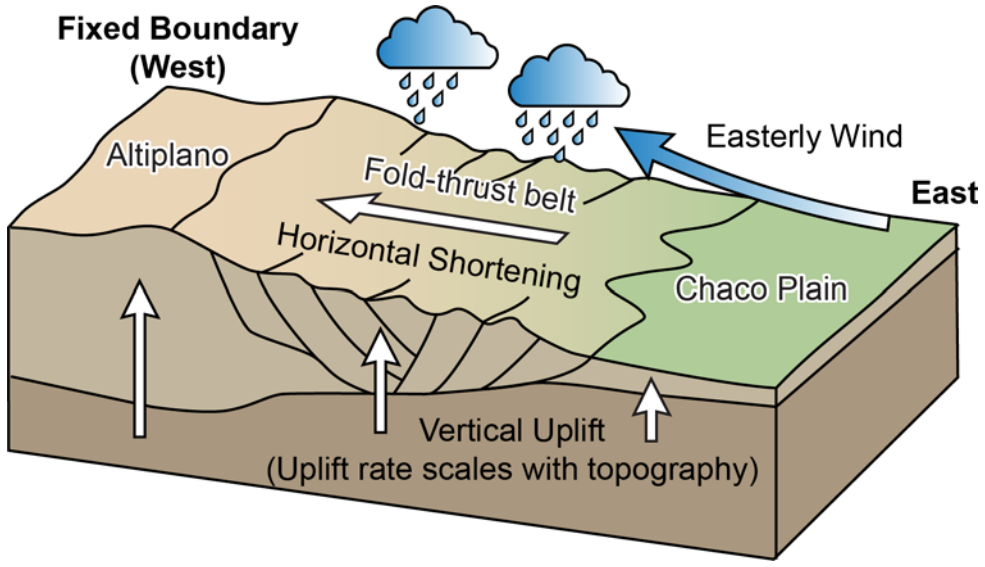

Figure 3. 3D conceptual model illustrating the coupling of vertical uplift, horizontal shortening, and orographic rainfall.

Setup 1: Altiplano uplift without fold (No Fold, NF)
We construct initial topography by scaling the modern DEM to match hypothesized paleoelevations at specific time periods (Table 1). First, we smooth the modern 30-m SRTM DEM of the eastern Central Andes (17°–24°S, 62°–67.5°W) using a Gaussian filter with a 30 km radius. The smoothing wavelength preserves first-order topographic features (part of the Altiplano, the eastern slope, and the foreland Chaco Plain) while removing the detailed drainage network and local relief of the modern topography. The smoothing approach minimizes the influence of the well-developed modern channel network on model evolution, allowing the model to self-organize and develop drainage patterns naturally under the imposed climatic and tectonic forcing. We scale this smoothed DEM (DEM_smoothed) by the ratio of paleoelevation to modern elevation to generate initial topography. For example, under the rapid uplift scenario, the Altiplano is 1.1 km high at 25 Ma compared to the modern 3.7 km. Therefore, DEM (25 Ma) = Modern DEM × 1.1/3.7 (Figure 4a). We assume that the spatial distribution of topography was similar in the past, with elevations proportionally lower.

We calculate uplift between time control points (Table 1). For example, the Altiplano rises from 1.1 to 1.2 km between 25 Ma and 10 Ma in the rapid uplift scenario. The field of uplift rate is: Uplift rate (25-10 Ma)=DEM_smoothed×((1.2-1.1)/3.7)/15 Myr. The uplift rate is applied uniformly across the model at each time step.

For rainfall, we impose easterly winds on a background rainfall rate of 800 mm/yr. While this approach does not precisely replicate the modern rainfall distribution, it enables the model to self-generate orographic rainfall patterns in response to evolving topography, thereby simulating spatial rainfall variability.

Setup 2: Altiplano uplift with vertical fold growth (Vertical Fold, VF)

To simulate the spatial complexity of deformation on the eastern flank, we superimpose vertical deformation of the fold-thrust belt onto the Altiplano uplift described above. We use 3D software (Blender) to extract the geometry of major folds with vertical relief exceeding 400 m, combining the DEM and structural maps (Gómez Tapias et al., 2019). These structures are particularly well defined in the Interandean and Subandean Zones, where N-S-striking folds are prominent. The fold topography is superimposed on DEM_smoothed to create a new modern topography (Figure 4b). Following the same approach as Setup 1, we scale the new modern topography to obtain the initial topography for past time periods. Uplift rates and rainfall changes are calculated using the same method as Setup 1.

Setup 3: Altiplano uplift with active fold shortening and growth (Fold Shortening, FS)

The tectonic evolution of the fold-thrust belt involves a large amount of horizontal shortening. Previous studies using balanced cross-sections and geophysical data estimate the total shortening of the entire retroarc thrust belt at 21°S to be 337 ± 69 km (Anderson et al., 2018; Anderson et al., 2017). Within our study area, the post-25 Ma shortening of the fold-thrust belt ranges from 170 to 220 km with latitudinal variations, reaching maximum values at 20°–21°S. To incorporate fold-thrust belt shortening while simplifying the model, we set uniform E-W shortening to 190 km with no latitudinal variation. We horizontally extend the initial topography from Setup 2 by 190 km in the E-W direction to create the initial topography for this Setup (Figure 4c). The western boundary of the model domain is fixed, and the topography progressively shortens westward during the simulation (Figures 3 and 4c). The shortening rate is calculated in the same manner as the uplift rate in Setup 1, which means the shortening rate is proportional to the uplift rate.

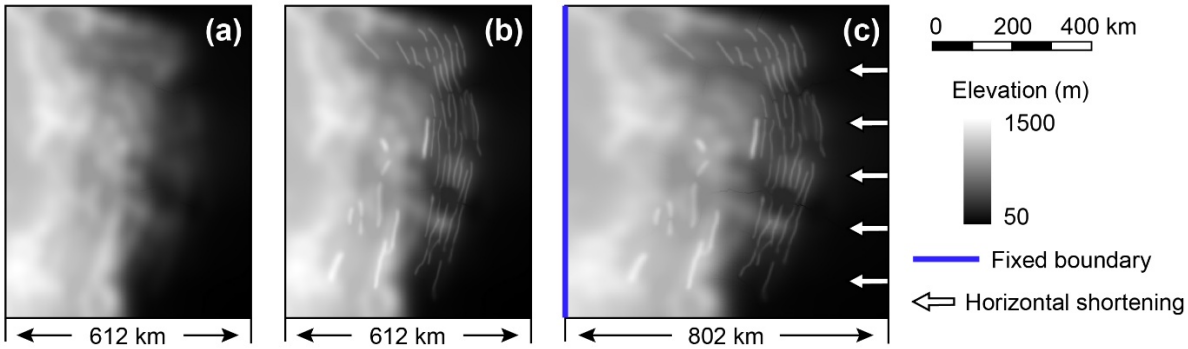

Figure 4. Three different initial topography maps used as model inputs. (a) Scaled and smoothed DEM used for the no-fold setup. (b) Scaled and smoothed DEM with folds used for the vertical-fold setup. (c) Extended (190 km E–W), scaled, and smoothed DEM with folds used for the fold-shortening setup.

We conduct a total of 15 modeling cases combining the five hypothesized uplift scenarios (Table 1) with the three model setups (Table 2). By comparing the results, we can evaluate which combinations of uplift history and perturbations produce landscape characteristics most consistent with the modern eastern Altiplano.

Table 2. Summary of fold-thrust setups in the model

Fold Setup	Tectonic configuration	Initial Topography	Rainfall input
Setup 1 (NF)	Altiplano uplift without folds	Smoothed scaled modern DEM	Background rainfall + easterly winds
Setup 2 (VF)	Altiplano uplift + fold uplift	Smoothed scaled modern DEM with fold topography	Background rainfall + easterly winds
Setup 3 (FS)	Altiplano uplift + fold uplift + horizontal shortening	Smoothed, scaled, and extended (190 km E-W) modern DEM with fold topography	Background rainfall + easterly winds

2.2 Modeling and Analyzing

We use the Badlands model to simulate landscape evolution from 25 Ma to the present. Badlands is an open-source surface-process model that simulates hillslope processes, fluvial incision using the stream-power law, sediment transport and deposition, and the coupled effects of spatially and temporally varying tectonics and climate (Salles and Howson, 2017; Salles and Hardiman, 2016). The model parameters include rainfall rate, erodibility, diffusion coefficient, etc. The choice of the erodibility is crucial. An excessively high erodibility will remove diagnostic landscape features, while an excessively low erodibility will fail to reflect the differentiated impacts of different tectonic uplifts on topography. To preserve

geomorphic variability while still allowing erosion, we select an intermediate erodibility value. Since the primary purpose of the study is to compare and test different uplift scenarios, the erodibility value remains constant in all cases. Detailed model parameters are listed in Supplementary Table S1.

We use TopoToolbox (Schwanghart and Scherler, 2014), a MATLAB-based toolbox for topographic analysis, to get geomorphic indices of both the modern DEM and the simulated landscapes. We focus on the four largest drainage basins that occupy most of the study area and have well-developed drainage networks. For the modern DEM, knickpoints located at mapped lithological boundaries are excluded to minimize lithological effects.

2.3 Geomorphic Indices

In quantitative geomorphic studies, various indices are employed to characterize landscape features, among which the normalized channel steepness index k_{sn} is one of the most widely applied parameters. It establishes a power-law relationship between channel slope *S* and upstream drainage area *A* based on the stream power law:

$$S = k_s A^{-\theta} \quad (1)$$

where k_s is the channel steepness index, and θ is the concavity index (Flint, 1974). Previous studies indicate that θ values in most regions range between 0.3 and 0.6 (e.g., Snyder et al., 2000; Flint, 1974; Hack, 1957). In this study, we adopt a standard reference concavity of $\theta_{ref} = 0.45$ to normalize k_s into k_{sn}. k_{sn} is frequently used to investigate the relative influences of tectonic forcing and climatic variations on landscape evolution (e.g., Whipple and Gasparini, 2014; Wolpert and Schoenbohm, 2025; Safran et al., 2005). In transient river systems affected by tectonic or climatic perturbations, knickpoints often develop. Knickpoints are boundaries that divide the river channel into two segments: an upstream relic channel, which has not adjusted to perturbations, and a downstream channel that has reached a steady state (Crosby and Whipple, 2006). The development of knickpoints is linked to k_{sn}, typically manifesting as a significant k_{sn} gradient where values in the adjacent downstream channel are higher than those in the adjacent upstream channel. Consequently, the amount and spatial distribution of knickpoints can help to study the history of transient landscape evolution.

In addition to k_{sn}, the integral quantity χ (chi) is widely used in quantitative landscape analysis. χ derives from the integration of the stream power law. The χ-transformation converts the longitudinal distance into a coordinate that accounts for the distribution of upstream drainage area. The integration method inherently suppresses the noise in

topographic data, making deviations from steady-state conditions, such as knickpoints, more distinguishable in χ-elevation space (Perron and Royden, 2013).

2.4 Quantitative Model Evaluation Strategy

To evaluate the similarity between simulated and observed landscapes, we use the Earth Mover's Distance (EMD), also known as the Wasserstein metric (Rubner et al., 2000). EMD is a measure of the difference between two probability distributions. Its intuitive meaning is: the minimum amount of work or cost required to 'transport' one distribution to another. In point cloud similarity calculation, point clouds are treated as discrete probability distributions. EMD can simultaneously account for the geometric positions and density distributions of point clouds. It has good robustness to noise and slight deformation.

We first normalize the χ and elevation values of the knickpoints to the maximum χ and elevation values within the study area, so that their range is [0, 1]. We then project the knickpoints onto normalized χ-elevation space to form point clouds. The similarity between the simulated and observed point clouds can be characterized using EMD. A lower EMD value indicates a higher degree of similarity between the simulated and modern landscapes.

3. RESULTS

3.1 Geomorphic Characteristics of the Modern Landscape

The mapped k_{sn} values show an increasing trend from east to west (Figure 5a). Downstream channels on the Chaco Plain are characterized by low k_{sn} values (<50) and lack knickpoints. Westward along the channels, N-S-striking tributaries develop, and k_{sn} increases, accompanied by the appearance of knickpoints. Farther west, channels generally have higher k_{sn} values (>150), and knickpoints are widespread in both tributaries and trunk streams. No knickpoints meeting the extraction criteria are identified on the low-relief Altiplano. In χ-elevation space, channel profiles are widely scattered and commonly display an upward-convex form. Knickpoints are mainly distributed at elevations of 1000-3500 m and χ values of 3000-9000 m (Figure 5b).

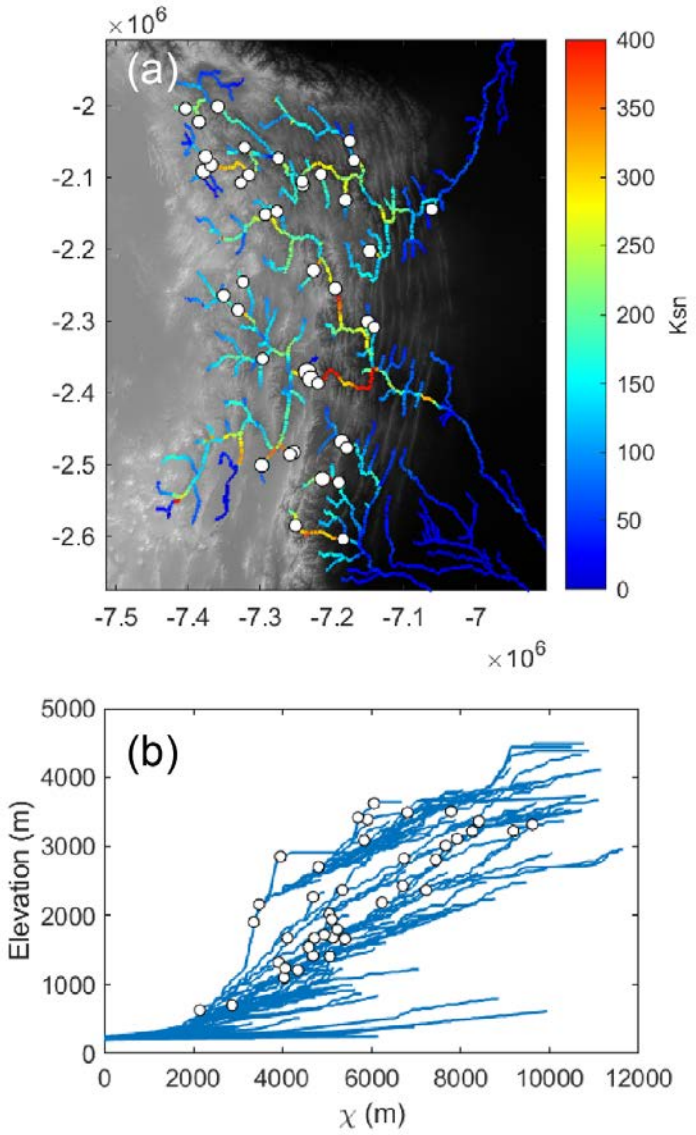

Figure 5. (a) k_{sn} maps with knickpoints (white dots) for the modern DEM of the study area. Each white dot represents a knickpoint. The coordinate system is WGS 84/World Mercator. (b) Channels and knickpoints in χ-elevation space.

3.2 Spatial Distribution of k_{sn} and Knickpoints of modeling landscapes

The modeling landscapes show that the drainage network, k_{sn} magnitude, and knickpoint development are significantly controlled by variations in fold setup and uplift scenarios (Figure 6).

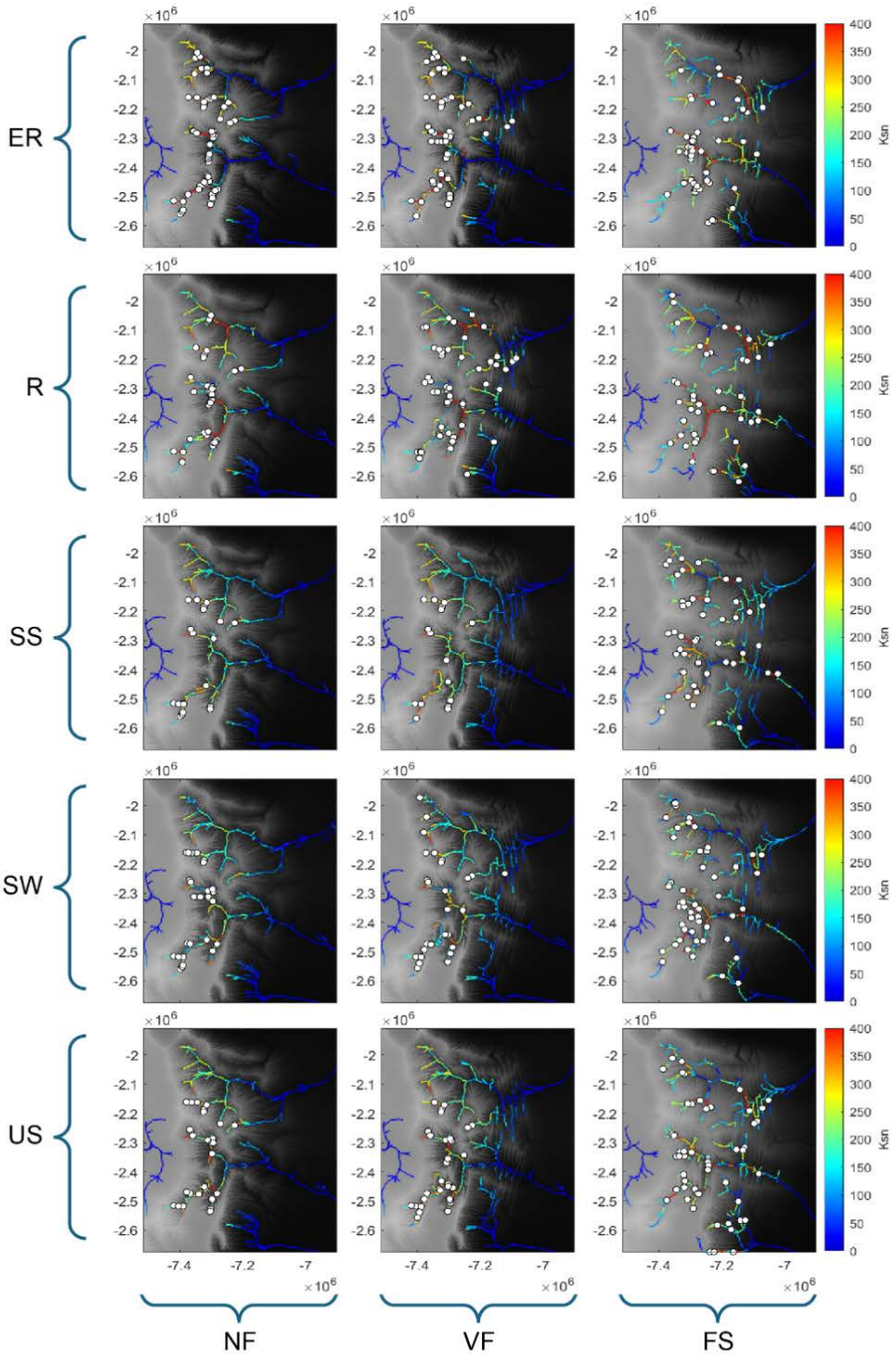

Uplift scenarios: Earlier Rapid (ER), Rapid (R), Slow and Steady (SS), Stepwise (SW), Uniform and Slow (US)

Fold setups: No Fold (NF), Vertical Fold (VF), and Fold Shortening (FS)

Figure 6. k_{sn} maps with knickpoints (white dots) for 15 modeling cases. Each white dot represents a knickpoint. Each row represents an uplift scenario: Earlier Rapid (ER), Rapid (R), Slow and Steady (SS), Stepwise (SW), and Uniform and Slow (US). Each column represents a fold setup: No Fold (NF), Vertical Fold (VF), and Fold Shortening (FS). The coordinate system for each map is WGS 84/World Mercator.

In the NF setup, N-S-striking tributaries are absent. k_{sn} values increase from east to west (upstream), with high values concentrated in the western area. k_{sn} values of eastern channels are generally lower than 100. In contrast, in the VF and FS setups, landscapes are characterized by the development of N-S-striking channels in the east. k_{sn} values of some channels are higher than 100. Notably, most channels across the drainage basin are high in k_{sn} value (> 100) in the FS setup.

The spatial distribution of knickpoints correlates closely with k_{sn}. Knickpoints cluster in the mid and upstream channels in the NF setup, while they are widely distributed in the FS setup. Regarding quantity, the NF setup produces fewer knickpoints than the FS setup, except in the ER uplift scenario (Figure 7). In the VF setup, the distribution and quantity of knickpoint depend on the uplift scenario. For SS, SW, and US scenarios, the distribution and count of knickpoints resemble those in the NF setup. However, for ER and R scenarios, some knickpoints develop along the N-S-striking channels, resulting in a higher total count. Notably, both the minimum (16 in the SS uplift scenario under the VF fold setup, VF-SS) and the maximum (59 in the ER uplift scenario under the VF fold setup, VF-ER) numbers of knickpoints across all 15 modeling cases occur under the VF setup.

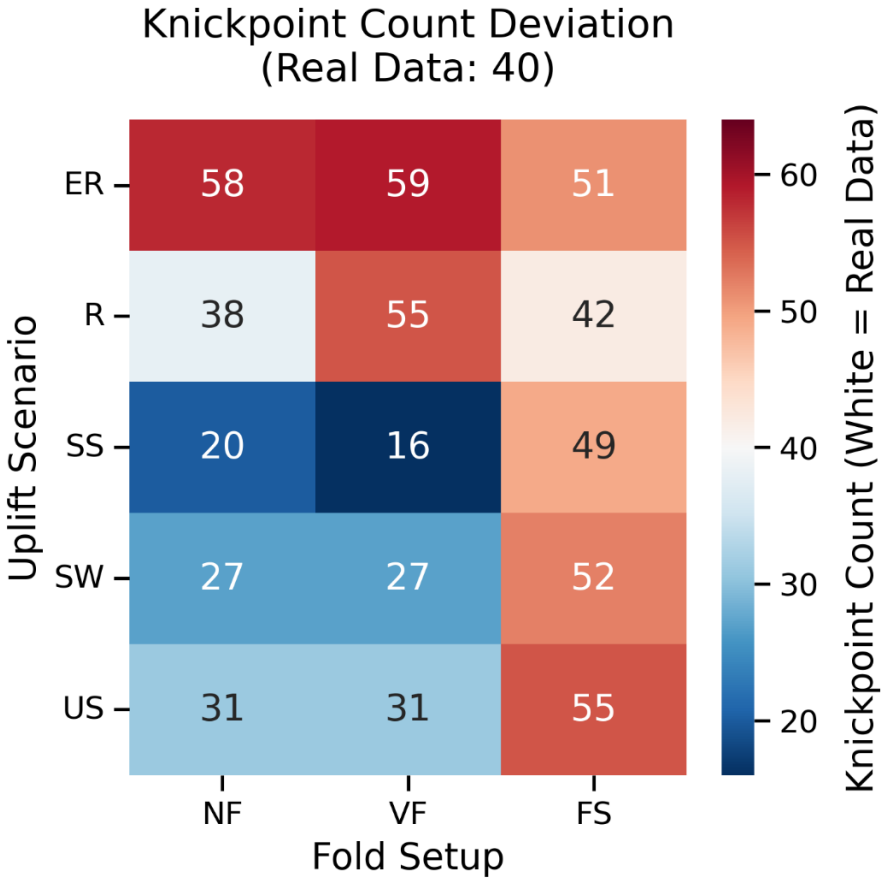

Figure 7. Heatmap of knickpoint count for 15 modeling cases.

3.3 Longitudinal Profiles of Modeling Landscapes in χ-Elevation Space

In χ–elevation space, channels on the Altiplano (~3700 m in elevation) plot as near-horizontal profiles and show no knickpoint development (Figure 8).

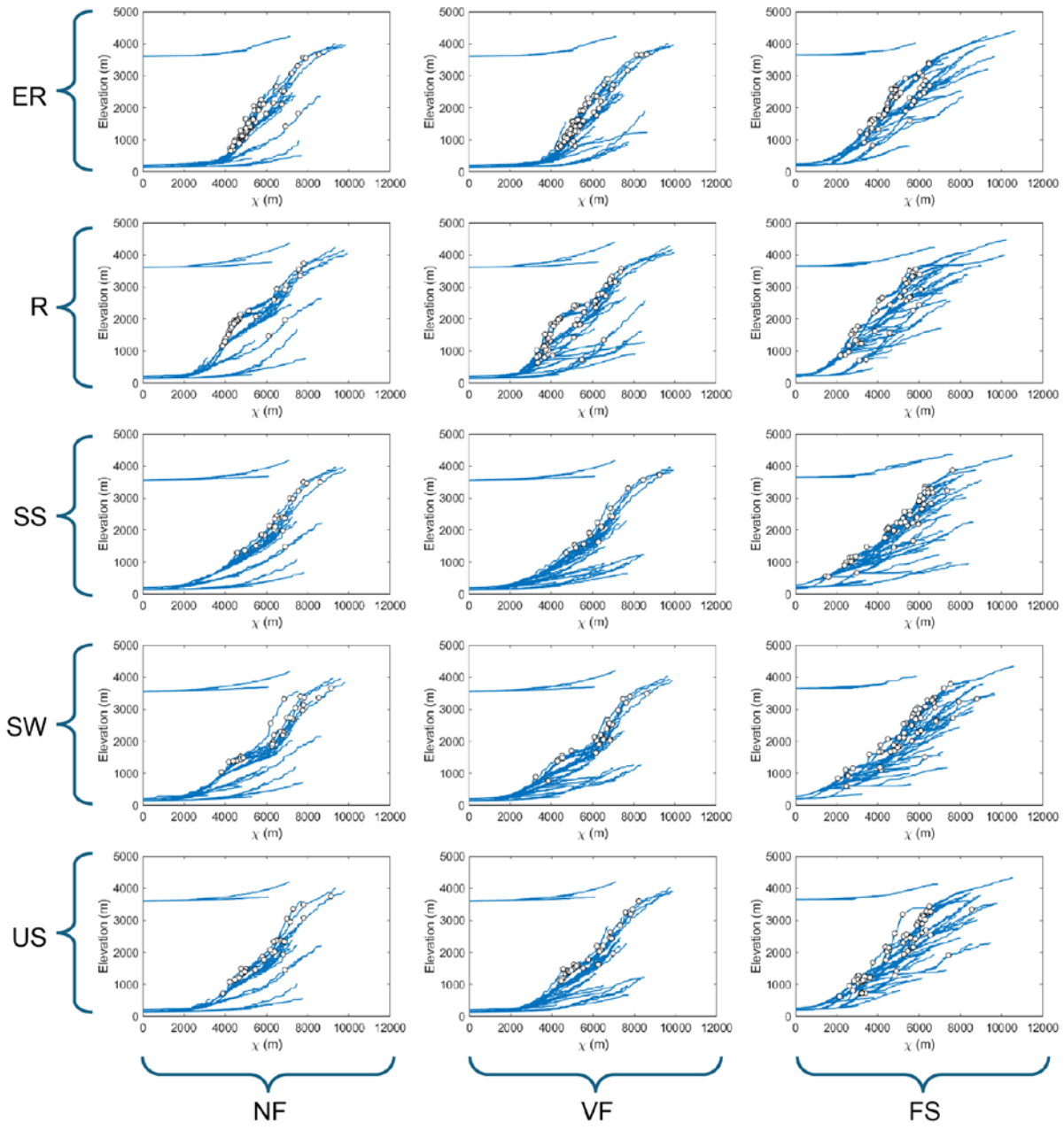

Figure 8. χ–elevation plots of channels for 15 modeling cases. Each white dot represents a knickpoint. Each row represents an uplift scenario: Earlier Rapid (ER), Rapid (R), Slow and Steady (SS), Stepwise (SW), and Uniform and Slow (US). Each column represents a fold setup: No Fold (NF), Vertical Fold (VF), and Fold Shortening (FS).

For drainage basins at lower elevations (downstream/east of the Altiplano), channel profiles under the FS setup are more dispersed in χ–elevation space than those under the VF and NF setups. Under the VF setup, channels form two different groups. One group consists of short channels restricted to low elevations (<1500 m). They are characterized by low slopes and an absence of knickpoints. Another group consists of long channels extending to high elevations. They have steeper slopes and abundant knickpoints. Under the R scenario, some channels display a convex-upward form within the χ range of 3000–6000 m, where knickpoints are densely clustered. Under the ER scenario, knickpoints are also concentrated, mainly within the χ range of 4000–6000 m. Under the NF setup, most channels extend to high elevations, and their χ–elevation morphology and knickpoint distribution resemble those of the high-elevation channel group in the VF setup. However, two key differences exist: first, there are fewer low-elevation channels, and the existing low-elevation channels are scattered in the NF setup; second, under the R scenario, the number of knickpoints in the NF setup is lower than in the VF setup.

3.4 Quantitative Model Evaluation via EMD Analysis

The Earth Mover's Distance (EMD) similarity heatmap quantifies the difference between the simulated and modern topographies, represented as knickpoint clouds in χ–elevation space (Figure 9). Lower EMD values indicate higher similarity (better match). The color bar indicates that blue represents low EMD values, while red represents high EMD values.

The results show that the fold setup has a significant impact on simulation accuracy. The FS setup consistently produces the lowest EMD values across all uplift scenarios. All values in the FS setup are below 0.10 (dark blue). In contrast, the NF and VF setups generally show higher EMD values (light red to dark red).

In all uplift scenarios, the two highest EMD values occur in the SS scenario, under the NF setup (0.2020) and the VF setup (0.1883). FS-SS is an exception with a low value (0.0860). The difference between the highest and lowest values in the SS scenario reaches 0.658. The R scenario shows relatively stable low values across all fold setups, with a difference between the highest and lowest values of 0.0089, the lowest difference among all uplift scenarios. The FS-SW case yields the lowest EMD value in all cases at 0.0758. The quantitative results indicate that the combination of the FS fold setup and the SW uplift scenario may produce the landscape most similar to the real landscape.

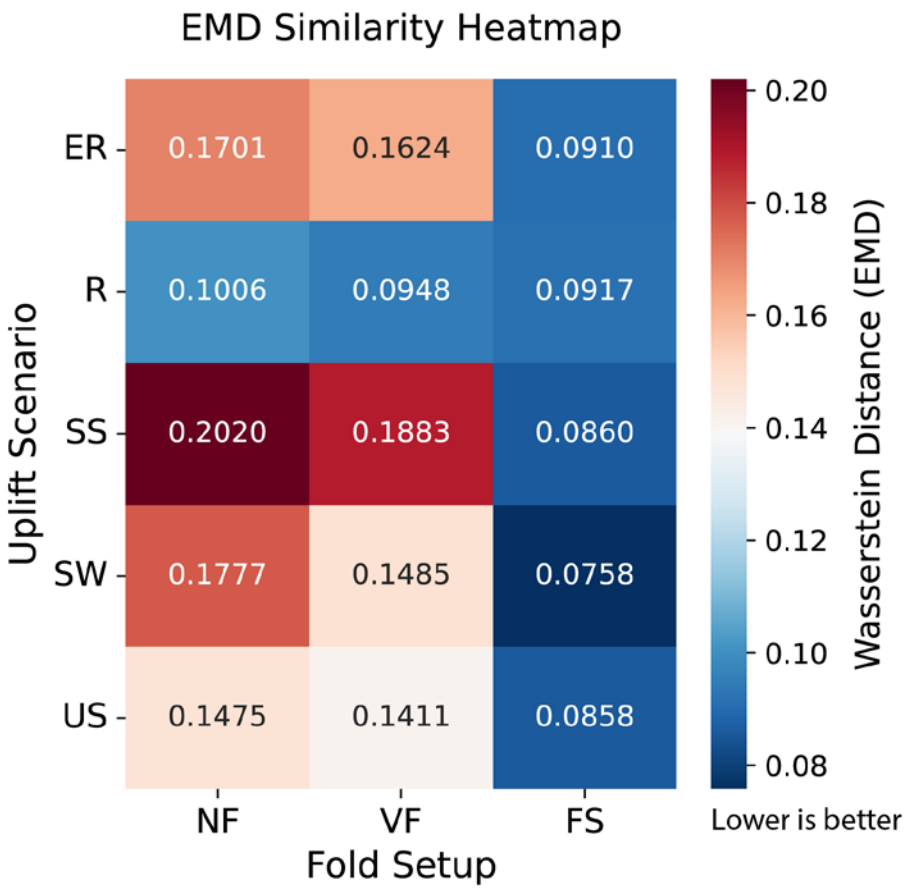

Figure 9. Earth Mover's Distance (EMD) similarity heatmap of 15 modeling cases. The lower the EMD value, the higher the similarity between the simulated knickpoint cloud and the real knickpoint cloud. Each row represents an uplift scenario: Earlier Rapid (ER), Rapid (R), Slow and Steady (SS), Stepwise (SW), and Uniform and Slow (US). Each column represents a fold setup: No Fold (NF), Vertical Fold (VF), and Fold Shortening (FS).

4. DISCUSSION

This study couples the fold setups and uplift scenarios to evaluate Altiplano uplift hypotheses using the landscape evolution model. The study results show that the combination of fold shortening (FS) and stepwise uplift (SW) produces the lowest EMD value, indicating that the FS-SW case best explains the landscape features of the modern eastern Andes.

4.1 The Role of Horizontal Shortening

The modeling results of the importance of horizontal shortening show that the setup of fold shortening (FS) produces the lowest EMD values in all uplift scenarios. The result highlights the essential role of horizontal shortening in shaping the landscape of the eastern Andes. The FS setup successfully reproduces the widely distributed N-S tributaries, the high k_{sn} value areas, and the distribution of knickpoints in the middle and lower

channels observed (Figure 6). The high degree of landscape similarity supports the geological evidence that fold-thrust shortening has continued on the eastern flank of the Altiplano since the Late Cenozoic (Anderson et al., 2018; Anderson et al., 2017). Regarding the geomorphological dynamics, horizontal shortening affects channel evolution through two mechanisms. First, horizontal advection causes surface features (divides, slopes, rivers, etc.) to continuously move westward and uplift, directly altering the physical length and drainage area of rivers. Second, due to the lateral compression of the river channel, its erosion base level rises. The continuous changes in the erosion base level mean that the river system remains in a state of long-term transient adjustment. The adjustment maintains high k_{sn} values in the middle and lower channels and triggers reorganization of the early channel network.

In contrast, although the vertical fold (VF) setup can show local changes in river flow direction, it fails to reproduce the complex distribution of knickpoints. The no fold (NF) and VF setups only simulate vertical uplift and lack horizontal motion components, so river erosion responds only in the vertical direction. The two setups reflect the first-order control of uplift on landscape elevation differences. However, they lack a mechanism for reorganizing the drainage system induced by horizontal motion, leading to deviations between simulated and observed modern landscapes.

4.2 Comparison of Uplift Scenarios

By comparing the simulation results of five uplift scenarios, we can assess the preservation potential and rationality of different tectonic histories in the landscape.

(1) Best-performing case: Stepwise Uplift (SW)

Among all the hypotheses tested, the FS-SW case shows the best fit with the modern landscape (EMD = 0.0758). The SW scenario represents a compromise between slow and rapid uplift. The SW scenario assumes that the Altiplano experienced uplift pulses during 10-6 Ma, but the uplift magnitude is less than ~2 km in the R scenario (Insel et al., 2012). The FS-SW case supports the existence of an uplift event in the late Miocene, which left transient response signals in the landscape (Hoke and Garzione, 2008; Garzione et al., 2008). However, it does not support the idea that these transient signals are caused by large-magnitude rapid uplift.

(2) Slow uplift scenarios: differences between SS and US

The SS scenario shows poor modeling results, especially in the absence of folds (NF), where the EMD value is highest (> 0.2). The SS scenario represents the traditional gradual uplift view (Insel et al., 2012). However, the modeling results indicate that a low uplift rate allows rivers sufficient time to balance the uplift through downcutting, thereby failing

to reproduce the observed distribution of high k_{sn} values. Unless fold shortening is introduced, simple slow uplift cannot maintain the high topographic relief of the modern eastern Central Andes. The US scenario significantly outperforms the SS scenario. Except for rapid uplift (R), compared to ER, SS, and SW, the US scenario has the lowest EMD values under all three fold setups. If not for the minimum EMD value of the FS-SW case, the most likely uplift model would be FS-US. The reason for the advantage of US is that, similar to SW, US includes a small uplift pulse (~1.5 km) during 11.5-6 Ma. The high degree of similarity between the landscapes simulated by FS-SW and FS-US and modern landscapes further indicates that uplift pulses can better explain the uplift history of the Altiplano.

(3) Rapid uplift scenarios: time differences between R and ER
The rapid uplift (R) and early rapid uplift (ER) scenarios highlight the importance of the timing of tectonic events. The recent rapid uplift (R) scenario consistently maintains low EMD values (~0.09-0.10) across all fold setups. Recent high-intensity tectonic uplift provides significant potential energy, generating strong headward-migrating erosion waves throughout the basin. The strong signals even mask the effects of local folding.

In contrast, under the NF and VF setups, the early rapid uplift (ER) scenario shows a poorer fit than the R scenario. The rapid uplift event in the ER scenario occurred earlier than in the R scenario. After a long period of evolution, the knickpoints formed early have migrated headward to the headwater area. The lack of clear remnants of the ER event in the modern landscape leads to a mismatch between the model and observations. The contrast strongly suggests that if a large-scale tectonic uplift event is the main factor shaping the modern eastern Andean landscape, it likely has occurred relatively late in geological history (e.g., Late Miocene-Pliocene), rather than earlier (Garzione et al., 2008; Ghosh et al., 2006). However, since both ER and R scenarios have EMD values greater than those in the SS, SW, and US scenarios under the more realistic FS setup, rapid uplift scenarios (R and ER) may not be suitable for explaining the uplift history of the Altiplano.

5. MODEL LIMITATIONS

Although the model considers the spatial variations in topography and rainfall, several simplifying assumptions remain. First, while the orographic rainfall effect is modeled using background rainfall and easterly wind input, the impact of long-term climate change (such as increased rainfall rate in the Late Miocene) (Poulsen et al., 2010) on erosion patterns is not considered. Spatial variations in rainfall rates are not well-represented in the model. Second, the initial topography is constructed based on scaling modern DEMs to represent paleotopography,

which does not fully account for pre-Andean topographic features. Tectonic uplift calculated from proportionally scaled topographic differences may not accurately reflect actual tectonic events.
Future research could pay more attention to identifying the initial tectonic and paleoclimatic conditions prior to the uplift of the Altiplano, which is the basis for landscape evolution modeling. Combined with higher-resolution paleoclimatic models, tectonic reconstruction data, and low-temperature thermochronology constraints, it is possible to further improve the study of landscape evolution in orogenic belts.

6. CONCLUSIONS

This study reconstructs the landscape evolution process in the eastern Central Andes through numerical modeling and quantitative analysis. The main conclusions are as follows:

(1) Horizontal shortening is a key tectonic factor in shaping landscapes: only considering vertical uplift (VF or NF setups) cannot reproduce the complex drainage system geometry and knickpoint distribution in the eastern Central Andes. The fold shortening (FS) setup can successfully induce river diversion and preserve the transient characteristics of the river channel through horizontal advection, which is a necessary condition for explaining modern landscape patterns.

(2) Support for the Late Miocene stepwise uplift scenario: among the five uplift scenarios tested, the combination case of fold shortening (FS) and stepwise uplift (SW) has the highest similarity with actual observed data (EMD=0.0758). This indicates that the formation of the Altiplano is not a single, long, slow process, but rather involves pulsed, accelerated uplift events during the late Miocene (approximately 10-6 Ma).

(3) The control and masking of landscape signals by uplift rate: high-intensity rapid uplift can generate overwhelming regional erosion signals, thereby “masking” the impact of local fold structures on river channels. On the contrary, slow and steady uplift makes it difficult to maintain a high k_{sn} value in the absence of strong tectonic interference due to the quasi-equilibrium between erosion and uplift.

ACKNOWLEDGEMENTS
The first author gratefully acknowledges the financial support from the China Scholarship Council (CSC) and the School of Geosciences at the University of Sydney.

AUTHOR CONTRIBUTIONS
Y.Z. designed and ran the simulations, analyzed the results, and wrote the manuscript. P.F.R. contributed to the result analysis and manuscript

revision. T.S. developed the model code and contributed to the manuscript revision.

DISCLOSURE STATEMENT

No potential conflict of interest was reported by the authors.

ORCID

Yinbing Zhu[1] (https://orcid.org/0000-0002-4115-3308)
Patrice F. Rey[1] (https://orcid.org/0000-0002-1767-8593)
Tristan Salles[1] (https://orcid.org/0000-0001-6095-7689)

DATA AVAILABILITY STATEMENT

Version 2.2.0 of Badlands used for the landscape and sedimentary evolution modeling is preserved at https://doi.org/10.5281/zenodo.1069573 (Salles & Howson, 2017), available via GNU General Public License v3.0 and developed openly at https://github.com/badlands-model/badlands.
The TopoToolbox v2.3.1 library is available at https://topotoolbox.wordpress.com/download/.
Tropical Rainfall Measuring Mission (TRMM) (2011), TRMM Combined Precipitation Radar and Microwave Imager Rainfall Profile L2 1.5 hours V7, Greenbelt, MD, Goddard Earth Sciences Data and Information Services Center (GES DISC), Accessed: 13/06/2025, https://disc.gsfc.nasa.gov/datacollection/TRMM_2B31_7.html
NASA JPL. (2013). NASA Shuttle Radar Topography Mission Global 1 arc second [Data set]. NASA Land Processes Distributed Active Archive Center. Accessed: 03/03/2025, https://doi.org/10.5067/MEASURES/SRTM/SRTMGL1.003.

REFERENCES

Anderson, R. B., Long, S. P., Horton, B. K., Calle, A. Z., and Ramirez, V.: Shortening and structural architecture of the Andean fold-thrust belt of southern Bolivia (21°S): Implications for kinematic development and crustal thickening of the central Andes, Geosphere, 13, 538-558, https://doi.org/10.1130/ges01433.1, 2017.

Anderson, R. B., Long, S. P., Horton, B. K., Thomson, S. N., Calle, A. Z., and Stockli, D. F.: Orogenic Wedge Evolution of the Central Andes, Bolivia (21°S): Implications for Cordilleran Cyclicity, Tectonics, 37, 3577-3609, https://doi.org/10.1029/2018tc005132, 2018.

Bookhagen, B. and Strecker, M. R.: Orographic barriers, high-resolution TRMM rainfall, and relief variations along the eastern Andes, Geophysical Research Letters, 35, https://doi.org/10.1029/2007gl032011, 2008.

Crosby, B. T. and Whipple, K. X.: Knickpoint initiation and distribution within fluvial networks: 236 waterfalls in the Waipaoa River, North Island, New Zealand, Geomorphology, 82, 16-38, https://doi.org/10.1016/j.geomorph.2005.08.023, 2006.

Ehlers, T. A. and Poulsen, C. J.: Influence of Andean uplift on climate and paleoaltimetry estimates, Earth and Planetary Science Letters, 281, 238-248, https://doi.org/10.1016/j.epsl.2009.02.026, 2009.

Evenstar, L. A., Hartley, A. J., and Mather, A. E.: Orogenic-orographic feedback and the rise of the Central Andes, Earth and Planetary Science Letters, 602, https://doi.org/10.1016/j.epsl.2022.117931, 2023.

Fiorella, R. P., Poulsen, C. J., Pillco Zolá, R. S., Jeffery, M. L., and Ehlers, T. A.: Modern and long-term evaporation of central Andes surface waters suggests paleo archives underestimate Neogene elevations, Earth and Planetary Science Letters, 432, 59-72, https://doi.org/10.1016/j.epsl.2015.09.045, 2015.

Flint, J.-J.: Stream gradient as a function of order, magnitude, and discharge, Water Resources Research, 10, 969-973, https://doi.org/10.1029/WR010i005p00969, 1974.

Garzione, C. N., Molnar, P., Libarkin, J. C., and MacFadden, B. J.: Rapid late Miocene rise of the Bolivian Altiplano: Evidence for removal of mantle lithosphere, Earth and Planetary Science Letters, 241, 543-556, https://doi.org/10.1016/j.epsl.2005.11.026, 2006.

Garzione, C. N., Auerbach, D. J., Smith, J. J. S., Rosario, J. J., Passey, B. H., Jordan, T. E., and Eiler, J. M.: Clumped isotope evidence for diachronous surface cooling of the Altiplano and pulsed surface uplift of the Central Andes, Earth and Planetary Science Letters, 393, 173-181, https://doi.org/10.1016/j.epsl.2014.02.029, 2014.

Garzione, C. N., Hoke, G. D., Libarkin, J. C., Withers, S., MacFadden, B., Eiler, J., Ghosh, P., and Mulch, A.: Rise of the Andes, Science, 320, 1304-1307, https://doi.org/10.1126/science.1148615, 2008.

Garzione, C. N., McQuarrie, N., Perez, N. D., Ehlers, T. A., Beck, S. L., Kar, N., Eichelberger, N., Chapman, A. D., Ward, K. M., Ducea, M. N., Lease, R. O., Poulsen, C. J., Wagner, L. S., Saylor, J. E., Zandt, G., and Horton, B. K.: Tectonic Evolution of the Central Andean Plateau and Implications for the Growth of Plateaus, Annual Review of Earth and Planetary Sciences, 45, 529-559, https://doi.org/10.1146/annurev-earth-063016-020612, 2017.

Ghosh, P., Garzione, C. N., and Eiler, J. M.: Rapid uplift of the Altiplano revealed through 13C-18O bonds in paleosol carbonates, Science, 311, 511-515, https://doi.org/10.1126/science.1119365, 2006.

Gómez, J., Schobbenhaus, C., Montes, N. E., and compilers: Geological Map of South America 2019. Scale 1:5 000 000. Commission for the Geological Map of the World (CGMW), Colombian Geological Survey, and Geological Survey of Brazil. Paris, https://doi.org/10.32685/10.143.2019.929, 2019.

GÓMez Tapias, J., Schobbenhaus, C., and Montes Ramírez, N.: Geological Map of South America 2019, https://doi.org/10.32685/10.143.2019.929, 2019.

Gregory-Wodzicki, K. M.: Uplift history of the Central and Northern Andes: A review, Geological Society of America Bulletin, 112, 1091-1105, https://doi.org/10.1130/0016-7606(2000)112<1091:uhotca>2.0.co;2, 2000.

Hack, J. T.: Studies of longitudinal stream profiles in Virginia and Maryland, https://doi.org/10.3133/pp294B, 1957.

Hoke, G. D. and Garzione, C. N.: Paleosurfaces, paleoelevation, and the mechanisms for the late Miocene topographic development of the Altiplano plateau, Earth and Planetary Science Letters, 271, 192-201, https://doi.org/10.1016/j.epsl.2008.04.008, 2008.

Houston, J. and Hartley, A. J.: The central Andean west-slope rainshadow and its potential contribution to the origin of hyper-aridity in the Atacama Desert, International Journal of Climatology, 23, 1453-1464, https://doi.org/10.1002/joc.938, 2003.

Insel, N., Poulsen, C. J., Ehlers, T. A., and Sturm, C.: Response of meteoric δ18O to surface uplift — Implications for Cenozoic Andean Plateau growth, Earth and Planetary Science Letters, 317-318, 262-272, https://doi.org/10.1016/j.epsl.2011.11.039, 2012.

Jordan, T. E., Kirk-Lawlor, N. E., Blanco, N. P., Rech, J. A., and Cosentino, N. J.: Landscape modification in response to repeated onset of hyperarid paleoclimate states since 14 Ma, Atacama Desert, Chile, Geological Society of America Bulletin, 126, 1016-1046, https://doi.org/10.1130/b30978.1, 2014.

Kar, N., Garzione, C. N., Jaramillo, C., Shanahan, T., Carlotto, V., Pullen, A., Moreno, F., Anderson, V., Moreno, E., and Eiler, J.: Rapid regional surface uplift of the northern Altiplano plateau revealed by multiproxy paleoclimate reconstruction, Earth and Planetary Science Letters, 447, 33-47, https://doi.org/10.1016/j.epsl.2016.04.025, 2016.

Lamb, S. and Hoke, L.: Origin of the high plateau in the central Andes, Bolivia, South America, Tectonics, 16, 623-649, https://doi.org/10.1029/97tc00495, 1997.

Leier, A., McQuarrie, N., Garzione, C., and Eiler, J.: Stable isotope evidence for multiple pulses of rapid surface uplift in the Central Andes, Bolivia, Earth and Planetary Science Letters, 371-372, 49-58, https://doi.org/10.1016/j.epsl.2013.04.025, 2013.

Perron, J. T. and Royden, L.: An integral approach to bedrock river profile analysis, Earth Surface Processes and Landforms, 38, 570-576, https://doi.org/10.1002/esp.3302, 2013.

Poulsen, C. J., Ehlers, T. A., and Insel, N.: Onset of convective rainfall during gradual late Miocene rise of the central Andes, Science, 328, 490-493, https://doi.org/10.1126/science.1185078, 2010.

Rech, J. A., Currie, B. S., Michalski, G., and Cowan, A. M.: Neogene climate change and uplift in the Atacama Desert, Chile, Geology, 34, https://doi.org/10.1130/g22444.1, 2006.

Rech, J. A., Currie, B. S., Jordan, T. E., Riquelme, R., Lehmann, S. B., Kirk-Lawlor, N. E., Li, S., and Gooley, J. T.: Massive middle Miocene gypsic paleosols in the Atacama Desert and the formation of the Central Andean rain-shadow, Earth and Planetary Science Letters, 506, 184-194, https://doi.org/10.1016/j.epsl.2018.10.040, 2019.

Rubner, Y., Tomasi, C., and Guibas, L. J.: The Earth Mover's Distance as a Metric for Image Retrieval, International Journal of Computer Vision, 40, 99-121, https://doi.org/10.1023/a:1026543900054, 2000.

Safran, E. B., Bierman, P. R., Aalto, R., Dunne, T., Whipple, K. X., and Caffee, M.: Erosion rates driven by channel network incision in the Bolivian Andes, Earth Surface Processes and Landforms, 30, 1007-1024, https://doi.org/10.1002/esp.1259, 2005.

Salles, T. and Hardiman, L.: Badlands: An open-source, flexible and parallel framework to study landscape dynamics, Computers & Geosciences, 91, 77-89, https://doi.org/10.1016/j.cageo.2016.03.011, 2016.

Salles, T. and Howson, I.: badlands-model/pyBadlands: Stable release version 2.0.0 (v2.0.0) [Software]. Zenodo, https://doi.org/10.5281/zenodo.1069573, 2017.

Schwanghart, W. and Scherler, D.: TopoToolbox 2 – MATLAB-based software for topographic analysis and modeling in Earth surface sciences,

Earth Surface Dynamics, 2, 1-7, https://doi.org/10.5194/esurf-2-1-2014, 2014.

Snyder, N. P., Whipple, K. X., Tucker, G. E., and Merritts, D. J.: Landscape response to tectonic forcing: Digital elevation model analysis of stream profiles in the Mendocino triple junction region, northern California, Geological Society of America Bulletin, 112, 1250-1263, https://doi.org/10.1130/0016-7606(2000)112<1250:lrttfd>2.0.co;2, 2000.

Strecker, M. R., Alonso, R. N., Bookhagen, B., Carrapa, B., Hilley, G. E., Sobel, E. R., and Trauth, M. H.: Tectonics and Climate of the Southern Central Andes, Annual Review of Earth and Planetary Sciences, 35, 747-787, https://doi.org/10.1146/annurev.earth.35.031306.140158, 2007.

Whipple, K. X. and Gasparini, N. M.: Tectonic control of topography, rainfall patterns, and erosion during rapid post–12 Ma uplift of the Bolivian Andes, Lithosphere, 6, 251-268, https://doi.org/10.1130/l325.1, 2014.

Wolpert, J. A. and Schoenbohm, L. M.: Channel Steepness Biases and Nonsteady Erosion in Landscapes Evolving Under Cyclical Climate, Geophysical Research Letters, 52, https://doi.org/10.1029/2024gl112229, 2025.

5 Discussion

5.1 Differences in Landscape Responses Driven by Uplift and Rainfall: Theoretical Synthesis

Identifying the respective contributions of climate change (e.g., rainfall rate changes) and tectonic activity (e.g., uplift) to landscape evolution has long been a major challenge in geomorphological research. By combining the first two numerical modeling studies in this thesis, we find that climatic and tectonic forcing produce distinct diagnostic signals in terms of headwater slope, landscape relaxation time, and divide migration.

The fundamental ways in which rainfall and uplift affect the landscape are different. Numerical modeling shows that river incision efficiency changes instantaneously following the change in rainfall rate, while the supply of sediment from hillslopes, constrained by topographic slope, lags significantly. This supply-demand imbalance leads to a "Transient Slope Change Reversal" in the slope of the headwater river channel. A decrease in rainfall rate reduces the incision rate faster than the rate of material supply from the hillslope, temporarily flattening the headwater channel, followed by an increase in slope and the attainment of a new equilibrium. Conversely, increased rainfall rate immediately intensifies river incision, causing a transient increase in the headwater channel slope, which then gradually decreases to a steady state.

In contrast, tectonic uplift is a boundary-like perturbation that typically propagates upwards in the form of a traceable erosion wave starting from the river outlet. Before the erosion wave arrives at the headwater, the slope of the headwater channel remains unchanged. When the erosion wave arrives, the slope shows a monotonic increase or decrease, without any reversals. Therefore, whether there is a transient reversal in the slope of the headwater river channel is an important indicator for distinguishing between climate and tectonic forcing.

The response pace of the landscape to perturbations also provides key information. Results show that landscapes respond asymmetrically to changes in rainfall rate. The time required for landscapes to adapt to an increase in rainfall rate (restore a steady state) is much shorter than the time required to adapt to a decrease in rainfall rate. The reason is that the erosion capacity of rivers has a non-linear (power-law) relationship with rainfall rate, and an increase in rainfall rate can more efficiently eliminate landscape imbalances. On the contrary, for the increase or decrease in the rate of tectonic uplift, the

relaxation/restoration time of the landscape is roughly equivalent (symmetry). The difference in relaxation time is more significant under orographic rainfall conditions.

Under orographic rain conditions, the impact of rainfall and uplift on divide stability varies. The migration of the divide is mainly controlled by the difference in erosion rates on both sides. The modeling results indicate that changes in rainfall rate can significantly amplify or reduce the rainfall gradient on both sides of the divide, leading to divide migration (up to several kilometers in the model). For example, an increase in rainfall rate drives the divide to migrate towards the windward slope, while a decrease in rainfall rate leads to its migration towards the leeward slope. In contrast, simple changes in the uplift rate, although altering the landscape height, have minimal impact on the rainfall gradient on both sides of the divide, resulting in minimal divide migration. The differences in divide response indicate that large-scale divide migration is more likely a signal of climate change (rainfall) than a simple result of tectonic uplift.

5.2 Application of Theory in the Uplift History of the Altiplano in the Central Andes

Based on the theoretical understanding of the geomorphic response mechanism mentioned above, we further quantitatively evaluate the uplift history of the Altiplano in the Central Andes using numerical models and Earth Mover's Distance (EMD).

The modeling results emphasize the key role of fold shortening (FS) in shaping the landscape of the eastern Central Andes. A model that considers only vertical uplift cannot reproduce the observed N-S tributary pattern and knickpoint distribution. After introducing horizontal shortening, the similarity between landscape features and modern observation data has significantly increased (with the lowest EMD value). The high degree of similarity not only confirms the controlling effect of horizontal movement on drainage system reorganization but also supports the theory in Article 1 that tectonics sets a boundary condition that controls the erosion base level. Horizontal shortening continuously changes the base level of the river, maintaining the system in a long-term transient adjustment.

Among the five uplift scenarios tested, "fold shortening + stepwise uplift" (FS-SW) has the best fit with the modern landscape. It supports the hypothesis that the Altiplano experienced an uplift pulse during the Late Miocene (approximately 10-6 Ma).

The elevation and normalized channel steepness index (k_{sn}) generated by the slow and steady model are lower than the observed values. In the eastern Central Andes, slow uplift is insufficient to offset erosion and maintain high elevation.

Results also show that recent large-scale rapid uplift (R uplift scenario) can generate overwhelming regional erosion signals, masking the impact of local fold structures on landscapes. The strong signal is similar to the fast migration erosion wave caused by strong tectonic forcing described in Article 1, which smooths out fine geomorphic differences.

5.3 Future work

The diagnostic framework proposed in this work provides new insights into the influence of climatic and tectonic forcing on landscape evolution. However, several limitations remain that point the way for future research.

First, extracting information from landscapes requires eliminating background noise caused by other factors. A more accurate numerical model needs to account for physical processes, including the combination of spatially and temporally variable rock types, weathering rates, and climate-dependent slope diffusion coefficients.

Second, combining thermochronological information with cosmogenic nuclide data can help verify the erosion history and rate patterns predicted by the model.

Third, by applying transport-limited or mixed bedrock-alluvial models, it is possible to investigate how landscapes respond to complex processes, including the "tools and cover" effect and channel adjustment.

Fourth, coupling mantle convection and landscape evolution models over longer time scales can provide insights into the interaction between deep processes and surface evolution.

Finally, applying theoretical models to mountain systems with different climatic and tectonic backgrounds (such as the Anatolian Plateau and the Tibet Plateau) can test the universality of these models and advance our understanding of landscape evolution.

6 Conclusion

This thesis studies the effects of rainfall and tectonic uplift on landscape evolution through a series of numerical experiments, from theoretical mechanisms to practical cases, and explores how to interpret climatic and tectonic history from modern landscapes. The main conclusions are as follows:

1. Headwater channel slope is a diagnostic signal for distinguishing the respective roles of climatic and tectonic forcing: changes in rainfall rate can cause a transient reversal of the headwater channel slope (first decreasing and then increasing or first increasing and then decreasing), which is caused by the time lag between hillslope diffusion and river incision. In contrast, changes in the uplift rate keep the headwater channel slope unchanged until the arrival of the erosion wave, after which it undergoes a monotonic change. The difference in the response of the headwater channel slope can serve as a key indicator for distinguishing between climate and tectonic forcing.

2. Asymmetric response time of landscape and divide sensitivity: the pace of landscape recovery from increased rainfall is faster than that from decreased rainfall, while the relaxation time of tectonic uplift is relatively symmetrical. Under orographic rainfall conditions, divide migration is highly sensitive to changes in rainfall rate and displays significant directional migration, while it is not sensitive to changes in tectonic uplift rate. The divide sensitivity to perturbation provides a theoretical basis for using divide dynamics to invert ancient climate change.

3. Horizontal shortening is the key to the formation of the landscape on the eastern flank of the Central Andes: vertical uplift alone cannot explain the complex drainage systems and knickpoints today. The Fold Shortening model, which includes horizontal motion, best reproduces the observed N-S tributaries and the area with high channel steepness, supporting the key role of horizontal tectonic movement in shaping landscapes.

4. The Altiplano experienced an uplift pulse in the Late Miocene: quantitative comparison (EMD analysis) shows that the scenario of "Fold Shortening + Stepwise Uplift" is most consistent with modern landscapes. The results indicate that the formation of the Altiplano was not a single long-term slow process but rather underwent an uplift pulse during the Late Miocene (approximately 10-6 Ma). Excessive uplift can mask local structural signals, while too slow uplift cannot maintain the current high topography.

Appendix A

Supplement Materials to Article 1:

Zhu, Y., Rey, P., & Salles, T. (2025). Rainfall and tectonic forcing lead to contrasting headwater slope evolutions. *Earth Surf. Dynam.*, 13(6), 1249-1261.

This supplement presents the results of a sensitivity test conducted with a finer grid resolution of 200 m. This test was performed to confirm that the primary findings of our study are robust and not an artifact of the 400 m grid spacing used in the main manuscript. The model run shown here is analogous to Models M2-M4 in the main text, which use a non-zero diffusion coefficient.

Figure S1 illustrates the resulting landscape morphology, which is consistent with the findings presented in the main text. Figure S2 demonstrates that the transient slope change reversal—a temporary decrease in headwater slope following a decrease in rainfall (Fig. S2 a2 and a3)—is clearly reproduced at this finer resolution. This confirms that the mechanism described in the main text is a robust feature of the model and not dependent on the chosen grid scale.

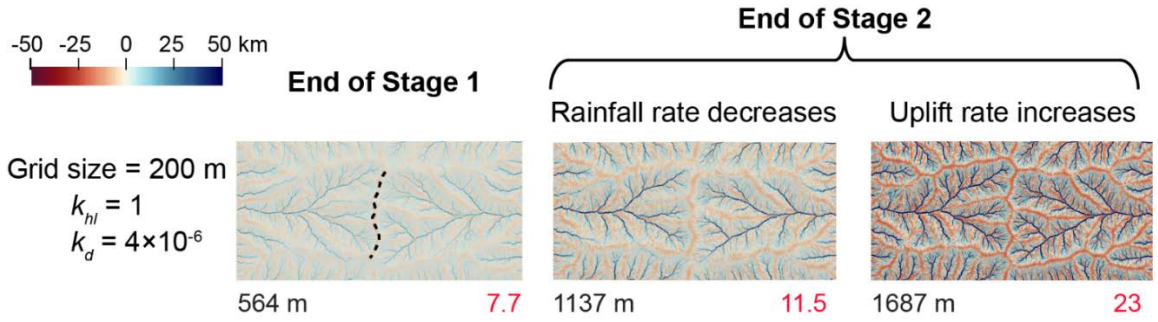

Figure S1. Hillshade maps showing cumulative erosion and deposition resulting from hillslope diffusion at the end of Stage 1 and the end of Stage 2. Blue areas indicate deposition, while red areas represent erosion. Color bar values indicate cumulative depositional (positive) and erosional (negative) amounts (km). Numbers below each map display the mean elevation (black) and roughness (red). Dashed lines on maps at the end of Stage 1 denote the divide. The divide in Stage 2 is similar to that in Stage 1 and is not marked in this stage.

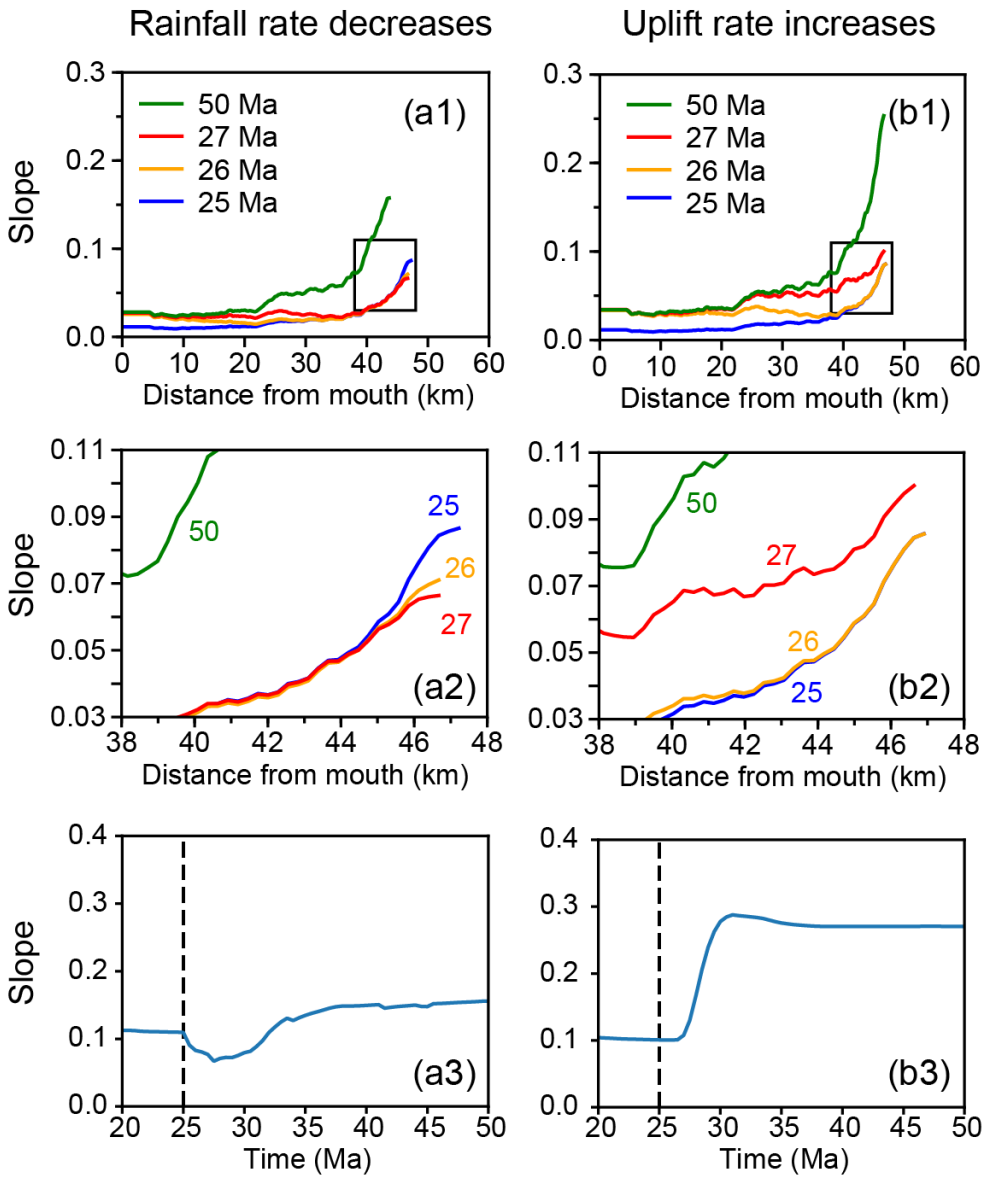

Figure S2. Evolution of trunk stream slope following a decrease in rainfall rate and an increase in uplift rate. (a1-b1) Longitudinal slope profiles of the trunk stream at selected time steps (colored lines). Black rectangles indicate the headwater regions. (a2-b2) Enlarged views of the headwater areas, corresponding to the boxed regions in (a1-b1). (a3-b3) Temporal evolution of the mean channel slope in the upper ~800 m of the trunk stream, capturing the dynamic slope response across model runs. Dashed vertical lines mark the timing of the change in rainfall or uplift rate (25 Ma).

Appendix B

Supplement Materials to Article 3:

Zhu, Y., Rey, P., & Salles, T. (2025). Evaluating Central Andean Altiplano uplift histories with numerical model: a quantitative comparison of fold setups and uplift scenarios. (Prepared for submission to *Earth Surface Processes and Landforms*)

Table S1. Common parameters used in Badlands models

Parameter	Value	Unit
Size of the model domain in NF and VF	612 × 767	km
Size of the model domain in FS	802 × 767	km
Grid resolution in NF and VF	1000	m
Grid resolution in VF	1310	m
Time step (d_t)	0.5	Myr
Total duration	25	Myr
Background rainfall	800	mm/yr
Easterly wind velocity	4	m/s
m (drainage area exponent)	0.45	-
n (slope exponent)	1	-
Erodibility (k_d)	5×10^{-7}	1/yr
Surface diffusion coefficient (k_h)	0.005	m^2/yr

Note: Three setups in the model are No Fold (NF), Vertical Fold (VF), and Fold Shortening (FS).

Bibliography

Ahmed, M. F., Ali, M. Z., Rogers, J. D., & Khan, M. S. (2019). A study of knickpoint surveys and their likely association with landslides along the Hunza River longitudinal profile. *Environmental Earth Sciences, 78*(5).

Ahnert, F. (1987). Approaches to dynamic equilibrium in theoretical simulations of slope development. *Earth Surface Processes and Landforms, 12*(1), 3-15.

Alavinia, M., Saleh, F. N., & Asadi, H. (2019). Effects of rainfall patterns on runoff and rainfall-induced erosion. *International Journal of Sediment Research, 34*(3), 270-278.

Allen;, P. A., & Allen, J. R. (2013). *Basin Analysis: Principles and Application to Petroleum Play Assessment*.

Anderson, R. B., Long, S. P., Horton, B. K., Calle, A. Z., & Ramirez, V. (2017). Shortening and structural architecture of the Andean fold-thrust belt of southern Bolivia (21°S): Implications for kinematic development and crustal thickening of the central Andes. *Geosphere, 13*(2), 538-558.

Barnhart, K. R., Hutton, E. W. H., Tucker, G. E., Gasparini, N. M., Istanbulluoglu, E., Hobley, D. E. J., et al. (2020a). Short communication: Landlab v2.0: a software package for Earth surface dynamics. *Earth Surface Dynamics, 8*(2), 379-397.

Barnhart, K. R., Tucker, G. E., Doty, S. G., Shobe, C. M., Glade, R. C., Rossi, M. W., & Hill, M. C. (2020b). Inverting Topography for Landscape Evolution Model Process Representation: 1. Conceptualization and Sensitivity Analysis. *Journal of Geophysical Research: Earth Surface, 125*(7).

Barnhart, K. R., Tucker, G. E., Doty, S. G., Shobe, C. M., Glade, R. C., Rossi, M. W., & Hill, M. C. (2020c). Inverting Topography for Landscape Evolution Model Process Representation: 2. Calibration and Validation. *Journal of Geophysical Research: Earth Surface, 125*(7).

Bierman, P. R., & Montgomery, D. R. (2019). Drainage basins. In *Key concepts in geomorphology* (2nd ed., pp. 235-270): W. H. Freeman and Company.

Bierman, P. R., & Montgomery, D. R. (2019). *Key Concepts in Geomorphology* (2 ed.): Macmillan Higher Education.

Bonnet, S., & Crave, A. (2003). Landscape response to climate change: Insights from experimental modeling and implications for tectonic versus climatic uplift of topography. *Geology, 31*(2), 123.

Braun, J., & Willett, S. D. (2013). A very efficient O(n), implicit and parallel method to solve the stream power equation governing fluvial incision and landscape evolution. *Geomorphology, 180-181*, 170-179.

Champagnac, J. D., Molnar, P., Sue, C., & Herman, F. (2012). Tectonics, climate, and mountain topography. *Journal of Geophysical Research: Solid Earth, 117*(B2).

Chen, A., Darbon, J., & Morel, J.-M. (2014). Landscape evolution models: A review of their fundamental equations. *Geomorphology, 219*, 68-86.

Davis, W. M. (1899). The Geographical Cycle. *The Geographical Journal, 14*(5), 481.

DiBiase, R. A., Whipple, K. X., Heimsath, A. M., & Ouimet, W. B. (2010). Landscape form and millennial erosion rates in the San Gabriel Mountains, CA. *Earth and Planetary Science Letters, 289*(1-2), 134-144.

Dietrich, R., Ivins, E. R., Casassa, G., Lange, H., Wendt, J., & Fritsche, M. (2010). Rapid crustal uplift in Patagonia due to enhanced ice loss. *Earth and Planetary Science Letters, 289*(1-2), 22-29.

Flament, N., Gurnis, M., & Müller, R. D. (2013). A review of observations and models of dynamic topography. *Lithosphere, 5*(2), 189-210.

Fraedrich, W. (2023). Glaciers Shape Landscapes. In *Traces of the Ice Age: Landscape Forms in Central Europe* (pp. 41-61). Berlin, Heidelberg: Springer Berlin Heidelberg.

Garzione, C. N., McQuarrie, N., Perez, N. D., Ehlers, T. A., Beck, S. L., Kar, N., et al. (2017). Tectonic Evolution of the Central Andean Plateau and Implications for the Growth of Plateaus. *Annual Review of Earth and Planetary Sciences, 45*(1), 529-559.

Guerrero, J., Gutiérrez, F., & Lucha, P. (2008). Impact of halite dissolution subsidence on Quaternary fluvial terrace development: Case study of the Huerva River, Ebro Basin, NE Spain. *Geomorphology, 100*(1-2), 164-179.

Hack, H. R. G. K. (2020). Weathering, Erosion, and Susceptibility to Weathering. In M. Kanji, M. He, & L. Ribeiro e Sousa (Eds.), *Soft Rock Mechanics and Engineering* (pp. 291-333). Cham: Springer International Publishing.

Hack, J. T. (1957). Studies of longitudinal stream profiles in Virginia and Maryland.

Han, J., Gasparini, N. M., & Johnson, J. P. L. (2015). Measuring the imprint of orographic rainfall gradients on the morphology of steady-state numerical fluvial landscapes. *Earth Surface Processes and Landforms, 40*(10), 1334-1350.

Heuret, A., & Lallemand, S. (2005). Plate motions, slab dynamics and back-arc deformation. *Physics of the Earth and Planetary Interiors, 149*(1-2), 31-51.

Hobley, D. E. J., Adams, J. M., Nudurupati, S. S., Hutton, E. W. H., Gasparini, N. M., Istanbulluoglu, E., & Tucker, G. E. (2017). Creative computing with Landlab: an open-source toolkit for building, coupling, and exploring two-dimensional numerical models of Earth-surface dynamics. *Earth Surface Dynamics, 5*(1), 21-46.

Hoggard, M., Austermann, J., Randel, C., & Stephenson, S. (2021). Observational Estimates of Dynamic Topography Through Space and Time. In *Mantle Convection and Surface Expressions* (pp. 371-411).

Horton, R. E. (1945). Erosional Development of Streams and Their Drainage Basins; Hydrophysical Approach to Quantitative Morphology. *Geological Society of America Bulletin, 56*(3).

Howard, A. D. (1994). A detachment-limited model of drainage basin evolution. *Water Resources Research, 30*(7), 2261-2285.

Insel, N., Poulsen, C. J., Ehlers, T. A., & Sturm, C. (2012). Response of meteoric δ18O to surface uplift — Implications for Cenozoic Andean Plateau growth. *Earth and Planetary Science Letters, 317-318*, 262-272.

Jiao, R., Herman, F., & Seward, D. (2017). Late Cenozoic exhumation model of New Zealand: Impacts from tectonics and climate. *Earth-Science Reviews, 166*, 286-298.

Kirby, E., & Whipple, K. X. (2012). Expression of active tectonics in erosional landscapes. *Journal of Structural Geology, 44*, 54-75.

Li, D., Overeem, I., Kettner, A. J., Zhou, Y., & Lu, X. (2021). Air Temperature Regulates Erodible Landscape, Water, and Sediment Fluxes in the Permafrost-Dominated Catchment on the Tibetan Plateau. *Water Resources Research, 57*(2).

Manea, V. C., Manea, M., Ferrari, L., Orozco-Esquivel, T., Valenzuela, R. W., Husker, A., & Kostoglodov, V. (2017). A review of the geodynamic evolution of flat slab subduction in Mexico, Peru, and Chile. *Tectonophysics, 695*, 27-52.

Mohamadi, M. A., & Kavian, A. (2015). Effects of rainfall patterns on runoff and soil erosion in field plots. *International Soil and Water Conservation Research, 3*(4), 273-281.

Molnar, P., & Tapponnier, P. (1975). Cenozoic Tectonics of Asia: Effects of a Continental Collision. *Science, 189*(4201), 419-426.

Moore, I. D., & Burch, G. J. (2010). Sediment Transport Capacity of Sheet and Rill Flow: Application of Unit Stream Power Theory. *Water Resources Research, 22*(8), 1350-1360.

Murphy, B. P., Johnson, J. P., Gasparini, N. M., & Sklar, L. S. (2016). Chemical weathering as a mechanism for the climatic control of bedrock river incision. *Nature, 532*(7598), 223-227.

Paola, C., Straub, K., Mohrig, D., & Reinhardt, L. (2009). The "unreasonable effectiveness" of stratigraphic and geomorphic experiments. *Earth-Science Reviews, 97*(1-4), 1-43.

Pelletier, J. D., & DeLong, S. (2004). Oscillations in arid alluvial-channel geometry. *Geology, 32*(8).

Roering, J. J., Almond, P., Tonkin, P., & McKean, J. (2002). Soil transport driven by biological processes over millennial time scales. *Geology, 30*(12).

Roering, J. J., Kirchner, J. W., & Dietrich, W. E. (1999). Evidence for nonlinear, diffusive sediment transport on hillslopes and implications for landscape morphology. *Water Resources Research, 35*(3), 853-870.

Salles, T. (2019). eSCAPE: Regional to Global Scale Landscape Evolution Model v2.0. *Geoscientific Model Development, 12*(9), 4165-4184.

Salles, T., Ding, X., & Brocard, G. (2018). pyBadlands: A framework to simulate sediment transport, landscape dynamics and basin stratigraphic evolution through space and time. *PLoS One, 13*(4), e0195557.

Salles, T., & Hardiman, L. (2016). Badlands: An open-source, flexible and parallel framework to study landscape dynamics. *Computers & Geosciences, 91*, 77-89.

Salles, T., Mallard, C., & Zahirovic, S. (2020). gospl: Global Scalable Paleo Landscape Evolution. *Journal of Open Source Software, 5*(56), 2804.

Scotese, C. R., & van der Pluijm, B. A. (2020). Deconstructing Tectonics: Ten Animated Explorations. *Earth and Space Science, 7*(11).

Smith, A. G. G., Fox, M., Schwanghart, W., & Carter, A. (2022). Comparing methods for calculating channel steepness index. *Earth-Science Reviews, 227*.

Snyder, N. P., Whipple, K. X., Tucker, G. E., & Merritts, D. J. (2003). Importance of a stochastic distribution of floods and erosion thresholds in the bedrock river incision problem. *Journal of Geophysical Research: Solid Earth, 108*(B2).

Sømme, T. O., Helland-Hansen, W., Martinsen, O. J., & Thurmond, J. B. (2009). Relationships between morphological and sedimentological parameters in source-to-sink systems: a basis for predicting semi-quantitative characteristics in subsurface systems. *Basin Research, 21*(4), 361-387.

Stern, R. J. (2002). Subduction zones. *Reviews of Geophysics, 40*(4).

Strahler, A. N. (1952). Hypsometric (Area-Altitude) Analysis of Erosional Topography. *Geological Society of America Bulletin, 63*(11).

Tada, R., Zheng, H., & Clift, P. D. (2016). Evolution and variability of the Asian monsoon and its potential linkage with uplift of the Himalaya and Tibetan Plateau. *Progress in Earth and Planetary Science, 3*(1).

Tanyaş, H., van Westen, C. J., Allstadt, K. E., & Jibson, R. W. (2018). Factors controlling landslide frequency–area distributions. *Earth Surface Processes and Landforms, 44*(4), 900-917.

Temme, A. J. A. M., & Vanwalleghem, T. (2016). LORICA – A new model for linking landscape and soil profile evolution: Development and sensitivity analysis. *Computers & Geosciences, 90*, 131-143.

Tucker, G. E., & Hancock, G. R. (2010). Modelling landscape evolution. *Earth Surface Processes and Landforms, 35*(1), 28-50.

Tucker, G. E., & Slingerland, R. (1997). Drainage basin responses to climate change. *Water Resources Research, 33*(8), 2031-2047.

Tucker, G. E., & Slingerland, R. L. (1994). Erosional dynamics, flexural isostasy, and long-lived escarpments: A numerical modeling study. *Journal of Geophysical Research: Solid Earth, 99*(B6), 12229-12243.

Turowski, J. M., Lague, D., & Hovius, N. (2007). Cover effect in bedrock abrasion: A new derivation and its implications for the modeling of bedrock channel morphology. *Journal of Geophysical Research: Earth Surface, 112*(F4).

Upadhyay, R. K. (2025). Earth's Internal Dynamics and Landforms. In R. K. Upadhyay (Ed.), *Geology and Mineral Resources* (pp. 139-212). Singapore: Springer Nature Singapore.

van der Meij, W. M., Temme, A. J. A. M., Lin, H. S., Gerke, H. H., & Sommer, M. (2018). On the role of hydrologic processes in soil and landscape evolution modeling: concepts, complications and partial solutions. *Earth-Science Reviews, 185*, 1088-1106.

Welivitiya, W. D. D. P., Willgoose, G. R., & Hancock, G. R. (2019). A coupled soilscape–landform evolution model: model formulation and initial results. *Earth Surface Dynamics, 7*(2), 591-607.

Welivitiya, W. D. D. P., Willgoose, G. R., Hancock, G. R., & Cohen, S. (2016). Exploring the sensitivity on a soil area-slope-grading relationship to

changes in process parameters using a pedogenesis model. *Earth Surface Dynamics, 4*(3), 607-625.

Whipple, K. X. (2004). Bedrock Rivers and the Geomorphology of Active Orogens. *Annual Review of Earth and Planetary Sciences, 32*(1), 151-185.

Whipple, K. X. (2009). The influence of climate on the tectonic evolution of mountain belts. *Nature Geoscience, 2*(2), 97-104.

Whipple, K. X., DiBiase, R. A., & Crosby, B. T. (2013). 9.28 Bedrock Rivers. In J. Shroder, Wohl, E. (Ed.), *Treatise on Geomorphology* (Vol. 9, Fluvial Geomorphology, pp. 550-573). San Diego, CA: Academic Press.

Whipple, K. X., & Tucker, G. E. (1999). Dynamics of the stream-power river incision model: Implications for height limits of mountain ranges, landscape response timescales, and research needs. *Journal of Geophysical Research: Solid Earth, 104*(B8), 17661-17674.

Wickert, A. D. (2016). Reconstruction of North American drainage basins and river discharge since the Last Glacial Maximum. *Earth Surface Dynamics, 4*(4), 831-869.

Willett, S. D., & Brandon, M. T. (2002). On steady states in mountain belts. *Geology, 30*(2), 175.

Willett, S. D., Hovius, N., Brandon, M. T., & Fisher, D. M. (2006). Introduction. In S. D. Willett, N. Hovius, M. T. Brandon, & D. M. Fisher (Eds.), *Tectonics, Climate, and Landscape Evolution* (Vol. 398, pp. vii–xi): Geological Society of America.

Willgoose, G. (2005). Mathematical Modeling of Whole Landscape Evolution. *Annual Review of Earth and Planetary Sciences, 33*(1), 443-459.

Willgoose, G., Bras, R. L., & Rodriguez-Iturbe, I. (2008). A coupled channel network growth and hillslope evolution model: 1. Theory. *Water Resources Research, 27*(7), 1671-1684.

Xie, C., Antić, N., Nadal-Romero, E., Yan, L., Tosti, T., Djogo Mračević, S., et al. (2022). The Influences of Climatic and Lithological Factors on Weathering of Sediments in Humid Badland Areas. *Frontiers in Earth Science, 10*.

Yin, A., & Harrison, T. M. (2000). Geologic Evolution of the Himalayan-Tibetan Orogen. *Annual Review of Earth and Planetary Sciences, 28*(1), 211-280.

Zhang, L., Ren, F., Li, H., Cheng, D., & Sun, B. (2021). The Influence Mechanism of Freeze-Thaw on Soil Erosion: A Review. *Water, 13*(8).